High Accuracy *ab initio* Quantum Chemistry on P, Si, and C-Containing Molecules

by

Tongxiang Lu

(Under the direction of Henry F. Schaefer III)

Abstract

The ground states and low-lying triplet states of P_2H_2 isomers and the associated isomerization transition states have been investigated systematically and the global minimum has been confirmed to be planar *trans*-HPPH diphosphene, lying 3.2 kcal mol^{-1} below *cis*-HPPH with the aug-cc-pVQZ CCSD(T) method upon inclusion of zero point vibrational energy corrections. This transition state for the *trans-cis* isomerization reaction exhibits multireference character and the reaction barrier is predicted to be 35.2 kcal mol^{-1} using the cc-pVQZ Mukherjee multi-reference coupled cluster (Mk-MRCCSD) (2e/2MO) method. The energy crossing of the singlet and triplet adiabatic potential energy surface is studied using Mk-MRCCSD method with the cc-pVQZ basis set, which predicts that the ^3B skewed HPPH is 1.4 kcal mol^{-1} lower in energy than corresponding ^1A skewed HPPH at the ^3B skewed HPPH optimized geometry. An accurate quartic force field for disilacyclopropenylidene-**1S** has been determined employing *ab initio* coupled-cluster (CC) with single and double excitations and perturbative treatment for triple excitations [CCSD(T)] method in combination with the correlation consistent core-valence quadruple zeta (cc-pCVQZ) basis set. The vibration-rotation coupling constants, equilibrium and zero-point vibration corrected rotational constants, centrifugal distortion constants, harmonic and fundamental vibrational frequencies for six isotopologues of disilacyclopropenylidene-**1S** are reported using vibrational

second-order perturbation theory (VPT2). The anharmonic corrections for the vibrational motions involving the H bridged bonds are found to be more than 5% with respect to the corresponding harmonic vibrational frequencies.

INDEX WORDS: coupled cluster theory, Mukherjee multi-reference coupled cluster, vibrational second-order perturbation theory, quartic force field, focal point analysis, basis set extrapolation, computational chemistry

High Accuracy *ab initio* Quantum Chemistry on P, Si, and C-Containing Molecules

by

Tongxiang Lu

B.S., Nankai University, Tianjin, China, 2003

M.S., University of Massachusetts, Amherst, 2007

A Dissertation Submitted to the Graduate Faculty

of The University of Georgia in Partial Fulfillment

of the

Requirements for the Degree

Doctor of Philosophy

Athens, Georgia

2011

High Accuracy *ab initio* Quantum Chemistry on P, Si, and C-Containing Molecules

by

Tongxiang Lu

Approved:

Major Professor: Henry F. Schaefer III

Committee: Geoffrey D. Smith
Nigel G. Adams

Electronic Version Approved:

Maureen Grasso
Dean of the Graduate School
The University of Georgia
May 2011

Dedication

To my parents and sister

Acknowledgments

I truly have to express my gratitude to a lot of people during the course of my research at the Center for Quantum Computational Chemistry (CCQC).

First of all, I am extremely indebted to my research advisor Professor Schaefer for his valuable guidance and constant encouragement throughout my graduate study at the CCQC. I would also like to thank him for his concern in both my professional and personal life. He provides the best academic research environment for graduate students at CCQC. He gives the freedom to allow me to study my personal interest in quantum chemistry. He has a kind and pleasure personality; he is generous, trustworthy. He is an excellent advisor and a true model of scientist.

Special thanks goes to Professor Nigel Adams and Professor Geoffrey Smith for being members of my committee. I have to give credit to Dr. Yukio Yamaguchi and Dr. Andy Simmonett. Dr. Yukio Yamaguchi taught me how to accomplish a project and write a scientific paper and how to become a better scientist. Dr Andy Simmonett gave answers for every questions related with the computers. I am thankful to Dr Steven Wheeler for being a great mentor. He has a gift to give answers even before I asked. Dr Yaoming Xie deserves a great deal of appreciation for for his answering my endless questions on quantum chemistry. I am grateful to the CCQC supporting staff Mrs. Linda Rowe, Amy Peterson, and Karen Branch for their assistance in my administrative needs.

I would like to thank all CCQC members for making these last few years enjoyable and fruitful. Dr Jun Zhang introduced me to quantum chemistry four years ago. My officemat, Dr Franceso Evangelista, let me know about the stock market. Jeremiah wilke gave the accurate and precise answer for the math questions. Dr Qiang Hao collaborated with me on several

papers. Professor Hao Feng discussed and cooperated with me on several projects. Certainly, I can not forget to thank Jowa Wu for his assistance in my first quantum chemistry class.

I would like to cordially thank my parents and my sister for always supporting my study. I dedicated this work to my parents because of their encouragement and support when I study abroad. They instilled in me a love for science at a young age, and teach me to work hard. They provide me the best eduction they can afford. Any accomplishment I achieve today is attributed to their love and considerations.

Table of Contents

Chapter 1

Introduction and Literature Review

1.1 Introduction

In modern chemistry computational quantum chemistry plays an important role, which has been employed to determine structures, evaluate vibrational frequencies and corresponding intensities, analyze chemical reactions, and shed light on other chemical and physical properties.

The Schrödinger equation, which is the foundation of quantum chemistry, is too complicated to be solved exactly for practical systems. Instead, the time-independent non-relativistic Schrödinger equation is simplified by the Born-Oppenheimer approximation, which separates the motions of nuclei and electrons. In principle, the nonrelativistic Schrödinger equation with Born-Oppenheimer approximation could be solved by the expansion of wavefunction using an infinite number of basis functions and slate determinants. In general, atom-centered Gaussian functions, which resemble the conventional "atomic orbitals", are adopted as basis functions. However, in practice, the usage of an infinite number of basis functions is not feasible. A limit amount of basis functions are used to approximately solve the problem, although the basis set error will be introduced.

The accurate determination of electron correlation is the main task for the post Hartree-Fock techniques. The electron correlation refers to that the motions of electrons is correlated by avoiding each other. The disparity for many post Hartree-Fock methods lies in the type of orbital occupation included and their weighting factor.

1.2 Theoretical Methods

Currently, the coupled cluster theory[1] is the most popular and efficient approach for the treatment of electron correlations. In coupled cluster, the wavefunction is expressed by,

$$\mid \Psi\rangle = e^{T} \mid \Psi\rangle \tag{1.1}$$

where T is excitation operator and $\mid \Phi\rangle$ is the Hartree-Fock wavefunction. In practice the truncation of the excitation operator at different orders gives rise to a family of coupled

cluster methods. For example, coupled cluster with single and double excitations (CCSD) is expressed as

$$T = T_1 + T_2, \tag{1.2}$$

The single excitations are provided by T_1, while double excitations are generated through the T_2 operator. The coupled cluster theory is superior to truncated CI approaches due to the property of size extensive at any level of truncation.

The main drawback for coupled cluster theory is that it is not viable for computation of large systems due to its time-consuming nature. The computational time using CCSD technique could scale as $O(o^2v^4)$, where v represents the number of unoccupied orbitals in the wavefunction and o indicates the number of occupied orbitals, whereas the scale is increased to $O(o^3v^4)$ for the popular CCSD(T) model.[2] The accuracy for a single CCSD(T) computation with a reasonable basis set for relative energies lies within 1-2 kcal mol^{-1}.

1.3 Convergence of the One-Particl Basis Set

The convergence of the Hartree-Fock energy with respect to the completeness of basis sets is relatively quick, which could be rationalized as follows. The Hartree-Fock equation is solved using average field approach, which imparts the one-particle nature into Hartree-Fock wavefunction. Consequently, the one-particle basis set can properly describe the wavefunction. Moreover, the Hartree-Fock energy depends only on the occupied molecular orbitals.

A cusp is formed at the coalescence point of the two electrons, which makes it difficult to describe correlated wavefunctions using one-particle basis sets.[3] Therefore, correlated wavefunctions more depends on basis sets. Moreover, the virtual orbitals are involved in the expansion of correlated wavefunctions. Although the virtual orbitals are required to be orthogonal to the occupied orbitals, it is difficult to optimize them due to the lack of real physical meaning.

Two approaches have been employed to improve the slow convergence of the correlation energy with respect to the one-particle basis. One is the so-call R_{12} method. This method includes the inter-electronic distance operator r_{12} in the correlated wavefunction, which can explicitly describe the electron cusp. As a result, the convergence of the correlation energy with regard to the complete basis set limit is more efficient compared with the conventional one-particle basis. The second approach, namely the extrapolation of energies (focal point analysis), are performed to reach the complete basis set limit.

1.4 Focal Point Analysis

Hartree-Fcok calculation with the complete basis set will not yield accurate results, since the electron correlations are not included in within the wavefunction. Likewise, the accuracy from a highly correlated wavefunction in combined with a small basis set is limited as well. In order to eliminate the error from both truncated correlation methods and limited basis set, the focal point analysis (FPA) was introduced by Allen and co-workers,[4,5] which improves the computational accuracy significantly.

In the FPA, the geometry of each structure optimized at the highest level of theory is adopted as the standard geometry for the whole extrapolation. Subsequently, a hierarchical series of single point energies are computed with the basis sets and correlation methods increased. In general, the family basis sets, cc-pVXZ constructed by Dunning,[6,7] are employed, where X is the "cardinal number" of the basis set. The primary advantage of this set of basis over other basis sets is that the energy increments are consistent with the increases of the cardinal number, which is accompanied by the addition of extra higher and lower angular momentum functions. This feature is very important to extrapolation. For the Hartree-Fock energy, the extrapolation could be expressed as[8]

$$E_{HF}(X) = A + Be^{-cX}, \tag{1.3}$$

where A, B, and C are fitting parameters by computations with three different basis sets. The complete basis set (CBS) limit could be obtained via

$$E_{HF}(\infty) = \lim_{x\to\infty} A + Be^{-CX} = A. \tag{1.4}$$

The extrapolation for the correlation energies could be performed using[9]

$$E_{corr}(X) = D + EX^{-3}. \tag{1.5}$$

Where D and E are fitting parameters. Correspondingly, the correlation energy in the complete basis set limit could be provided by

$$E_{corr}(\infty) = \lim_{x\to\infty} D + EX^{-3} = D. \tag{1.6}$$

It is noteworthy that the basis sets cc-pVTZ and cc-pVQZ or higher basis sets are required to perform the extrapolation. However, it is too expensive to perform the calculation at a large basis set in combined with a higher level theory *e.g.*, CCSDT or higher levels of theory. Fortunately, it has been found that the energy differences between the higher levels of theory are less dependent on basis sets, which makes it feasible to employ the additivity approximation. Within the additivity approximation, the energy difference between two correlation treatments is obtained using a small basis and appended to the final extrapolated energy from a lower level of theory in the complete basis set limit. The relative energies, which is more usually more important in the reactions relative to absolute energies, are more accurately determined given a large degree of error cancellation. All of the energies computed with lower levels of theory and small basis sets are deposited in focal point table as well, which could serve as an indicator for the energy convergence with respect to level of theory. The error bars can also be evaluated from the FPA table.

To achieve accuracy to 0.2 kcal mol^{-1}, additional corrections must be appended to the energies obtained using FPA. As mentioned above, the current computations are on the basis of the Born-Oppenheimer approximation neglecting relativity. The Born-Oppenheimer approximation is assumed that the electronic motion is much faster than that of the nuclei,

which could be rationalized by the large ratio of nuclear mass to the electronic mass. In this light, the system involving light atoms, such as hydrogen atoms may violate this approximation. In general, diagonal Born-Oppenheimer correction (DBOC)[10–14] is employed to improve the accuracy within 0.1 kcal mol^{-1}.

1.5 Anharmonicity and Vibration-Rotation Interaction

1.5.1 Anharmonicity

In general, second order vibrational perturbation theory (VPT2)[15–19] and vibrational variational methods are the two main theoretical approaches utilized to obtain the fundamental frequencies. The vibrational perturbation theory will alway invoke massive amount of basis sets, which prevents the application of this theory on systems with more than six atoms. As an alternative, VPT2 is suitable to determine fundamental frequencies for large systems. However, it should keep in mind that VPT2 theory may fail in weakly-bound systems, since the harmonic oscillator hamiltonian is chosen to be the zeroth-order hamiltonian for the perturbation theory.

The harmonic frequencies are obtained assuming that the vibrational potential energy is harmonic around the equilibrium (stationary) point. This approximation always leads to that the resultant harmonic frequencies frequencies are consistently higher than the real fundamental frequencies. In order to include the deviation of potential surface from the harmonic curvature, the vibrational potential energy ($\overline{V}$) may be expanded in terms of displacement symmetry internal coordinates (Δ S_i) in the vicinity of the equilibrium point (E_e) as

$$\overline{V} = E_e + \frac{1}{2}\sum_{ij} F_{ij}\Delta S_i \Delta S_j + \frac{1}{6}\sum_{ijk} F_{ijk}\Delta S_i \Delta S_j \Delta S_k + \frac{1}{24}\sum_{ijkl} F_{ijkl}\Delta S_i \Delta S_j \Delta S_k \Delta S_l + \cdots \quad (1.7)$$

where F_{ij}, F_{ijk}, and F_{ijkl} denote quadratic, cubic, and quartic force constants. S represents the symmetric coordinates.

When the terms higher than quartic force constants are neglected from the vibrational potential energy expansion, the vibrational energy levels of an asymmetric top molecule are given by

$$G(v) = \sum_r \omega_r (v_r + \frac{1}{2}) + \sum_{r \geq s} \chi_{rs} (v_r + \frac{1}{2})(v_s + \frac{1}{2}). \tag{1.8}$$

The rth anharmonic (fundamental) vibrational frequency (ν_r) is determined using the following equation:[15,19–21]

$$\nu_r = \omega_r + 2\chi_{rr} + \frac{1}{2} \sum_{s \neq r} \chi_{rs} \tag{1.9}$$

where ω_r is an rth harmonic vibrational frequency and χ_{rs} are anharmonic vibrational constants. The formulae obtained from perturbation theory for the χ_{rs} values are[15,19,21]

$$\chi_{rr} = \frac{1}{16}\phi_{rrrr} - \frac{1}{16} \sum_s \frac{\phi_{rrs}^2 (8\omega_r^2 - 3\omega_s^2)}{\omega_s (4\omega_r^2 - \omega_s^2)} \tag{1.10}$$

for the diagonal elements and

$$\begin{aligned} \chi_{rs} &= \frac{1}{4}\phi_{rrss} - \frac{1}{4} \sum_t \frac{\phi_{rrt}\phi_{sst}}{\omega_t} - \frac{1}{2} \sum_t \frac{\phi_{rst}^2 \omega_t (\omega_t^2 - \omega_r^2 - \omega_s^2)}{\Big[(\omega_r + \omega_s)^2 - \omega_t^2\Big]\Big[(\omega_r - \omega_s)^2 - \omega_t^2\Big]} \\ &+ \Big[A_e (\zeta_{r,s}^{(a)})^2 + B_e (\zeta_{r,s}^{(b)})^2 + C_e (\zeta_{r,s}^{(c)})^2\Big]\Big(\frac{\omega_r}{\omega_s} + \frac{\omega_s}{\omega_r}\Big) \end{aligned} \tag{1.11}$$

for the off-diagonal elements. Here, ϕ_{rrss} represents the quartic force constant in terms of dimensionless normal coordinates, and $\zeta_{(r,s)}^{(b)}$ denotes the Coriolis interaction constants. When either of the following relationships is satisfied accidentally for an asymmetric top molecule, $2\omega_r \approx \omega_s$ and $\phi_{rrs} \neq 0$ (overtone-type Fermi resonance); $\omega_r + \omega_s \approx \omega_t$ and $\phi_{rst} \neq 0$, (combination-type Fermi resonance), the quantities χ_{rr} and χ_{rs} may become indefinitely large and the perturbation theory may fail. In the case of overtone-type Fermi resonance, the terms can be decomposed into three factors as follows:

$$\frac{\phi_{rrs}^2 (8\omega_r^2 - 3\omega_s^2)}{16\omega_s (4\omega_r^2 - \omega_s^2)} = \frac{\phi_{rrs}^2}{32}\Big[\frac{1}{2\omega_r + \omega_s} - \frac{1}{2\omega_r - \omega_s} + \frac{4}{\omega_s}\Big] \tag{1.12}$$

and the second factor involving the resonances may be deleted following Nielsen's treatments.[15]

The reduced normal coordinate systems are mass-dependent. The nonlinear transformation from the symmetry internal coordinates to the mass independent Cartesian coordinates for quadratic, cubic, and quartic force constants permits the convenient evaluation of the force constants for each individual isotopic variant; therefore, the full set of quartic force constants, ϕ_{ijkl}, are computed in our analyses in lieu of the most-common computation of only semi-diagonal quartic force constants, ϕ_{iijj}.

1.5.2 Vibration-Rotation Interaction

The vibration-rotation interaction corrections to the equilibrium rotational constants, B_{e}, may be expressed by the following equation[19]

$$B_v = B_{\mathrm{e}} - \sum_r \alpha_r^B (v + 1/2) + \text{higher terms} \tag{1.13}$$

where B_v (v being a vibrational quantum number) is the rotational constant and the sums run over all normal modes. Similar expressions hold for the vibrational dependence of the rotational constants A_v and C_v.

The vibration-rotation coupling constants α_r^B for an asymmetric top from perturbation theory are given by[19]

$$\begin{aligned} -\alpha_r^B &= \frac{2B_e^2}{\omega_r}\Bigg[\sum_\xi \frac{3\left(a_r^{(b\xi)}\right)^2}{4I_\xi} + \sum_s \left(\zeta_{r,s}^{(b)}\right)^2 \frac{(3\omega_r^2+\omega_s^2)}{\omega_r^2-\omega_s^2} \\ &+ \pi\left(\frac{c}{h}\right)^{\frac{1}{2}} \sum_s \phi_{rrs} a_s^{(bb)} \left(\frac{\omega_r}{\omega_s^{3/2}}\right)\Bigg] \end{aligned} \tag{1.14}$$

where ω_r is the rth harmonic vibrational frequency, I_ξ is the ξth principal moment of inertia, $\zeta_{r,s}^{(b)}$ is the Coriolis coupling constant about the b axis, and ϕ_{rrs} is the cubic force constants in terms of dimensionless normal coordinates. In this equation the $a_r^{\alpha\beta}$ constants are the derivatives of the matrix elements of the inertia tensor with respect to the rth normal coordinate Q_r

$$a_r^{(\alpha\beta)} = \left(\frac{\partial I_{\alpha\beta}}{\partial Q_r}\right)_e \tag{1.15}$$

The Coriolis resonances will be manifested in the second term in the square brackets of the equation for the vibration-rotation coupling constants when two vibrational frequencies are sufficiently close, *i.e.*, $\omega_r \approx \omega_s$. In this light, it was pointed out by East, Johnson, and Allen that the B_0 constant (v=0) may be determined without terms involving the Coriolis resonances by taking the sums of the α_r^B constants over all normal modes in lieu of their individual values.[22]

1.6 Overview of Chapters

We proceed by systematical investigation of equilibrium structure P_2H_2 and the associated isomerization transition states. In particular, the transition state between the *trans* and *cis* isomerization reaction exhibits multireference character and is evaluated using Mukherjee multi-reference coupled cluster (Mk-MRCCSD) (2e/2MO) method. In chapter 3, the triplet potential energy surface (PES) of P_2H_2 is presented, based on systematically extrapolated coupled cluster energies, and accounting for core-valence correlation, zero-point vibrational energy, and diagonal Born-Oppenheimer effects. The energy crossing of the singlet and triplet adiabatic PES is studied using Mk-MRCCSD method with the cc-pVQZ basis set. In chapter 4, the vibration-rotation coupling constants, equilibrium and zero-point vibration corrected rotational constants, centrifugal distortion constants, harmonic and fundamental vibrational frequencies for six isotopologues of disilacyclopropenylidene (Si_2CH_2-**1S**) are predicted using vibrational second-order perturbation theory (VPT2). A brief summary is provided in Chapter 5.

1.7 References

[1] Crawford, T. D.; Schaefer, H. F. *Rev. comput. Chem.* **2000**, *14*, 33–136

[2] Raghavachari, K.; Trucks, G. W.; Pople, J. A.; Head-Gordon, M. *Chem. Phys. Lett.* **1989**, *157*, 479–483

[3] Kato, T. *Commun. Pure Appl. Math.* **1957**, *10*, 151–177

[4] East, A. L. L.; Allen, W. D. *J. Chem. Phys.* **1993**, *99*, 4638–4650

[5] Császár, A. G.; Allen, W. D.; Schaefer, H. F. *J. Chem. Phys.* **1998**, *108*, 9751–9764

[6] Dunning, T. H. **1989**, *90*, 1007–1023

[7] Woon, D. E.; Dunning, T. H. **1993**, *98*, 1358–1371

[8] Feller, D. *J. Chem. Phys.* **1993**, *98*, 7059–7071

[9] Helgaker, T.; Klopper, W.; Koch, H.; Noga, J. *J. Chem. Phys.* **1997**, *106*, 9639–9646

[10] Sellers, H.; Pualy, P. *Chem. Phys. Lett.* **1984**, *103*, 463–465

[11] Handy, N. C.; Yamaguchi, Y.; Schaefer, H. F. *J. Chem. Phys.* **1986**, *84*, 4481–4484

[12] Ioannou, A. G.; Amos, R. D.; Handy, N. C. *Chem. Phys. Lett.* **1996**, *251*, 52–58

[13] Handy, N. C.; Lee, A. M. *Chem. Phys. Lett.* **1996**, *252*, 425–430

[14] Kutzelnigg, W. *Mol. Phys.* **1997**, *90*, 909–916

[15] Nielsen, H. H. *Rev. Mod. Phys.* **1951**, *23*, 90

[16] Clabo, D. A.; Allen, W. D.; Remington, R. B.; Yamaguchi, Y.; Schaefer, H. F. *Chem. Phys.* **1988**, *123*, 187

[17] Allen, W. D.; Yamaguchi, Y.; Császár, A. G.; Clabo, D. A.; Remington, R. B.; Schaefer, H. F. *Chem. Phys.* **1990**, *145*, 427

[18] Aarset, K.; Császár, A. G.; Sibert, E. L.; Allen, W. D.; Schaefer, H. F.; Klopper, W.; Noga, J. *J. Chem. Phys.* **2000**, *112*, 4053

[19] Mills, I. M. In *Molecular Spectroscopy: Modern Research*; Rao, K. N., Mathews, C. W., Eds.; Academic, New York, 1972; pp 115–140

[20] Nielsen, H. H. *Phys. Rev.* **1941**, *60*, 794

[21] Nielsen, H. H. *Phys. Rev.* **1945**, *68*, 181

[22] East, A. L. L.; Johnson, C. S.; Allen, W. D. *J. Chem. Phys.* **1993**, *98*, 1299

Chapter 2

Diphosphene and Diphosphinylidene[1]

[1]T. Lu, A. C. Simmonett, F. A. Evangelista, Y. Yamaguchi, and H. F. Schaefer, J. Phys. Chem. A **113** 13227 (2009). Reprinted here with permission of the American Chemical Society.

2.1 Introduction and Literature Review

2.1.1 abstract

The equilibrium structures of P_2H_2 isomers and the associated isomerization transition states have been investigated systematically starting from self-consistent-field theory and proceeding to coupled cluster methods using a wide range of basis sets. For each structure the geometry, energy, dipole moment, harmonic vibrational frequencies, and infrared intensities have been predicted. The global minimum has been confirmed to be planar *trans*-HPPH diphosphene, lying 3.2 kcal mol^{-1} below *cis*-HPPH with the aug-cc-pVQZ CCSD(T) method upon inclusion of zero point vibrational energy corrections. Diphosphinylidene, which has the connectivity PPH_2 and C_{2v} symmetry lies 25.2 kcal mol^{-1} above the global minimum. The *trans-cis* isomerization reaction occurs via internal rotation with a barrier of 35.2 kcal mol^{-1} using the cc-pVQZ Mk-MRCCSD (2e/2MO) method. This transition state exhibits multireference character and consequently properties were evaluated using CASSCF, MRCI, CASPT2, and Mk-MRCCSD methods with various basis sets. At the aug-cc-pVQZ CCSD(T) level, the transition state for the isomerization reaction between *trans*-HPPH and diphosphinylidene (planar PPH_2) was predicted to be nonplanar with a torsional angle of 101.1°. The corresponding barrier is estimated to be 48.2 kcal mol^{-1}.

2.1.2 Introduction

Heavier main group elements with low coordination numbers have attracted much attention over the last two decades.[1–7] The interest in such compounds stems from their reactivity towards a diverse range of chemical reagents and their unique electrochemical and photochemical properties.[1,8–12] More recent research suggests that secondary diphosphines and diphosphenes (HPPH) are potential candidates for use in chemical hydrogen storage systems.[13]

In the absence of steric factors, these small phosphorus compounds with low coordination numbers often tend to form oligomers due to thermodynamic preferences.[14] The preparation of the first stable diphophene was reported in 1981 by Yoshifuji and co-workers,[15] who used sterically bulky substituents (RP=PR, R=2,4,6-tri-tert-butylphenyl) to achieve kinetic stability. Since then, the synthesis, structure, and reactivity of various doubly-bonded phosphorous compounds have been examined, typically employing bulky ligands to ensure stability.[6,16–22] More recently, a carbene stabilized diphosphorus compound was synthesized in which the phosphorus behaves as an electron acceptor.[22] The geometries of several diphosphenes have been determined using X-ray crystallographic analyses.[23] The PP bond length varies in the range of 2.001 to 2.034 Å, which shows that the PP bond has double-bond character.[24] The large difference between the bond angles of TbtP=PTbt (Tbt=2,4,6-tris[bis(trimethylsilyl)methyl]phenyl) (106.4° and 104.5°) and the ideal sp^2 hybridized bond angle (120°) may be caused by the lower tendency of second row or higher atoms to form hybridized orbitals.[12,20] The activation free energy for the *trans-cis* conversion of Mes*PPMes* (2,4,6-tri-tert-butylphenyl or supermesityl) was deduced to be 20.3 kcal mol^{-1} at 0°C through laser irradiation.[25] Moreover, the vibrational frequency of PP stretching of Mes*PPMes* was determined to be 610 cm^{-1} from Raman spectra.[26]

In order to further understand these small phosphorus compounds with low coordination numbers, theoretical investigations of their bonding and reactivity have been performed using simplified model systems as prototypes.[27–36] Theoretical calculations have shown that the singlet state of diphosphinylidene is stabilized via implantation of alkyl and/or amino groups at the β-position due to π donating and steric effects. Moreover, bulky substituents destabilize the triplet state.[37] Furthermore, it has been demonstrated that the triplet state of PPF_2 lies below the singlet state, in contrast to PPHCl and PPHF whose ground states are singlets.[38] Diphosphene has a larger singlet-triplet separation of about 1.2 eV,[28] which is relatively small compared to the first-row isolobal HNNH molecule (2 eV)[39] or the triply-bonded HCCH molecule (3.5 eV).[40]

In the present research we investigate the prototypical doubly-bonded phosphorous systems by characterizing the closed-shell structures of diphosphene (HPPH) and diphosphinylidene (PPH_2) using high-accuracy *ab initio* methods in concert with large gaussian basis sets; these structures are depicted in Figure 2.1. Special emphasis is placed on the analysis of the isomerization transition state between *trans*- and *cis*-HPPH diphosphene structures. The latter system requires multireference theoretical treatments. Finally, the transition state for the isomerization reaction between *trans*-HPPH and diphosphinylidene, which involves a hydrogen migration, is investigated. For brevity we shall hereafter refer to diphoshinylidene simply as planar PPH_2.

2.2 Electronic Structure Considerations

In previous theoretical studies, the electronic ground state of the diphosphene molecule was found[28] to have a C_{2h}-symmetric *trans*-HPPH structure with an electron configuration of

$$[(\text{core})(5a_g)^2(5b_u)^2(6b_u)^2(6a_g)^2(7a_g)^2(2a_u)^2],$$

where (*core*) denotes the ten lowest-lying core orbitals (P:1s, 2s, 2p-like). The $2a_u$ molecular orbital is the highest occupied molecular orbital (HOMO), while the $2b_g$ molecular orbital represents the lowest unoccupied molecular orbital (LUMO), as shown in Figure 2.7. A C_{2v}-symmetric *cis*-isomer, with an electron configuration of

$$[(\text{core})(5a_1)^2(5b_2)^2(6a_1)^2(7a_1)^2(6b_2)^2(2b_1)^2],$$

is also located on the lowest closed-shell singlet surface. The $2b_1$ molecular orbital (HOMO), which is depicted in Figure 2.8a, represents the bonding π orbital; the $2a_2$ orbital (LUMO) in Figure 2.8b represents the antibonding π orbital.

On the same closed shell singlet surface there exists another isomer of vinylidene type, the C_{2v}-symmetric diphosphinylidene (PPH_2) molecule. The latter's frontier orbitals are illustrated in Figure 2.9. The electron configuration of PPH_2 may be described as

$$[(\text{core})(7a_1)^2(8a_1)^2(3b_2)^2(9a_1)^2(3b_1)^2(4b_2)^2].$$

The C_2 symmetric transition state for the isomerization reaction of *trans*- to *cis*-HPPH via rotation about the H-P-P-H torsional angle is minimally represented by a linear combination of the electron configurations

$$[(\text{core})(6a)^2(6b)^2(7a)^2(7b)^2(8a)^2(9a)^2]$$

and

$$[(\text{core})(6a)^2(6b)^2(7a)^2(7b)^2(8a)^2(8b)^2]$$

and therefore requires multi-determinant methods to be described correctly. Moreover, active space orbitals are shown in Figure 2.10. Finally the transition state for an isomerization reaction between *trans*-HPPH and planar PPH_2 possesses the following electronic configuration

$$[(\text{core})(11a)^2(12a)^2(13a)^2(14a)^2(15a)^2(16a)^2];$$

the HOMO and LUMO are demonstrated in Figure 2.11.

2.3 Theoretical Procedures

In this research, the correlation-consistent family of basis sets cc-pVXZ (X=D, T, and Q) and aug-cc-pVXZ (X=D, T, and Q) developed by Dunning and coworkers was used.[41,42] The zeroth-order description was obtained using one-configuration restricted close-shell Hartree-Fock (RHF) wave functions. The effects of electron correlation were systematically explored using configuration interaction with single and double excitations (CISD),[43–45] coupled cluster with single and double excitations (CCSD),[46,47] CCSD with perturbative triple excitations [CCSD(T)],[48–50] complete active space self-consistent-field (CASSCF),[51,52] internally contracted multireference CI (MRCI)[53,54](based on the CASSCF reference), CAS second-order perturbation theory(CASPT2),[55–57] and the state-specific multireference coupled cluster approach suggested by Mukherjee and co-workers (Mk-MRCCSD).[58–60] For Mk-MRCCSD calculations two-configuration SCF (TCSCF) orbitals were employed. The active space orbitals were canonicalized by transforming to the natural orbital basis. In the

correlated procedures the ten lowest-lying core orbitals (P:1s, 2s, 2p- like) were frozen, in keeping with the design of the basis sets used. At the SCF, CCSD, and CCSD(T) levels of theory, geometries, harmonic vibrational frequencies, and infrared (IR) intensities were obtained using analytic derivative methods, while at the CISD, CASSCF, MRCI, CASPT2, and Mk-MRCCSD levels of theory numerical differentiation was used. For *trans*-HPPH, *cis*-HPPH, and the isomerization transition state between them, the number of configuration state functions (CSFs) are 3620, 3620, and 13860, respectively, at the (12e/10MO) CASSCF level of theory. The computations were carried out using the MOLPRO,[61] MAB-ACESII,[62,63] and PSI3[64] *ab initio* quantum chemistry packages. The Mk-MRCCSD calculations were performed with the PSI3 and MCSCF codes.[65,66]

2.4 Results and Discussion

2.4.1 Energy Minima

Selected optimized geometrical parameters for the minimum energy structures are reported in Figures 2.2-2.4. Harmonic vibrational frequencies and physical properties for *trans*-HPPH, *cis*-HPPH, and PPH_2 are given in Tables 2.1, 2.2, and 2.3, respectively, while total energies and relative energies for these structures are presented in Table 2.4.

In order to correctly capture the multireference character of the isomerization transition state between the *trans* and *cis* structures, the (12e/10MO) CASSCF and MRCI wavefunctions of these closed-shell structures were constructed using a variety of basis sets. This active space spans the full valence space of the orbitals and electrons in the constituent atoms. For the *trans* isomer, the aug-cc-pVTZ CASSCF wavefunction is written, in terms of natural

orbitals, as

$$\begin{aligned}
\Psi &= 0.945\Phi_1[(\text{core})(5a_g)^2(5b_u)^2(6b_u)^2(6a_g)^2(7a_g)^2(2a_u)^2] \\
&- 0.207\Phi_2[(\text{core})(5a_g)^2(5b_u)^2(6b_u)^2(6a_g)^2(7a_g)^2(2b_g)^2] \\
&- 0.055\Phi_3[(\text{core})(5a_g)^2(5b_u)^2(6b_u)^2(6a_g)^2(2a_u)^2(7b_u)^2] \\
&- 0.053\Phi_4[(\text{core})(5a_g)^2(5b_u)^2(6b_u)^2(6a_g)^2(7a_g\alpha)(2a_u\beta)(2b_g\alpha)(7b_u\beta)] \\
&- 0.051\Phi_5[(\text{core})(5a_g)^2(5b_u)^2(6b_u)^2(6a_g)^2(7a_g\beta)(2a_u\alpha)(2b_g\beta)(7b_u\alpha)] \\
&+ \cdots\cdots\cdots\cdots\cdots .
\end{aligned}$$

The analogous aug-cc-pVTZ MRCI wavefunction is described, in terms of natural orbitals, by

$$\begin{aligned}
\Psi &= 0.901\Phi_1[(\text{core})(5a_g)^2(5b_u)^2(6b_u)^2(6a_g)^2(7a_g)^2(2a_u)^2] \\
&- 0.189\Phi_2[(\text{core})(5a_g)^2(5b_u)^2(6b_u)^2(6a_g)^2(7a_g)^2(2b_g)^2] \\
&+ 0.063\Phi_3[(\text{core})(5a_g)^2(5b_u)^2(6b_u)^2(6a_g)^2(7a_g\alpha)(2a_u\beta)(2b_g\alpha)(7b_u\alpha)] \\
&+ 0.050\Phi_4[(\text{core})(5a_g)^2(5b_u)^2(6b_u\beta)(6a_g\alpha)(7a_g)^2(2a_u)^2(8b_u\beta)(8a_g\alpha)] \\
&+ 0.050\Phi_5[(\text{core})(5a_g)^2(5b_u)^2(6b_u)^2(6a_g)^2(7a_g\alpha)(2a_u\alpha)(2b_g\beta)(7b_u\beta)] \\
&+ \cdots\cdots\cdots\cdots\cdots .
\end{aligned}$$

Only the configuration state functions (CSFs) whose absolute CI coefficients are larger than 0.05 are shown. These confirm the predominantly single-reference nature of the *trans* isomer. The most dominant excited configuration present, denoted Φ_2, corresponds to a HOMO (in Figure 2.7a) to LUMO (in Figure 2.7b) double excitation, $[(2a_u)^2 \rightarrow (2b_g)^2]$. The aug-cc-

pVTZ MRCI wavefunction for *cis*-HPPH is represented, in terms of natural orbitals, by

$$
\begin{aligned}
\Psi &= 0.900\Phi_1[(\text{core})(5a_1)^2(5b_2)^2(6a_1)^2(7a_1)^2(6b_2)^2(2b_1)^2] \\
&- 0.193\Phi_2[(\text{core})(5a_1)^2(5b_2)^2(6a_1)^2(7a_1)^2(6b_2)^2(2a_2)^2] \\
&- 0.072\Phi_3[(\text{core})(5a_1)^2(5b_2)^2(6a_1)^2(7a_1\alpha)(6b_2)^2(2b_1\beta)(2a_2\beta)(7b_2\alpha)] \\
&- 0.069\Phi_4[(\text{core})(5a_1)^2(5b_2)^2(6a_1)^2(7a_1\alpha)(6b_2)^2(2b_1\alpha)(2a_2\beta)(7b_2\beta)] \\
&+ 0.057\Phi_5[(\text{core})(5a_1)^2(5b_2)^2(6a_1\alpha)(7a_1)^2(6b_2\beta)(2b_1)^2(8a_1\alpha)(8b_2\beta)] \\
&- 0.056\Phi_6[(\text{core})(5a_1)^2(5b_2)^2(6a_1)^2(7a_1)^2(2b_1)^2(8a_1)^2] \\
&- 0.052\Phi_7[(\text{core})(5a_1)^2(5b_2)^2(6a_1)^2(6b_2)^2(2b_1)^2(7b_2)^2] \\
&+ \cdots\cdots\cdots\cdots\cdots .
\end{aligned}
$$

Again, the second CSF corresponds to a HOMO (in Figure 2.8a) to LUMO (in Figure 2.8b) double excitation, $[(2b_1)^2 \rightarrow (2a_2)^2]$, while the dominant configuration has a CI coefficient of 0.9, indicating only marginal multi-reference character.

Increasing the presence of electron correlation elongates both the P-P and P-H bond lengths in all three of these isomers (in Figures 2.2–2.4), which is consistent with the extra anti-bonding character introduced into the correlated wavefunction. The PPH_2 structure presents the shortest P-P bond length, while the *cis*-HPPH has the longest. The similar trend is observed amongst the H-P bond lengths, with PPH_2 possessing the shortest out of the three minima investigated here. The H-P bond lengths in the *cis*- and *trans*-HPPH structures are nearly equal, but slightly shorter in the *cis* isomer. At the CISD, CCSD, and CCSD(T) levels of theory the HPP bond angles of *trans* and *cis* structures decrease compared with the SCF predictions. However, with the application of correlated methods, the PPH bond angle in the PPH_2 structure increases gradually. The (12e/10MO) CASSCF and MRCI methods seem to overestimate the bond lengths and bond angles of *trans* and *cis* structures compared to the more reliable CCSD and CCSD(T) methods. In contrast, at the (2e/2MO) Mk-MRCCSD level of theory, the bond angles and bond lengths are consistent with the

CCSD prediction. This further proves that these isomers only possess little multi-reference character.

With the aug-cc-pVQZ CCSD(T) method, the magnitudes of the dipole moments for *trans*-HPPH, *cis*-HPPH, and PPH_2 are 0 (by symmetry), 1.1, and 2.3 D, respectively (in Tables 2.1-2.3). The planar PPH_2 isomer exhibits a larger dipole moment than the *cis* isomer, whose C_2 axis is perpendicular to the PP bond. This is expected, given that the PPH_2 isomer is more extended along the C_2 axis, which is defined by the PP bond. The orientation of the C_2 axes in these systems gives rise to dipole moments that are parallel to the PP bond in planar PPH_2, but perpendicular in *cis*-HPPH.

The harmonic vibrational frequencies of these structures (in Tables 2.1-2.3) decrease by about 100 cm^{-1} proceeding from SCF to CCSD(T); consequently, the zero point vibrational energy (ZPVE) decreases with a more complete description of correlation effects. This behavior is symptomatic of reduced force constants, which result from the extra antibonding character in the correlated wavefunctions. The harmonic vibrational frequencies in the *trans*- and *cis*-HPPH structures from the treatment of (12e/10MO) CASSCF and MRCI are in reasonable agreement with the other levels of theory used.

The asymmetric PH stretching mode (ω_5) of *trans*-HPPH (in Table 2.1) presents the strongest infrared (IR) intensity, which is about an order of magnitude larger than the asymmetric bending (ω_6). However, the intensities for the other vibrational frequencies are zero by symmetry; the intensity for the torsion mode (ω_4) is almost equal to zero although it is allowed according to IR selection rules. In the *cis*-HPPH isomer (in Table 2.2), the most intense vibrational mode originates from the symmetric PH stretching mode (ω_1), while the PP stretching mode (ω_3) is the weakest IR active mode. As observed for the vibrational frequencies, the (12e/10MO) CASSCF and MRCI methods provide IR intensities that are in reasonable accord with coupled cluster theory. The IR intensities computed for the vibrational modes of PPH_2 (in Table 2.3) are comparable to those for *trans*-HPPH and *cis*-HPPH, exhibiting only a slight dependence on the level of theory employed.

As shown in Table 2.4, the classical energetic difference between *trans*- and *cis*-HPPH isomers is predicted to be 3.5 (SCF), 3.5 (CISD), 3.4 (CCSD), and 3.4 kcal mol^{-1} [CCSD(T)] with the aug-cc-pVQZ basis set. Multireference treatments predict slightly smaller differences of 3.1 [(12e/10MO)(CASSCF)], 3.3 kcal mol^{-1} (MRCI) with the aug-cc-pVTZ basis set, and 3.3 kcal mol^{-1} [(2e/2MO)(Mk-MRCCSD)] with cc-pVQZ basis set. Employing our most reliable method, aug-cc-pVQZ CCSD(T), the final ZPVE-corrected *trans-cis* energy gap is predicted to be 3.2 kcal mol^{-1}.

The energy difference between *trans*-HPPH and the planar PPH_2 structure is estimated to fall within the range of 24.2-26.2 kcal mol^{-1}. With the more complete treatment of electron correlation effects, the difference increases gradually. At our most reliable level of theory, aug-cc-pVQZ CCSD(T), the ZPVE-corrected energy gap is predicted to be 25.2 kcal mol^{-1}.

2.4.2 Transition States

In Figure 2.5 and Figure 2.6 the representative optimized structures of the two isomerization transition states are depicted. The harmonic vibrational frequencies and dipole moments are shown in Table 2.5 and Table 2.6. In Table 2.7 the total energies and ZPVE-corrected energies for the transition states are reported.

The 1,2 hydrogen shift in similar model systems (SCH_2, NPH_2 and PPH_2) demonstrates two different transition states, an in-plane transition state with C_s symmetry or out-of-plane transition state with C_1 symmetry.[67] However, as for PPH_2 the in-plane stationary point possesses more than one imaginary frequencies (a second-order saddle point) and higher energy barrier. Nguyen and Ha suggested that the migrating hydrogen behaves as a proton in the out-of-plane transition state between *trans*-HPPH and planar PPH_2.[67] The $P_2P_1H_3$ bond angle at the transition state is about 104°, as shown in Figure 2.5, which is larger than that of the *trans* structure (94°), but smaller than for the planar PPH_2 structure (128°). The $P_1P_2H_4$ bond angle is about 47°, which is roughly half of that of the *trans* structure. This indicates that the H_4 proton moves above the PP bond, forming a 3-center

bond. Moreover, the $H_3P_1P_2H_4$ dihedral angle, which is about 101°, demonstrates that the 3-center bonding involves the P_1H_3 bond as well. It should be noted that the dihedral angle is sensitive to degree of correlation and is about 10° smaller at the CCSD(T) level of theory than at the SCF level. Using the P_2H_4 bond length as a measure of the reaction progress, an later transition state, *i.e.* one that more closely resembles PPH_2, is predicted with increasing correlation. These trends are mirrored by the relative energies of the *trans*-HPPH and planar PPH_2 species in Table 2.4, with a later transition state correlating with a more endothermic reaction, in keeping with the Hammond postulate.[68]

The harmonic vibrational frequencies of this isomerization transition state are shown in Table 2.5. The magnitude of the imaginary vibrational frequency decreases by about 370 cm^{-1} going from SCF to CCSD(T), showing a large dependence upon the theoretical model used. The imaginary vibrational frequency decreases with increasing basis set size as well. Despite the high sensitivity of the imaginary frequency, the real vibrational frequencies are less sensitive to the level of theory. The dipole moment for this transition state is determined to be 1.25 D with CCSD(T), as shown in Table 2.5. At the aug-cc-pVQZ CCSD(T) level of theory, the *trans*-HPPH→ PPH_2 isomerization barrier is predicted to be 50.3 kcal mol^{-1}, which drops to 48.2 kcal mol^{-1} upon inclusion of ZPVE corrections (in Table 2.7). This is 3.2 kcal mol^{-1} lower than the barrier height of 51.4 kcal mol^{-1} determined by Nguyen using MP4/6-311++G (df,p).[67] At the aug-cc-pVQZ CCSD(T) level of theory, the barrier for the reverse process, PPH_2→ *trans*-HPPH is determined to be 23.0 kcal mol^{-1}.

Conversion between *trans*- and *cis*-HPPH may occur either by internal rotation about the P-P bond or through a structure with a linear P-P-H bond ("inversion"). It has previously been shown[28] that the rotational reaction path exhibits a much lower reaction barrier. During the rotational reaction path, the molecule possesses C_2 symmetry. However, the *trans* and *cis* structures have different orbital occupation in the C_2 subgroup [*trans*: $(9a^2 7b^2)$, *cis*: $(8a^2 8b^2)$]. Consequently, this process is forbidden according to Woodward-Hoffmann rules, and multireference methods are required to properly describe the transition state. Here, CASSCF and

MRCI, each with two different defined active spaces (2e/2MO and 12e/10MO) are applied to characterize the transition state. In addition, (2e/2MO) CASPT2 and (2e/2MO) Mk-MRCCSD are also employed to characterize the transition state. The aug-cc-pVTZ CASSCF (2e/2MO) wavefunction for the transition state is represented, in terms of natural orbitals, by

$$\begin{aligned}\Psi &= 0.708\Phi_1[(\text{core})(6a)^2(6b)^2(7a)^2(7b)^2(8a)^2(9a)^2] \\ &- 0.705\Phi_2[(\text{core})(6a)^2(6b)^2(7a)^2(7b)^2(8a)^2(8b)^2] \\ &+ \cdots\cdots\cdots\cdots\cdots,\end{aligned}$$

and at the corresponding MRCI level it is

$$\begin{aligned}\Psi &= 0.663\Phi_1[(\text{core})(6a)^2(6b)^2(7a)^2(7b)^2(8a)^2(9a)^2] \\ &- 0.659\Phi_2[(\text{core})(6a)^2(6b)^2(7a)^2(7b)^2(8a)^2(8b)^2] \\ &+ \cdots\cdots\cdots\cdots\cdots,\end{aligned}$$

and the analogous CASPT2 method gives

$$\begin{aligned}\Psi &= 0.709\Phi_1[(\text{core})(6a)^2(6b)^2(7a)^2(7b)^2(8a)^2(9a)^2] \\ &- 0.704\Phi_2[(\text{core})(6a)^2(6b)^2(7a)^2(7b)^2(8a)^2(8b)^2] \\ &+ \cdots\cdots\cdots\cdots\cdots.\end{aligned}$$

The above wavefunctions are composed of two CSFs with almost equal CI coefficients. We would expect these two configurations to provide a faithful description of the system; this is corroborated by the multireference computations employing a larger active space (full valence, 12e/10MO). The aug-cc-pVTZ MRCI wavefunction of the transition state is

described, in terms of natural orbitals, by

$$\begin{aligned}
\Psi &= 0.652\Phi_1[(\text{core})(6a)^2(6b)^2(7b)^2(7a)^2(8a)^2(9a)^2] \\
&- 0.648\Phi_2[(\text{core})(6a)^2(6b)^2(7b)^2(7a)^2(8a)^2(8b)^2] \\
&+ 0.058\Phi_3[(\text{core})(6a)^2(6b)^2(7b)^2(7a)^2(8a\alpha)(9a\beta)(8b\alpha)(9b\beta)] \\
&- 0.057\Phi_4[(\text{core})(6a)^2(6b)^2(7b)^2(7a)^2(9a)^2(9b)^2] \\
&+ 0.057\Phi_5[(\text{core})(6a)^2(6b)^2(7b)^2(7a)^2(8b)^2(9b)^2] \\
&+ \cdots\cdots\cdots\cdots\cdots .
\end{aligned}$$

The two CSFs [$(9a)^2(7b)^2$ and $(8a)^2(8b)^2$] whose coefficients are greater than 0.6 are the same as those in the smaller active space (2e/2MO) computations. This indicates that a (2e/2MO) active space may be sufficient to describe the transition state, particularly if dynamical correlation is added through MRCI, CASPT2, or Mk-MRCCSD.

The PP bond length (in Figure 2.6) at the *trans-cis* transition state significantly increases because the alignment of p orbitals is no longer forming a π bond. The bond order drops to one, *i.e.* only one σ bond is left. At the transition state the dihedral angle is almost 90°, which indicates that the transition state lies about half way between reactant and product; this is expected given the small energy difference between *trans*-HPPH and *cis*-HPPH (in Table 2.4). All of the methods predict a similar structure; however, most of the real frequencies, shown in Table 2.6, decrease by roughly 100 cm^{-1} from (2e/2MO) CASSCF to (2e/2MO) Mk-MRCCSD due to the additional dynamical correlation. In contrast, the imaginary frequency increases with additional dynamical correlation. Furthermore, the dipole moment is predicted to be 0.8 D, which is intermediate between the *trans*- and *cis*-HPPH structures. The *trans-cis* isomerization barrier is estimated to be 35.2 kcal mol^{-1}(in Table 2.7) using our most reliable level of theory, (2e/2MO) Mk-MRCCSD with the cc-pVQZ basis set. This is significantly lower than the barrier from *trans*-HPPH to planar PPH_2.

Attempts to synthesize phosphines have typically employed bulky substituent groups to prevent oligomerization; matrix isolation should, in principle, also achieve this. However, in

isolation, unimolecular isomerization is still possible. Using the standard transistion state theory (TST) reaction rate[69]

$$k(T) = \left(\frac{k_B T}{h}\right) \frac{Q^{\ddagger}}{Q} e^{-\frac{E_0}{k_B T}}. \tag{2.1}$$

where the partition functions for *trans*-HPPH (Q) and the transition states ($Q^{\ddagger}$) are evaluated using direct summation over rigid rotor and harmonic oscillator energy levels, we can compute the rate of isomerization of *trans*-HPPH to both *cis*-HPPH and planar PPH_2. Even at a temperature as high as 298 K, we compute the rates for isomerization to [*cis*-HPPH, planar PPH_2] to be just [3×10^{-12}, 2×10^{-23}] s^{-1} at the [aug-cc-pVTZ MRCI, aug-cc-pVQZ CCSD(T)] levels of theory, which correspond to half lives of [3×10^{11}, 4×10^{22}] seconds, respectively. If the same analysis is performed with our lowest levels of theory, [SCF aug-cc-pVTZ, CASSCF, cc-pVDZ] , the rates become [5×10^{-11}, 2×10^{-23}] s^{-1}, respectively which confirms the insensitivity of the reaction rates to level of theory employed.

According to the simple Wigner tunnelling correction,[70] this rate is accelated by a factor of

$$k_W(T) = 1 + \frac{1}{24}\left(\frac{h\nu_i}{k_B T}\right) \tag{2.2}$$

where ν_i is the magnitude of the imaginary vibrational frequency connecting reactants and products. The values of k_W at 4 Kelvin are just [7433, 3241] for isomerization reactions to form [*cis*-HPPH, planar PPH_2] at the [aug-cc-pVTZ MRCI, aug-cc-pVQZ CCSD(T)] levels of theory. Given the sensitivity of the imaginary frequencies, we also computed the Wigner correction using [cc-pVDZ CASSCF, aug-cc-pVTZ SCF] vibrational frequencies at 4 K, resulting in classical rate increases by a factor of [5877, 7180]. These confirm that although the imaginary vibrational frequencies exhibit significant dependence upon the level of theory, the resulting tunnelling corrections, and hence the halflives, are of the same order of magnitude. The fact that these isomerization rates are so small, even at high temperatures, and that the tunnelling is not significant even at low temperatures bolsters the feasibility of experimentally characterizing *trans*-HPPH.

2.5 Concluding Remarks

Trans- and *cis*-HPPH diphosphene as well as planar PPH_2 diphosphinylidene have been studied using highly correlated *ab initio* electronic structure theory. Multireference wavefunctions were required to investigate the isomerization transition state between the *trans* and *cis* structures. The *trans-cis* isomerization transition state barrier is predicted to be 35.2 kcal mol^{-1} using the Mk-MRCCSD method. At the highest level of theory, aug-cc-pVTZ CCSD(T), the barrier for the isomerization transition state between *trans*-HPPH and planar PPH_2 is predicted to be 48.2 kcal mol^{-1}. The results for this unusual non-planar transition state should be of aid in understanding the nature of 1,2 hydrogen shifts for phosphorus compounds involving the PP double bond.

2.6 Acknowledgments

T. L. thanks Dr. S. E. Wheeler for insightful discussions. This research was supported by the U.S. Department of Energy, Office of Basic Energy Sciences, Grant No. DE-FG02-00ER14748 and used resources of the National Energy Research Scientific Computing Center, which is supported by the Office of Science of the U.S. Department of Energy under Contract No. DE-AC02-05CH11231.

2.7 References

[1] Cowley, A. H. *Acc. Chem. Res.* **1984**, *17*, 386

[2] Scherer, O. J. *Angew. Chem. Int. Ed.* **1990**, *29*, 1104

[3] Klinkhammer, K. W. *Angew. Chem. Int. Ed.* **1997**, *36*, 2320

[4] Power, P. P. *J. Chem. Soc. Dalton Trans.* **1998**, *18*, 2939

[5] Robinson, G. H. *Acc. Chem. Res.* **1999**, *32*, 773

[6] Power, P. P. *Chem. Rev.* **1999**, *99*, 3463

[7] Grützmacher, H.; Fässler, T. F. *Chem. Eur. J.* **2000**, *6*, 2317

[8] Cowley, A. H. *Polyhedron* **1984**, *3*, 389

[9] Geoffroy, M.; Jouaiti, A.; Terron, G.; Cattani-Lorente, M.; Ellinger, Y. *J. Phys. Chem.* **1992**, *96*, 8241

[10] Binder, H.; Riegel, B.; Heckmann, G.; Moscherosch, M.; Kaim, W.; von Schnering, H.-G.; Hönle, W.; Flad, H.-J.; Savin, A. *Inorg. Chem.* **1996**, *35*, 2119

[11] Kawasaki, S.; Nakamura, A.; Toyota, K.; Yoshifuji, M. *Bull. Chem. Soc. Japan* **2005**, *78*, 1110

[12] Sasamori, T.; Tokitoh, N. *Dalton Trans.* **2008**, *11*, 1395

[13] Matus, M. H.; Nguyen, M. T.; Dixon, D. A. *J. Phys. Chem. A* **2007**, *111*, 1726

[14] Shah, S.; Concolino, T.; Rheingold, A. L.; Protasiewicz, J. D. *Inorg. Chem.* **2000**, *39*, 3860

[15] Yoshifuji, M.; Shima, I.; Inamoto, N.; Hirotsu, K.; Higuchi, T. *J. Am. Chem. Soc.* **1981**, *103*, 4587

[16] Cowley, A. H.; Decken, A.; Norman, N. C.; Krüger, C.; Lutz, F.; Jacobsen, H.; Ziegler, T. *J. Am. Chem. Soc.* **1997**, *119*, 3389

[17] Yoshifuji, M. *J. Chem. Soc. Dalton Trans.* **1998**, *20*, 3343

[18] Twamley, B.; Power, P. P. *Chem. Comm.* **1998**, *18*, 1979

[19] Twamley, B.; Sofield, C. D.; Olmstead, M. M.; Power, P. P. *J. Am. Chem. Soc.* **1999**, *121*, 3357

[20] Sasamori, T.; Takeda, N.; Tokitoh, N. *J. Phys. Org. Chem.* **2003**, *16*, 450

[21] Mathey, F. *Angew. Chem. Int. Ed.* **2003**, *42*, 1578

[22] Wang, Y.; Xie, Y.; Wei, P.; King, R. B.; Schaefer, H. F.; v. R. Schleyer, P.; Robinson, G. H. *J. Am. Chem. Soc.* **2008**, *130*, 14970

[23] Weber, L. *Chem. Rev.* **1992**, *92*, 1839

[24] Tokitoh, N. *J. Organomet. Chem.* **2000**, *611*, 217

[25] Caminade, A.-M.; Verrier, M.; Ades, C.; Paillous, N.; Koenig, M. *J. Chem. Soc. Chem. Commun.* **1984**, *13*, 875

[26] Hamaguchi, H.; Tasumi, M.; Yoshifuji, M.; Inamoto, N. *J. Am. Chem. Soc.* **1984**, *106*, 508

[27] Trinquier, J. *J. Am. Chem. Soc.* **1982**, *104*, 6969

[28] Allen, T. L.; Scheiner, A. C.; Yamaguchi, Y.; Schaefer, H. F. *J. Am. Chem. Soc.* **1986**, *24*, 7579

[29] Nguyen, M. T. *Chem. Phys.* **1986**, *109*, 277

[30] Ito, K.; Nagase, S. *Chem. Phys. Lett.* **1986**, *126*, 531

[31] Nagase, S.; Suzuki, S.; Kurakake, T. *J. Chem. Soc. Chem. Commun.* **1990**, *23*, 1724

[32] Allen, T. L.; Scheiner, A. C.; Schaefer, H. F. *J. Phys. Chem.* **1990**, *94*, 7780

[33] Jin, S.; Colegrove, B. T.; Schaefer, H. F. *Inorg. Chem.* **1991**, *30*, 2969

[34] Mahé, L.; Barthelat, J.-C. *J. Phys. Chem.* **1995**, *99*, 6819

[35] Cheng, H.-M.; Lin, C.-F.; Chu, S.-Y. *J. Phys. Chem. A* **2007**, *111*, 6890

[36] Amatatsu, Y. *J. Phys. Chem. A* **2008**, *112*, 8824

[37] Olkowska-Oetzel, J.; Pikies, J. *Appl. Organometal. Chem.* **2003**, *17*, 28

[38] Nguyen, M. T.; van Keer, A.; Vanquickenborne, L. G. *J. Org. Chem.* **1996**, *61*, 7077

[39] Kim, K.; Shavitt, I.; Del Bene, J. E. *J. Chem. Phys.* **1992**, *96*, 7573

[40] Wetmore, R. W.; Schaefer, H. F. *J. Chem. Phys.* **1978**, *69*, 1648

[41] Dunning, T. H. *J. Chem. Phys.* **1989**, *90*, 1007

[42] Woon, D. E.; Dunning, T. H. *J. Chem. Phys.* **1993**, *98*, 1358

[43] Brooks, B. R.; Laidig, W. D.; Saxe, P.; Goddard, J. D.; Yamaguchi, Y.; Schaefer, H. F. *J. Chem. Phys.* **1980**, *72*, 4652

[44] Osamura, Y.; Yamaguchi, Y.; Schaefer, H. F. *J. Chem. Phys.* **1982**, *77*, 383

[45] Rice, J. E.; Amos, R. D.; Handy, N. C.; Lee, T. J.; Schaefer, H. F. *J. Chem. Phys.* **1986**, *85*, 963

[46] Hampel, C.; Peterson, K. A.; Werner, H.-J. *Chem. Phys. Lett.* **1992**, *190*, 1

[47] Watts, J. D.; Gauss, J.; Bartlett, R. J. *Chem. Phys. Lett.* **1992**, *200*, 1

[48] Raghavachari, K.; Trucks, G. W.; Pople, J. A.; Head-Gordon, M. *Chem. Phys. Lett.* **1989**, *157*, 479

[49] Watts, J. D.; Gauss, J.; Bartlett, R. J. *J. Chem. Phys.* **1993**, *98*, 8718

[50] Stanton, J. F. *Chem. Phys. Lett.* **1997**, *281*, 130

[51] Knowles, P. J.; Werner, H.-J. *Chem. Phys. Lett.* **1985**, *115*, 259

[52] Werner, H.-J.; Knowles, P. J. *J. Chem. Phys.* **1985**, *82*, 5053

[53] Knowles, P. J.; Werner, H.-J. *Chem. Phys. Lett.* **1988**, *145*, 514

[54] Werner, H.-J.; Knowles, P. J. *J. Chem. Phys.* **1988**, *89*, 5803

[55] Roos, B. O.; Linse, P.; Siegbahn, P. E. M.; Blomberg, M. R. A. *Chem. Phys.* **1982**, *66*, 197

[56] Andersson, K.; Malmqvist, P. Å.; Roos, B. O.; Sadlej, A. J.; Wolinski, K. *J. Phys. Chem.* **1990**, *94*, 5483

[57] Andersson, K.; Malmqvist, P. Å.; Roos, B. O. *J. Chem. Phys.* **1992**, *96*, 1218

[58] Mahapatra, U. S.; Datta, B.; Mukherjee, D. *Mol. Phys.* **1998**, *94*, 157

[59] Evangelista, F. A.; Allen, W. D.; Schaefer, H. F. *J. Chem. Phys.* **2006**, *125*, 154113

[60] Evangelista, F. A.; Allen, W. D.; Schaefer, H. F. *J. Chem. Phys.* **2007**, *127*, 024102

[61] Werner, H.-J. et al. *MOLPRO, version 2006.1, a package of ab initio programs*, see http://www.molpro.net

[62] J. F. Stanton, J. Gauss, J. D. Watts, P. G. Szalay, R. J. Bartlett with contributions from A. A. Auer, D. E. Bernholdt, O. Christiansen, M. E. Harding, M. Heckert, O. Heun, C. Huber, D. Jonsson, J. Jusélius, W. J. Lauderdale, T. Metzroth, C. Michauk, D. P. O'Neill, D. R. Price, K. Ruud, F. Schiffmann, A. Tajti, M. E. Varner, J. Vázquez and the integral packages: MOLECULE (J. Almlöf and P. R. Taylor), PROPS (P. R. Taylor), and ABACUS (T. Helgaker, H. J. Aa. Jensen, P. Jørgensen, and J. Olsen). Current version see http://www.aces2.de.

[63] Stanton, J. F.; Gauss, J.; Watts, J. D.; Lauderdale, W. J.; Bartlett, R. J. *Int. J. Quant. Chem.* **1992**, *44 (S26)*, 879

[64] Crawford, T. D.; Sherrill, C. D.; Valeev, E. F.; Fermann, J. T.; King, R. A.; Leininger, M. L.; Brown, S. T.; Janssen, C. L.; Seidl, E. T.; Kenny, J. P.; Allen, W. D. *J. Comp. Chem.* **2007**, *28*, 1610

[65] Evangelista, F. A. MCSCF *is a program for multi-configuration self-consistent field calculations.*, 2008

[66] Evangelista, F. A.; Simmonett, A. C. PSIMRCC *is a computer code written at the University of Georgia to perform multireference coupled cluster computations*, 2007, See http://www.ccc.uga.edu/psimrcc

[67] Nguyen, M. T.; Ha, T.-K. *Chem. Phys. Lett.* **1989**, *158*, 135

[68] Hammond, G. S. *J. Am. Chem. Soc.* **1953**, *77*, 334

[69] Levine, R. D. *Molecular Reaction Dynamics*; Cambridge University Press: Cambridge, UK, 2005

[70] Wigner, E. *Z.Phys.Chem.B* **1932**, *19*, 203

Table 2.1: Theoretical prediction of harmonic vibrational frequencies (in cm^{-1}), infrared intensities (in parentheses in km mol^{-1}), and zero point vibrational energies (ZPVE, in kcal mol^{-1}) for the ^1A_g *trans*-HPPH molecule.

Theory	$\omega_1(a_g)$	$\omega_2(a_g)$	$\omega_3(a_g)$	$\omega_4(a_u)$	$\omega_5(b_u)$	$\omega_6(b_u)$	ZPVE
aug-cc-pVTZ HF	2493	1045	696	849	2509 (128.3)	736 (17.4)	11.91
aug-cc-pVQZ HF	2495	1048	698	852	2511 (126.7)	737 (17.7)	11.92
cc-pVTZ CISD[a]	2438	1001	659	811	2453	697	11.52
cc-pVQZ CISD	2446	1005	667	814	2461	701	11.57
aug-cc-pVTZ CISD	2437	999	658	807	2452	699	11.51
aug-cc-pVQZ CISD	2445	1004	666	813	2460	702	11.57
cc-pVTZ CCSD	2382	978	629	782	2396 (113.9)	683 (10.8)	11.22
cc-pVQZ CCSD	2390	983	638	787	2405 (99.3)	688 (11.7)	11.28
aug-cc-pVTZ CCSD	2379	977	628	778	2394 (103.0)	685 (12.0)	11.21
aug-cc-pVQZ CCSD	2388	982	637	785	2403 (96.4)	689 (12.3)	11.28
cc-pVTZ CCSD(T)	2358	963	601	762	2373 (110.4)	671 (10.0)	11.05
cc-pVQZ CCSD(T)	2366	968	611	767	2381 (95.6)	676 (10.8)	11.11
aug-cc-pVTZ CCSD(T)	2354	961	599	758	2370 (100.4)	673 (11.1)	11.03
aug-cc-pVQZ CCSD(T)	2363	967	610	765	2379 (93.4)	677 (11.2)	11.10
cc-pVDZ CASSCF[b]	2243	956	568	746	2260 (178.3)	672 (10.1)	10.64
cc-pVTZ CASSCF	2237	958	578	752	2256 (150.6)	668 (11.1)	10.65
aug-cc-pVDZ CASSCF	2242	951	568	738	2259 (139.9)	669 (11.5)	10.62
aug-cc-pVTZ CASSCF	2241	956	578	751	2259 (135.5)	668 (13.0)	10.65
cc-pVDZ MRCI	2340	964	576	749	2356 (158.9)	674 (9.8)	10.95
cc-pVTZ MRCI	2331	969	594	761	2352 (121.7)	665 (11.4)	10.97
aug-cc-pVDZ MRCI	2324	955	572	733	2340 (126.5)	669 (11.7)	10.86
aug-cc-pVTZ MRCI	2329	967	593	758	2350 (110.0)	666 (12.8)	10.96

[a] The algorithm used to compute the CISD energies did not afford dipole moments or derivatives thereof.

[b] The active space is defined as (12e/10MO).

Table 2.2: Theoretical prediction of harmonic vibrational frequencies (in cm^{-1}), infrared intensities (in parentheses in km mol^{-1}), zero point vibrational energies (ZPVE, in kcal mol^{-1}), and dipole moments (μ_e, in Debye) for the $^1A_1$ *cis*-HPPH molecule.

Theory	μ_e	$\omega_1(a_1)$	$\omega_2(a_1)$	$\omega_3(a_1)$	$\omega_4(a_2)$	$\omega_5(b_2)$	$\omega_6(b_2)$	ZPVE
aug-cc-pVTZ HF	1.347	2522 (95.0)	806 (21.6)	690 (1.2)	769	2497 (28.4)	935 (12.6)	11.75
aug-cc-pVQZ HF	1.342	2525 (93.7)	808 (21.9)	692 (1.2)	771	2499 (28.4)	937 (13.3)	11.77
cc-pVTZ CISD[a]		2468	765	649	730	2443	881	11.35
cc-pVQZ CISD		2477	772	657	732	2452	884	11.40
aug-cc-pVTZ CISD		2467	769	647	725	2442	878	11.33
aug-cc-pVQZ CISD		2475	773	656	732	2451	883	11.39
cc-pVTZ CCSD	1.134	2411 (87.2)	747 (13.7)	618 (1.4)	702	2387 (18.0)	859 (15.5)	11.04
cc-pVQZ CCSD	1.146	2420 (75.7)	755 (14.5)	627 (1.7)	705	2396 (16.2)	862 (16.9)	11.10
aug-cc-pVTZ CCSD	1.102	2408 (79.5)	751 (14.6)	616 (1.8)	698	2383 (15.6)	855 (16.8)	11.03
aug-cc-pVQZ CCSD	1.128	2417 (74.0)	756 (14.9)	626 (1.8)	705	2393 (15.5)	861 (17.1)	11.09
cc-pVTZ CCSD(T)	1.106	2387 (85.6)	731 (12.5)	587 (1.5)	681	2364 (15.9)	839 (16.4)	10.85
cc-pVQZ CCSD(T)	1.115	2395 (73.5)	740 (13.2)	598 (1.7)	685	2372 (14.4)	842 (17.7)	10.91
aug-cc-pVTZ CCSD(T)	1.065	2383 (78.3)	737 (13.3)	586 (1.9)	677	2359 (13.9)	836 (17.4)	10.83
aug-cc-pVQZ CCSD(T)	1.092	2392 (72.3)	741 (13.5)	597 (1.9)	685	2369 (13.8)	842 (17.8)	10.90
cc-pVDZ CASSCF[b]	1.307	2265 (137.6)	729 (12.3)	556 (0.9)	673	2239 (31.6)	851 (16.5)	10.45
cc-pVTZ CASSCF	1.232	2264 (117.1)	724 (12.7)	567 (1.2)	679	2235 (25.8)	845 (17.9)	10.46
aug-cc-pVDZ CASSCF	1.243	2266 (111.3)	730 (13.0)	556 (1.3)	669	2240 (23.2)	842 (18.2)	10.44
aug-cc-pVTZ CASSCF	1.234	2267 (106.6)	725 (14.0)	566 (1.5)	677	2238 (22.8)	843 (19.9)	10.46
cc-pVDZ MRCI	1.188	2365 (125.4)	736 (11.8)	563(1.1)	670	2340 (22.2)	848 (18.0)	10.75
cc-pVTZ MRCI	1.156	2367 (95.9)	728 (12.9)	581(1.5)	680	2337 (17.4)	838 (18.2)	10.76
aug-cc-pVDZ MRCI	1.092	2352 (101.7)	734 (13.1)	559 (1.7)	650	2326 (16.4)	828 (19.2)	10.65
aug-cc-pVTZ MRCI	1.134	2365 (87.7)	732 (13.9)	580 (1.8)	676	2334 (15.1)	834 (19.9)	10.75

[a] The algorithm used to compute the CISD energies did not afford dipole moments or derivatives thereof.

[b] The active space is defined as (12e/10MO).

Table 2.3: Theoretical prediction of harmonic vibrational frequencies (in cm^{-1}), infrared intensities (in parentheses in km mol^{-1}), zero point vibrational energies (ZPVE, in kcal mol^{-1}), and dipole moments (μ_e, in Debye) for the $^1A_1$ planar PPH_2 structure.

Theory	μ_e	$\omega_1(a_1)$	$\omega_2(a_1)$	$\omega_3(a_1)$	$\omega_4(b_1)$	$\omega_5(b_2)$	$\omega_6(b_2)$	ZPVE
aug-cc-pVTZ HF	2.460	2590 (32.0)	1228 (66.9)	707 (2.9)	367 (46.6)	2595 (22.6)	700 (0.0)	11.71
aug-cc-pVQZ HF	2.455	2592 (33.4)	1234 (68.5)	712 (2.5)	379 (45.6)	2596 (22.6)	707 (0.0)	11.75
cc-pVTZ CISD[a]		2513	1200	712	407	2514	667	9.45
cc-pVQZ CISD		2519	1199	720	415	2520	672	9.50
aug-cc-pVTZ CISD		2512	1190	709	403	2515	660	9.43
aug-cc-pVQZ CISD		2517	1196	719	414	2518	671	9.50
cc-pVTZ CCSD	2.226	2451 (46.9)	1180 (80.1)	694 (0.0)	387 (23.3)	2452 (49.5)	644 (0.3)	11.16
cc-pVQZ CCSD	2.276	2457 (45.5)	1177 (77.3)	702 (0.0)	392 (24.7)	2458 (35.7)	651 (0.7)	11.20
aug-cc-pVTZ CCSD	2.276	2450 (47.9)	1168 (77.0)	690 (0.0)	382 (26.9)	2452 (32.9)	639 (1.2)	11.12
aug-cc-pVQZ CCSD	2.288	2455 (46.7)	1173 (76.7)	701 (0.0)	391 (26.7)	2456 (30.4)	649 (1.2)	11.19
cc-pVTZ CCSD(T)	2.211	2415 (56.1)	1173 (87.0)	681 (0.0)	394 (20.4)	2412 (56.7)	630 (0.8)	11.01
cc-pVQZ CCSD(T)	2.258	2418 (53.9)	1168 (83.5)	689 (0.0)	397 (21.8)	2420 (40.9)	636 (1.3)	11.05
aug-cc-pVTZ CCSD(T)	2.262	2412 (57.5)	1159 (83.7)	676 (0.0)	388 (23.7)	2412 (38.1)	624 (2.1)	10.97
aug-cc-pVQZ CCSD(T)	2.271	2417 (55.5)	1164 (82.9)	687 (0.0)	395 (23.5)	2417 (34.9)	633 (2.0)	11.03

[a] The algorithm used to compute the CISD energies did not afford dipole moments or derivatives thereof.

Table 2.4: Theoretical predictions of the total energies (in E_h) for the three structures. Relative energies (ΔE_e) and ZPVE-corrected relative energies (ΔE_0) are in kcal mol^{-1} relative to the *trans*-HPPH closed-shell structure obtained by the same method and basis set.

Theory	^1A_g *trans*-HPPH	$^1A_1$ *cis*-HPPH			$^1A_1$ planar PPH_2		
	Energy	Energy	ΔE_e	ΔE_0	Energy	ΔE_e	ΔE_0
aug-cc-pVTZ HF	-682.643184	-682.637648	3.47	3.32	-682.604043	24.56	24.36
aug-cc-pVQZ HF	-682.650899	-682.645323	3.50	3.34	-682.612349	24.19	24.02
cc-pVTZ CISD	-682.936526	-682.931052	3.43	3.26	-682.895999	25.43	23.37
cc-pVQZ CISD	-682.960652	-682.955068	3.50	3.33	-682.921286	24.70	22.63
aug-cc-pVTZ CISD	-682.941826	-682.936285	3.48	3.30	-682.901282	25.44	23.37
aug-cc-pVQZ CISD	-682.962771	-682.957158	3.52	3.35	-682.923366	24.73	22.65
cc-pVTZ CCSD	-682.972302	-682.967008	3.32	3.14	-682.930975	25.93	25.87
cc-pVQZ CCSD	-682.998244	-682.992861	3.38	3.19	-682.958224	25.11	25.03
aug-cc-pVTZ CCSD	-682.978383	-682.973065	3.34	3.15	-682.937109	25.90	25.81
aug-cc-pVQZ CCSD	-683.000584	-682.995192	3.38	3.20	-682.960555	25.12	25.03
cc-pVTZ CCSD(T)	-682.991391	-682.986079	3.33	3.14	-682.949601	26.22	26.19
cc-pVQZ CCSD(T)	-683.019299	-683.013909	3.38	3.19	-682.979005	25.28	25.23
aug-cc-pVTZ CCSD(T)	-682.998344	-682.993045	3.32	3.13	-682.956710	26.13	26.06
aug-cc-pVQZ CCSD(T)	-683.021992	-683.016610	3.38	3.18	-682.981711	25.28	25.21
cc-pVDZ CASSCF[a]	-682.704374	-682.699485	3.07	2.88			
cc-pVTZ CASSCF	-682.730516	-682.725698	3.02	2.83			
aug-cc-pVDZ CASSCF	-682.708350	-682.703552	3.01	2.83			
aug-cc-pVTZ CASSCF	-682.731578	-682.726666	3.08	2.89			
cc-pVDZ MRCI	-682.882814	-682.877507	3.33	3.13			
cc-pVTZ MRCI	-682.964468	-682.959187	3.31	3.11			
aug-cc-pVDZ MRCI	-682.897281	-682.892168	3.21	3.00			
aug-cc-pVTZ MRCI	-682.969841	-682.964526	3.34	3.13			
cc-pVDZ Mk-MRCCSD[b]	-682.887132	-682.881902	3.28				
cc-pVTZ Mk-MRCCSD	-682.974905	-682.969709	3.26				
cc-pVQZ Mk-MRCCSD	-683.000833	-682.995548	3.32				

[a] The active space is defined as (12e/10MO).

[b] The active space for the reference wavefuntions is defined as (2e/2MO).

Table 2.5: Theoretical prediction of harmonic vibrational frequencies (in cm^{-1}), zero point vibrational energies (ZPVE, in kcal mol^{-1}), and dipole moments (μ_e, in Debye) for the isomerization transition state between the *trans*-HPPH and planar PPH_2 structures.

Theory	μ_e	$\omega_1(a)$	$\omega_2(a)$	$\omega_3(a)$	$\omega_4(a)$	$\omega_5(a)$	$\omega_6(a)$	ZPVE
aug-cc-pVTZ HF	1.44	2372	1777	1094	894	626	$1154i$	9.67
aug-cc-pVQZ HF	1.43	2373	1781	1101	899	629	$1148i$	9.70
cc-pVTZ CISD[a]		2308	1777	1084	854	590	$975i$	9.45
cc-pVQZ CISD		2317	1788	1083	860	600	$951i$	9.50
aug-cc-pVTZ CISD		2311	1771	1078	850	588	$964i$	9.43
aug-cc-pVQZ CISD		2317	1786	1082	859	599	$949i$	9.50
cc-pVTZ CCSD	1.25	2253	1766	1004	830	562	$912i$	9.17
cc-pVQZ CCSD	1.27	2261	1776	1002	836	573	$885i$	9.22
aug-cc-pVTZ CCSD	1.26	2256	1756	997	826	560	$899i$	9.14
aug-cc-pVQZ CCSD	1.26	2261	1773	1000	835	571	$881i$	9.21
cc-pVTZ CCSD(T)	1.23	2226	1791	922	812	541	$821i$	9.00
cc-pVQZ CCSD(T)	1.25	2234	1800	914	817	552	$781i$	9.03
aug-cc-pVTZ CCSD(T)	1.25	2229	1779	913	808	538	$803i$	8.96
aug-cc-pVQZ CCSD(T)[b]		2233	1795	912	817	550	$775i$	9.02

[a] The algorithm used to compute the CISD energies did not afford dipole moments.

[b] The aug-cc-pVQZ CCSD(T) vibrational frequencies were computed using numerical differentiation of energies, which did not afford dipole moments.

Table 2.6: Theoretical prediction of harmonic vibrational frequencies (in cm^{-1}), zero point vibrational energies (ZPVE, in kcal mol^{-1}), and dipole moments (μ_e, in Debye) for the isomerization transition state between the *trans*- and *cis*-HPPH structures.

Theory	μ_e	$\omega_1(a)$	$\omega_2(a)$	$\omega_3(a)$	$\omega_4(a)$	$\omega_5(b)$	$\omega_6(b)$	ZPVE
(2e/2MO)								
cc-pVTZ CASSCF	0.832	2485	781	464	982i	2484	784	10.01
cc-pVQZ CASSCF	0.832	2489	784	465	1002i	2488	785	10.02
aug-cc-pVTZ CASSCF	0.835	2487	781	465	992i	2486	783	10.01
aug-cc-pVQZ CASSCF	0.831	2489	784	465	1004i	2488	785	10.02
cc-pVTZ MRCI	0.780	2418	732	454	1091i	2418	736	9.66
cc-pVQZ MRCI	0.786	2428	737	461	1137i	2427	740	9.71
aug-cc-pVTZ MRCI	0.768	2417	733	454	1107i	2417	736	9.66
aug-cc-pVQZ MRCI	0.780	2427	737	460	1142i	2426	740	9.71
cc-pVTZ CASPT2	0.799	2401	702	456	1052i	2401	705	9.53
cc-pVQZ CASPT2	0.800	2403	705	460	1081i	2404	707	9.55
aug-cc-pVTZ CASPT2	0.796	2395	702	454	1064i	2396	705	9.51
aug-cc-pVQZ CASPT2	0.796	2400	704	459	1086i	2401	707	9.54
cc-pVDZ Mk-MRCCSD		2331	707	447	1045i	2331	714	9.34
cc-pVTZ Mk-MRCCSD		2339	704	464	1132i	2339	701	9.36
(12e/10MO)								
cc-pVDZ CASSCF	0.870	2205	701	388	1044i	2206	708	8.87
cc-pVTZ CASSCF	0.802	2204	705	400	1127i	2206	709	8.90
aug-cc-pVDZ CASSCF	0.802	2205	701	392	1093i	2207	706	8.88
aug-cc-pVTZ CASSCF	0.796	2207	705	400	1144i	2209	708	8.91
cc-pVDZ MRCI	0.771	2300	698	404	1034i	2300	706	9.16
cc-pVTZ MRCI	0.748	2305	698	425	1152i	2306	703	9.20
aug-cc-pVDZ MRCI	0.686	2288	692	403	1078i	2288	699	9.11
aug-cc-pVTZ MRCI	0.727	2303	699	425	1174i	2305	703	9.20

Table 2.7: Theoretical predictions of the total energies (in E_h) for the isomerization reactions. Relative energies (ΔE_e) and ZPVE-corrected relative energies (ΔE_0) are in kcal mol^{-1} relative to the *trans*-HPPH closed-shell structure obtained by the same method and basis set.

Theory	^1A_g *trans*-HPPH	Transition State connecting *trans*-HPPH and planar PPH_2			Transition State connecting *trans*-HPPH and *cis*-HPPH		
	Energy	Energy	ΔE_e	ΔE_0	Energy	ΔE_e	ΔE_0
aug-cc-pVTZ HF	-682.643184	-682.562425	50.68	48.44			
aug-cc-pVQZ HF	-682.650899	-682.570127	50.69	48.46			
cc-pVTZ CISD	-682.936526	-682.856358	50.31	48.24			
cc-pVQZ CISD	-682.960652	-682.880883	50.06	47.99			
aug-cc-pVTZ CISD	-682.941826	-682.862282	49.91	47.84			
aug-cc-pVQZ CISD	-682.962771	682.883196	49.93	47.86			
cc-pVTZ CCSD	-682.972302	-682.892356	50.17	48.11			
cc-pVQZ CCSD	-682.998244	-682.918799	49.85	47.79			
aug-cc-pVTZ CCSD	-682.978383	-682.899205	49.69	47.62			
aug-cc-pVQZ CCSD	-683.000584	-682.921380	49.70	47.63			
cc-pVTZ CCSD(T)	-682.991391	-682.910189	50.95	48.90			
cc-pVQZ CCSD(T)	-683.019299	-682.938821	50.50	48.43			
aug-cc-pVTZ CCSD(T)	-682.998344	-682.918093	50.36	48.29			
aug-cc-pVQZ CCSD(T)	-683.021992	-682.941811	50.31	48.23			
cc-pVDZ CASSCF[a]	-682.704374				-682.651100	33.43	31.66
cc-pVTZ CASSCF	-682.730516				-682.675189	34.72	32.97
aug-cc-pVDZ CASSCF	-682.708350				-682.654713	33.66	31.92
aug-cc-pVTZ CASSCF	-682.731578				-682.676062	34.84	33.09
cc-pVDZ MRCI	-682.882814				-682.830555	32.79	31.01
cc-pVTZ MRCI	-682.964468				-682.908903	34.87	33.11
aug-cc-pVDZ MRCI	-682.897281				-682.844974	32.82	31.07
aug-cc-pVTZ MRCI	-682.969841				-682.913988	35.05	33.29
cc-pVDZ Mk-MRCCSD[b]	-682.881732				-682.835028	32.70	
cc-pVTZ Mk-MRCCSD	-682.974905				-682.920341	34.24	
cc-pVQZ Mk-MRCCSD	-682.000833				-682.944749	35.19	

[a] The active space is defined as (12e/10MO).

[b] The active space for the reference wavefunctions is defined as (2e/2MO).

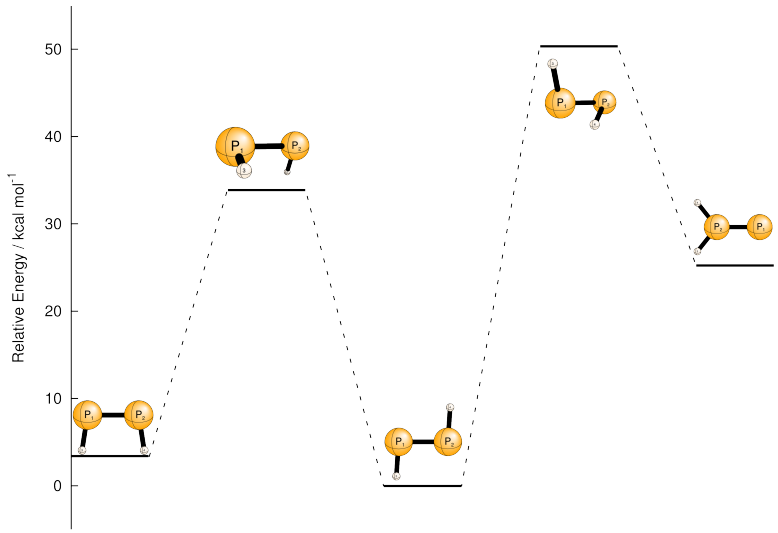

Figure 2.1: Schematic potential energy surface showing *cis*-HPPH (left), *trans*-HPPH (center), planar PPH_2 (right), and two isomerization transition states connecting them.

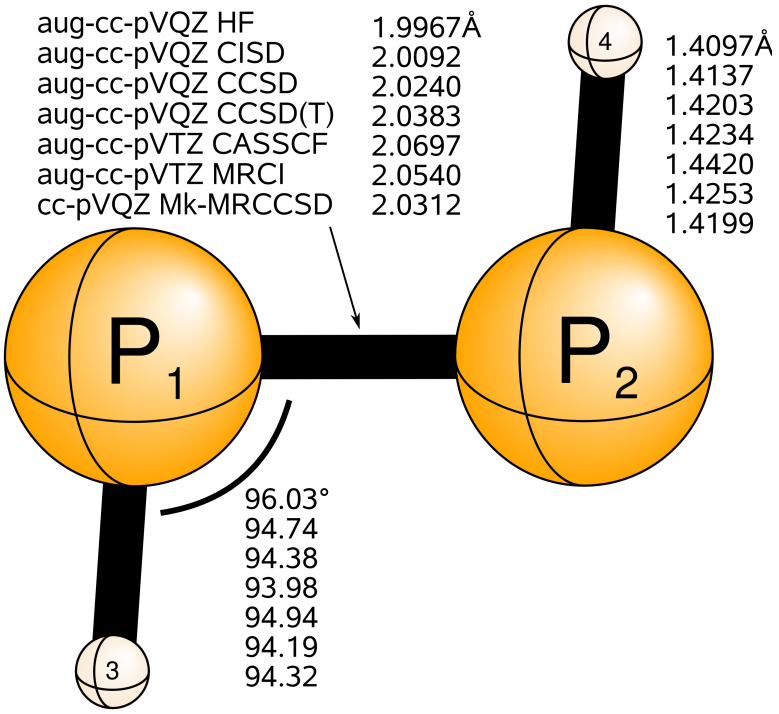

Figure 2.2: Theoretical geometries for *trans*-HPPH.

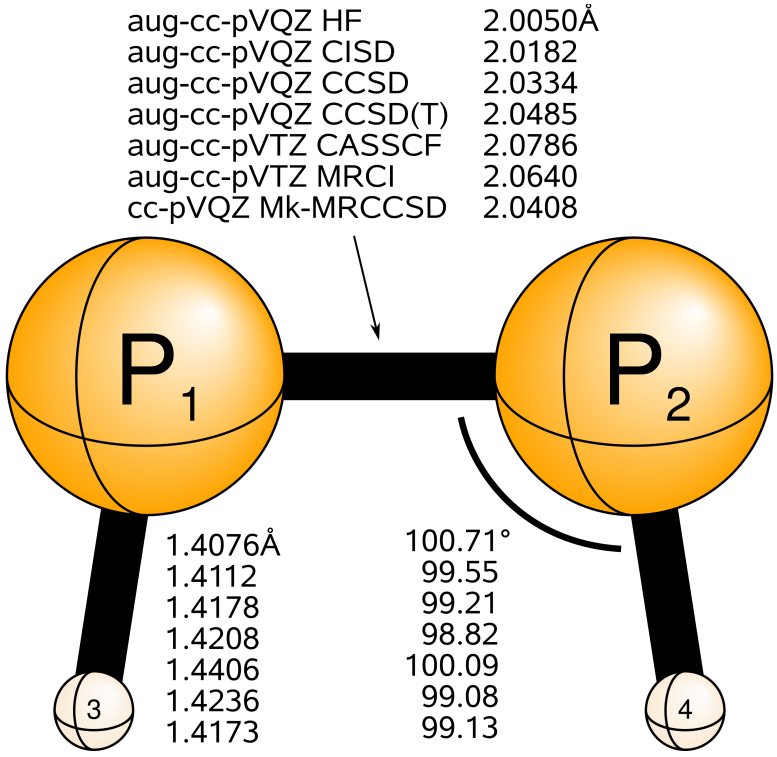

Figure 2.3: Theoretical geometries for *cis*-HPPH.

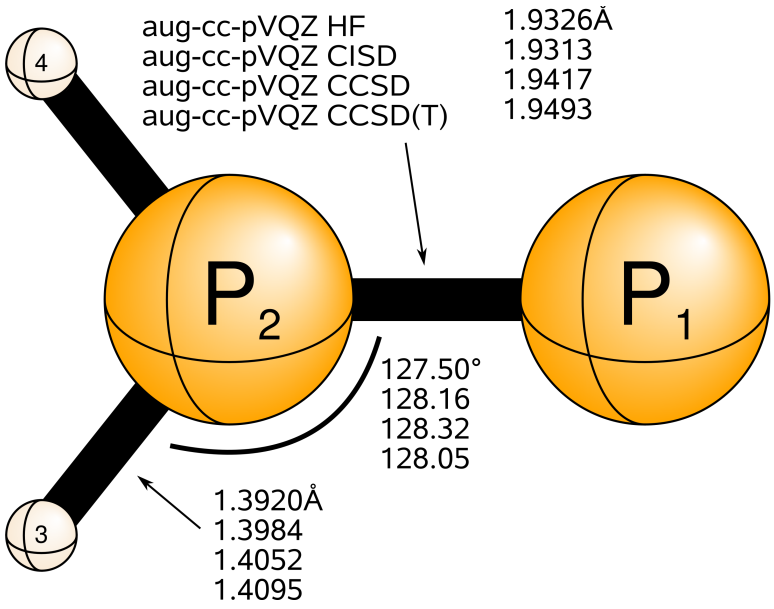

Figure 2.4: Theoretical geometries for planar PPH_2.

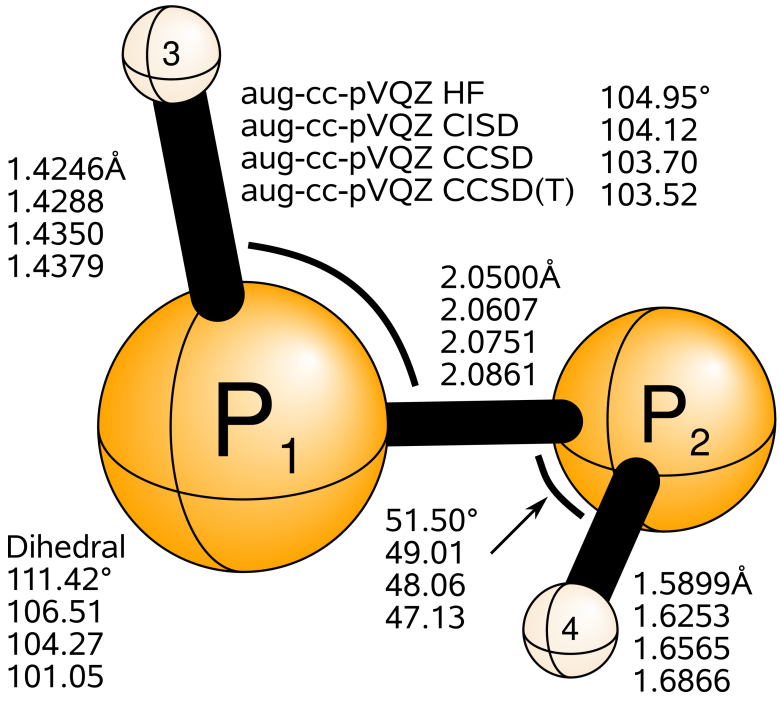

Figure 2.5: Theoretical geometries for the isomerization transition state linking *trans*-HPPH and planar PPH_2.

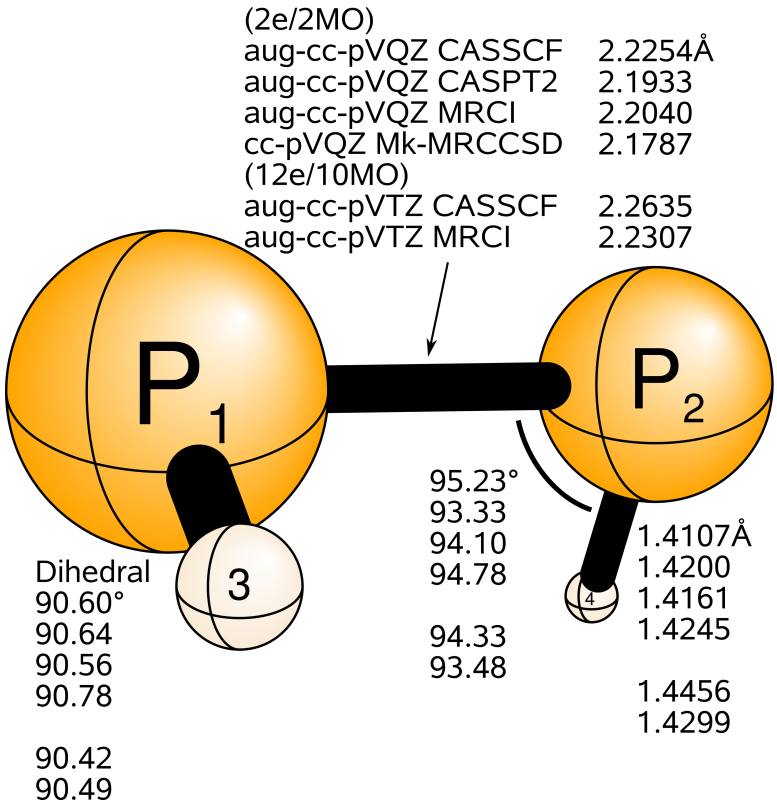

Figure 2.6: Theoretical geometries for the isomerization transition state linking *trans*-HPPH and *cis*-HPPH.

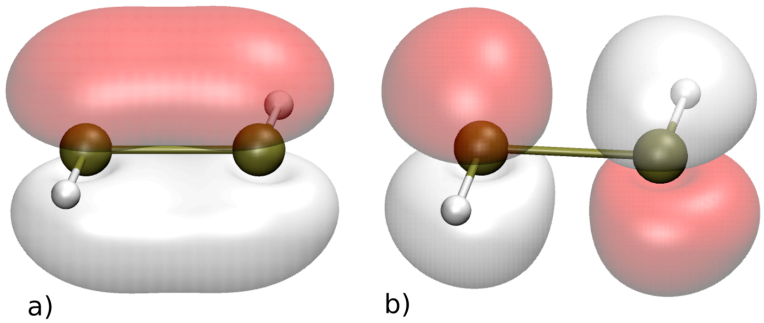

Figure 2.7: The $2a_u$ (HOMO) (a) and $2b_g$ (LUMO) (b) molecular orbitals for ^1A_g *trans*-HPPH at the cc-pVTZ SCF level of theory.

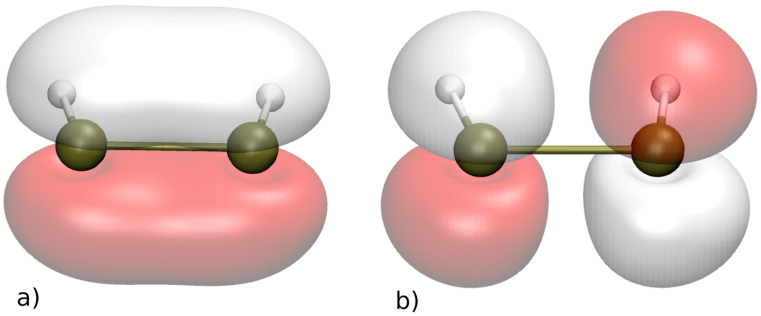

Figure 2.8: The $2b_1$ (HOMO) (a) and $2a_2$ (LUMO) (b) molecular orbitals for $^1A_1$ *cis*-HPPH at the cc-pVTZ SCF level of theory.

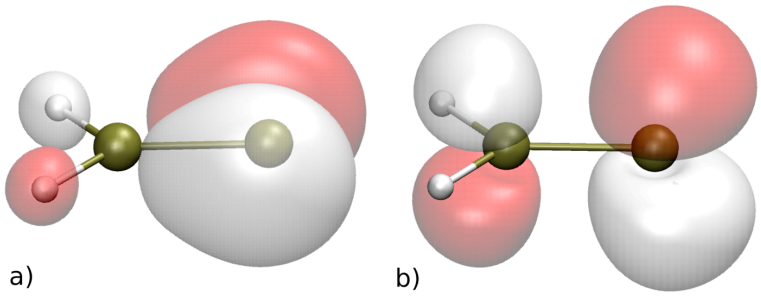

Figure 2.9: The $4b_2$ (HOMO) (a) and $4b_1$ (LUMO) (b) molecular orbitals for $^1A_1$ planar PPH_2 at the cc-pVTZ SCF level of theory.

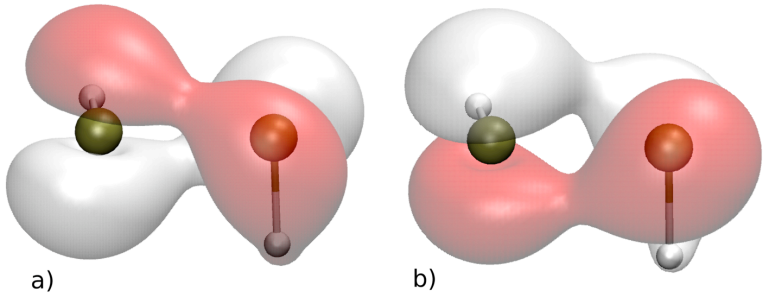

Figure 2.10: The $9a$ (a) and $8b$ (b) molecular orbitals for the isomerization transition state between *trans*-HPPH and *cis*-HPPH at the cc-pVTZ CASSCF level of theory.

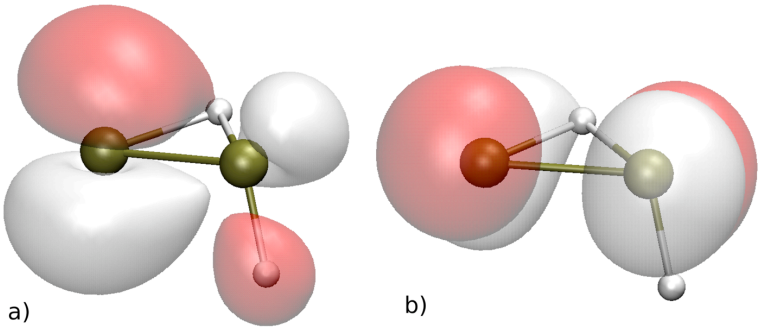

Figure 2.11: The HOMO (a) and LUMO (b) for the isomerization transition state (1,2 hydrogen shift) between *trans*-HPPH and planar PPH_2 at the cc-pVTZ SCF level of theory.

Chapter 3

Low-Lying Triplet States of Diphosphene and Diphosphinylidene[1]

[1]T. Lu, Q. Hao, A. C. Simmonett, F. A. Evangelista, Y. Yamaguchi, D.-C. Fang, and H. F. Schaefer, J. Phys. Chem. A **114** 10850 (2010). Reprinted here with permission of the American Chemical Society.

3.1 Introduction and Literature Review

3.1.1 abstract

In this research six low-lying triplet states of diphosphene (HPPH) and disphosphinylidene (PPH_2) are systematically investigated starting from self-consistent-field theory and proceeding to multi-reference coupled cluster methods using a wide range of basis sets. For each structure, the geometry, energy, dipole moment, harmonic vibrational frequencies, and infrared intensities are predicted. The triplet potential energy surface (PES) of P_2H_2 is presented, based on systematically extrapolated coupled cluster energies, and accounting for core-valence correlation, zero-point vibrational energy, and diagonal Born-Oppenheimer effects. Both $^3A''$ pyramidal PPH_2 and ^3B skewed HPPH are minima on the triplet PES, and lie 27.4±0.3 kcal mol^{-1} and 32.4±0.3 kcal mol^{-1} above the global minimum structure closed-shell ^1A_g *trans*-HPPH, respectively. The energy barrier for isomerization reaction [^3B skewed HPPH→ $^3A''$ pyramidal PPH_2] is predicted to be 16.4±0.3 kcal mol^{-1}. On this triplet PES two equivalent ^3B skewed HPPH are converted via ^3B_u *trans*-HPPH transition state with a barrier of 9.1±0.3 kcal mol^{-1}, or via $^3B_2$ *cis*-HPPH transition state with a barrier of 11.1±0.3 kcal mol^{-1}. Moreover, the two equivalent $^3A''$ pyramidal PPH_2 structures are connected through $^3A_2$ planar PPH_2 transition state with a barrier of 18.6±0.3 kcal mol^{-1}. The energy crossing of the singlet and triplet adiabatic PES is studied using Mukherjee multi-reference coupled cluster method with the cc-pVQZ basis set, which predicts that the ^3B skewed HPPH is 1.4 kcal mol^{-1} lower in energy than corresponding ^1A skewed HPPH at the ^3B skewed HPPH optimized geometry.

3.1.2 Introduction

The potential application of organic π conjugated systems in molecular electronic devices has stimulated tremendous research interest;[1–3] most visibly the 2000 Nobel Prize was awarded to MacDiarmid, Heeger, and Shirakawa for their pioneering work in this field. The electronic

properties of these materials can be tuned via manipulation of chemical structures.[4–6] In particular, the conductivity of the material can be modulated by tuning the band gap of the conjugated linker.[7] Recently PP double bonds have been incorporated into π conjugated systems as building blocks for the development of molecular electronics.[8–13] Accordingly, it is important to elucidate the excited states of diphosphenes in order to further this burgeoning area of material science.[14]

Diphosphene compounds usually have the symmetry allowed ($\pi \rightarrow \pi^*$) (intense) and symmetry forbidden ($n \rightarrow \pi^*$) (weak) electronic transitions.[15] It was found using resonance Raman excitation spectroscopy that the PP symmetric stretching mode is enhanced much more strongly in resonance with the allowed electron $\pi \rightarrow \pi^*$ transition than with the forbidden $n \rightarrow \pi^*$ transition. This is attributed to differences in the geometries of the excited states and to the different mechanisms of enhancement of resonance with allowed and forbidden electronic absorption.[16] It was also demonstrated that electron-donating substituents at the para position in diphosphenes protected by bulky groups strongly affect the $n \rightarrow \pi^*$ transition, but not the $\pi \rightarrow \pi^*$ transition.[17] The incorporation of low coordinate phosphorus centers into conjugated materials is a viable strategy for accessing the materials featuring smaller band gaps than those observed in all-carbon analogues. Moreover, in oligomers featuring P=P units the red shift of $\pi \rightarrow \pi^*$ absorptions are observed with increasing oligomer chain length.[12] In contrast to the phosphaalkene polymer, featuring P=C units, the poly(phenylenevinylene)s (PPVs) incorporating P=P linkage are not fluorescent, which may be ascribed to fluorescent quenching by interaction with phosphorus lone pairs.[13] More recently, ferrocenyl diphosphenes have been successfully synthesized.[18–21] Electronic excitation of these systems give rise to a metal-ligand charge transfer at 542 nm.[19]

Theoretical investigations have also been performed to gain insight into the different excitation processes.[22–35] PPFH has a singlet ground state, while PPF_2 has a triplet ground state. On the contrary, the singlet states are the ground states for both PPHCl and $PPCl_2$.[36,37] Moreover, the excitation energies of doubly bonded systems of group 15 elements decrease

proceeding down the periodic table.[38] The absorption band of PhPPPh (Ph=phenyl) can be adjusted by twisting the phenyl ligands, since the highest occupied molecular orbital (HOMO) and HOMO-1 mix and are concomitantly stabilized, while the lowest unoccupied molecular orbital (LUMO) is unaffected during twisting of the phenyl ligands.[39]

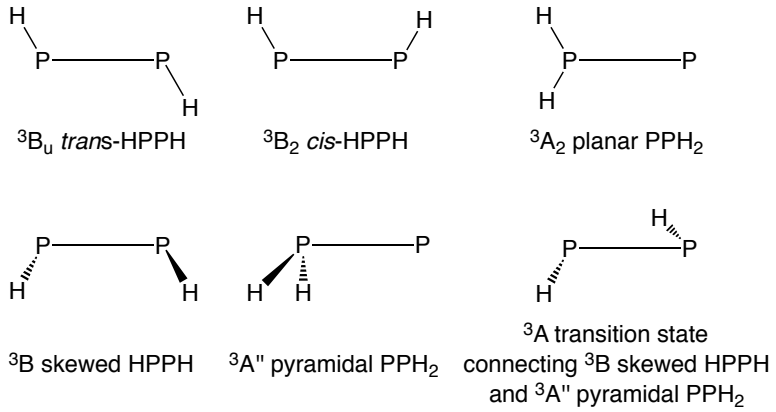

Scheme 1. Six triplet structures of HPPH and PPH_2.

In our previous paper the potential energy surface (PES) of singlet ground states of HPPH and PPH_2 has been studied.[40] The closed-shell *trans*-HPPH, *cis*-HPPH, and planar PPH_2 are minima on the singlet potential energy surface, while the skewed HPPH structure is the transition state connecting *trans*- and *cis*-HPPH on the singlet PES. The transition state for the isomerization reaction between *trans*-HPPH and planar PPH_2 is predicted to be nonplanar with a torsional angle of 101.1°. In the current paper six structures of triplet electronic states of diphosphene (HPPH) and diphosphinylidene (PPH_2) depicted in Scheme 1 are systematically investigated using highly accurate *ab initio* methods in concert with large gaussian basis sets. In order to determine the reliable relative energies and energy barriers of isomerization reactions between these structures, focal point analyses (FPA) are performed. Moreover, the crossing of singlet and triplet potential energy surfaces is also discussed.

3.2 Theoretical Procedures

In this research the correlation-consistent family of basis sets cc-pVXZ (X=D, T, Q, 5, and 6) and aug-cc-pVXZ (X=D, T, and Q) developed by Dunning and co-workers were

used.[41–43] Due to the phosphorus atom belonging to the second row, the aug-cc-pV(Q+d)Z basis sets were also employed to compare with the aug-cc-pVQZ basis sets, given that previous studies have noted the importance of the additional d function.[44] The zeroth-order descriptions of stationary points were obtained using one-configuration restricted open-shell Hartree-Fock (ROHF) and unrestricted HF (UHF) wavefunctions. The effects of electron correlation were systematically explored using coupled cluster with single and double excitations (CCSD),[45–48] CCSD with perturbative triple excitations [CCSD(T)],[49–52] full triple excitations CCSDT,[53–56] as well as CCSDT with a perturbative correction for quadruple excitations [CCSDT(Q)].[57,58] In this report the CC wavefunctions adopting ROHF reference functions are denoted as RCCSD, RCCSD(T), and RCCSDT, while those with UHF references are designated as UCCSD, UCCSD(T), UCCSDT, and UCCSDT(Q). It is important to note that the coupled cluster treatment is fully unrestricted for ROHF reference. In order to analyze changes in geometries and physical properties of these triplet states with respect to the level of correlation treatment, full valence 12 electrons in 10 molecular orbitals (12e/10MO) complete active space self-consistent-field (CASSCF)[59,60] wavefunctions with the aug-cc-pVQZ basis set were constructed at the aug-cc-pVQZ RCCSD(T) optimized geometries. The energy crossing of singlet and triplet PES has been investigated by applying the state-specific multi-reference coupled cluster approach suggested by Mukherjee and co-workers (Mk-MRCCSD).[61–63] For the Mk-MRCCSD calculations, two configuration SCF(TCSCF) orbitals with two active electrons were employed. The active space orbitals were canonicalized by transforming to the natural orbital basis. In the correlated procedures the ten lowest-lying core orbitals (P:1s,2s,2p-like) were frozen, in keeping with the design of the basis sets used. However, for the core valence correlation correction, where aug-cc-pCVQZ basis sets combined with RCCSD(T) were applied, only the two lowest-lying core orbitals (P:1s-like) were frozen.

At the RCCSD and RCCSD(T) levels of theory, geometries, harmonic vibrational frequencies, and dipole moments were obtained using numerical differentiation of the total energies;

on the other hand, at the ROHF, UHF, UCCSD, and UCCSD(T) levels of theory, analytic second derivative methods were used to compute the molecular properties including the infrared (IR) intensities. The computations were carried out using the MOLPRO,[64] the Mainz-Austin-Budapest version of ACESII (MAB-ACESII),[65] and PSI3[66] *ab initio* quantum chemistry packages. The Mk-MRCCSD calculations were performed with the PSI3 and MCSCF codes.[67,68]

The focal point analysis (FPA)[69–75] paradigm provides a framework within which one executes dual one- and n-particle expansions, extrapolating to the complete basis set limit (CBS) using the correlation consistent polarized valence hierarchy (cc-pVXZ). Electron correlation is treated through Møller-Plesset second-order perturbation theory (MP2), followed primarily by RCCSD and [RCCSD(T)], as well as RCCSDT. The CCSDT(Q) method is not yet implemented for ROHF reference functions; therefore, corrections to the RCCSDT energies for the quadruple excitations were estimated by the difference between spin-unrestricted UCCSDT(Q) and UCCSDT computations. Since high-order coupled-cluster wave functions are only very weakly dependent on the reference orbitals, the use of an unrestricted formalism is expected to have negligible effects, even in the presence of some spin contamination. The UCCSDT(Q) computations were carried out using the MRCC code of Kállay, through the MAB-ACESII interface.[58,76,77] Hartree-Fock energies were extrapolated using a standard exponential form[78]

$$E_{HF} = a + be^{-cX};$$

while the correlation energies were extrapolated via[79]

$$E_{corr} = d + eX^{-3}.$$

where a-e are fitting parameters for energies, and X is the cardinal number corresponding to the maximum angular momentum of the basis set.

Core-valence correlation corrections were computed as energy differences between all electron (excluding P 1s-like) and frozen-core (P:1s,2s,2p-like) aug-cc-pCVQZ RCCSD(T).[80]

The diagonal Born-Oppenheimer corrections (DBOC),[81–85] which constitute the first-order perturbative correction to the Born-Oppenheimer energy, were evaluated at the aug-cc-pVQZ ROHF level of theory. All computations required for the focal point method were performed at the aug-cc-pVQZ RCCSD(T) optimized geometries.

3.3 Electronic Structure Considerations and CASSCF Wavefunctions

The aug-cc-pVQZ CASSCF wavefunctions at the aug-cc-pVQZ RCCSD(T) optimized geometries are described in terms of CASSCF natural orbitals (NOs). The reference configuration (Φ_1) and several excited configurations with large CI coefficients ($|C_I| \geq 0.060$) are presented in Table A1, while the electron occupation numbers of valence MOs of the CASSCF wavefunctions are provided in Table A2 as supporting information in Appendix A. The electronic singlet ground state of the *trans*-HPPH molecule has C_{2h} symmetry with electron configuration[22,40]

$$[(\text{core})(5a_g)^2(5b_u)^2(6b_u)^2(6a_g)^2(7a_g)^2(2a_u)^2] \qquad \widetilde{X} \qquad {}^1A_g, \tag{3.1}$$

where (core) denotes the ten lowest-lying core orbitals (P:1s,2s,2p-like). The six triplet structures studied in this research are shown in Scheme 1. The lowest-lying triplet state of *trans*-HPPH exhibits electron configuration

$$[(\text{core})(5a_g)^2(5b_u)^2(6b_u)^2(6a_g)^2(7a_g)^2(2a_u\alpha)(2b_g\alpha)] \qquad {}^3B_u, \tag{3.2}$$

which corresponds to the $\pi \rightarrow \pi^*$ excitation relative to the ground state.

The electronic configuration of the lowest-lying triplet state of *cis*-HPPH is represented by

$$[(\text{core})(5a_1)^2(5b_2)^2(6a_1)^2(7a_1)^2(6b_2)^2(2b_1\alpha)(2a_2\alpha)] \qquad {}^3B_2, \tag{3.3}$$

which is generated from the ground state of *cis* structure by the $\pi \rightarrow \pi^*$ excitation.

The skewed structure of ${}^3B$ HPPH with C_2 symmetry displays electron configuration

$$[(\text{core})(6a)^2(6b)^2(7a)^2(7b)^2(8a)^2(9a\alpha)(8b\alpha)] \qquad {}^3B. \tag{3.4}$$

On the same triplet potential energy surface another local minimum $^3A''$ PPH_2 with pyramidal structure exists, and its electron configuration would be described by

$$[(\text{core})(9a')^2(10a')^2(3a'')^2(11a')^2(12a')^2(4a''\alpha)(13a'\alpha)] \qquad ^3A''. \tag{3.5}$$

The electron configuration of $^3A_2$ planar PPH_2 with C_{2v} symmetry may be written as

$$[(\text{core})(7a_1)^2(8a_1)^2(3b_2)^2(9a_1)^2(3b_1)^2(4b_2\alpha)(4b_1\alpha)] \qquad ^3A_2, \tag{3.6}$$

which is attributed to the $n \rightarrow \pi^*$ excitation from the ground state. The transition state connecting $^3A''$ pyramidal PPH_2 and ^3B skewed HPPH has electron configuration

$$[(\text{core})(11a)^2(12a)^2(13a)^2(14a)^2(15a)^2(16a\alpha)(17a\alpha)] \qquad ^3A. \tag{3.7}$$

T_1 diagnostics[75,86] for all of these structures are lower than 0.026 at the aug-cc-pVQZ CCSD(T) level of theory, which indicates the single reference character for all structures. Furthermore, each of the six triplet structures has only one dominant determinant with the CASSCF CI coefficient greater than 0.96 (C_1 in Table A1), confirming the single reference nature. In the ^3B_u *trans*-HPPH wavefunction, the determinant with the second largest CI coefficient (Φ_2) corresponds to the $(7a_g)^2 \rightarrow (7b_u)^2$ double excitation $[n(\sigma)^2 \rightarrow \sigma^{*2}]$. In a similar manner, in all of the other structures the second largest determinants (Φ_2) are generated by $n(\sigma)^2 \rightarrow \sigma^{*2}$ double excitations.

3.4 Results and Discussion

In Figure 3.1 the optimized geometries for the six triplet P_2H_2 structures at the aug-cc-pVQZ RCCSD(T) level of theory are depicted, while in Table 3.1 the total energies and physical properties at the same level of theory are presented. Selected optimized geometrical parameters for the six triplet structures are reported in Figures A1-A6. The harmonic vibrational frequencies and dipole moments at all the levels of theory are given in Tables A3-A8, while the total energies and barriers for isomerization reactions are provided in Tables A9-A15.

3.4.1 Geometries

In Figure 3.1 (also in Figure A1), it is seen that the PP bond length in the ^3B_u *trans*-HPPH structure is predicted to be 2.291 Å at the aug-cc-pVQZ RCCSD(T) level of theory, a distance being much longer than 2.038 Å of ^1A_g closed-shell ground state *trans*-HPPH with the same theoretical treatment,[40] and also longer than the PP single bond length (2.238 Å) of H_2PPH_2.[87] This feature is clearly due to the $\pi \rightarrow \pi^*$ excitation as shown in Eq. (2). However, the PH bond lengths in the ground and excited states are almost the same, around 1.42 Å. At the RCCSD(T) level of theory, both of the aug-cc-pVQZ and aug-cc-pV(Q+d)Z basis sets predict the PP bond length to be around 2.29 Å, although the extra tight d function slightly shortens the PP bond distance. Not surprising, all of trends observed in the *trans*-HPPH are also present in the $^3B_2$ *cis*-HPPH structure in Figure 3.1 (also in Figure A2).

The optimized geometries for the ^3B skewed HPPH structure are depicted in Figure 3.1 (also in Figure A3). The PP bond length of this structure is predicted to be considerably shorter than those of the ^3B_u *trans*- and $^3B_2$ *cis*-HPPH structures at all levels of theory. Since the dihedral angle of the ^3B skewed HPPH is around 90°, the formation of the π and π^* PP bonds are strictly prohibited, enhancing the PP σ bond. As with the *trans*-HPPH and *cis*-HPPH, the geometrical parameters computed at the aug-cc-pV(Q+d)Z RCCSD(T) level of theory are almost the same as those from the aug-cc-pVQZ RCCSD(T) treatment.

Although the PPH_2 has a planar equilibrium structure on the singlet PES,[22,40] the triplet PPH_2 presents a non-planar (pyramidalized) equilibrium structure as shown in Figure 3.1 (also in Figure A4). The pyramidal angle with respect to the planar structure is around 80°, which implies less efficient hybridization of the P atom, compared to the first row atoms. The $^3A_2$ planar PPH_2 in Figure 3.1 (also in Figure A5) which presents a transition state on the triplet PES (*vide infra*), possesses a much longer PP bond distance (2.092 Å) than that of the ground state $^1A_1$ planar PPH_2 (1.949 Å). This is consistent with decreasing by one bond order due to the $n \rightarrow \pi^*$ excitation in Eq. (6). The P(2)-H(4) bond length of the transition state connecting ^3B skewed HPPH and $^3A''$ pyramidal PPH_2 isomers (see Figure 3.1 and

Figure A6 for numbering) is significantly elongated compared to the PH bond distance of the ^3B skewed HPPH. This structural change accompanies the decrease of the P(1)-P(2)-H(4) bond angle, demonstrating the migration of H(4) from P(2) to P(1) to form the $^3A''$ pyramidal PPH_2 isomer.

3.4.2 Dipole Moments

The dipole moment of $^3B_2$ *cis*-HPPH in Table A4 decreases with the inclusion of correlation effects and its magnitude [0.964 debye, at the aug-cc-pVQZ RCCSD(T) level of theory] is comparable to that of the ground state closed-shell *cis*-HPPH [1.092 debye, at the same level of theory]. The former feature is associated with the double excitation Φ_2 $[(7a_1)^2 \rightarrow (7b_1)^2]$ in Table A1, which shifts the electron from $7a_1$ MO (parallel to the C_2 axis) to the $7b_2$ MO (perpendicular to the C_2 axis). The dipole moment of $^3A_2$ planar PPH_2 is predicted to be 1.30 debye at the aug-cc-pVQZ RCCSD(T) level of theory, while the dipole moment of the corresponding ground state is determined to be 2.27 debye with the same treatment of theory. This significant decrease may be ascribed to the $n \rightarrow \pi^*$ excitation $[(4b_2) \rightarrow (4b_1)]$ in Eq. (6), which redistributes the electrons from in-plane orbital $4b_2$ MO to out of plane $4b_1$ MO. Unlike the $^3B_2$ *cis*-HPPH structure, the dipole moment of $^3A_2$ planar PPH_2 in Table A7 increases with inclusion of correlation effects. This phenomenon is related to the double excitations Φ_2 and Φ_3 in Table A1, which shift the electron from the $9a_1$ MO (less polar) to the $10a_1$ MO (more polar) along the C_2 axis.

3.4.3 Harmonic Vibrational Frequencies and Associated IR Intensities

The *trans*-HPPH, *cis*-HPPH, and planar PPH_2, which are minima on the ground singlet state PES,[22,40] become transition states on the triplet PES. Two equivalent skewed HPPH on the triplet PES are converted via *trans*-HPPH or *cis*-HPPH transition states, while $^3A_2$ planar PPH_2 is the transition state which connects two equivalent $^3A''$ pyramidal PPH_2 (*vide infra*).

As shown in Table 3.1 (and Table A3), the torsional vibrational frequency of ^3B_u *trans*-HPPH is imaginary (486i cm^{-1}), which demonstrates this structure is a transition state on the triplet PES, whereas the ground state *trans*-HPPH is a minimum. The PP stretching mode [426 cm^{-1} at the aug-cc-pVQZ RCCSD(T) level of theory] of ^3B_u *trans*-HPPH has a lower frequency than that (610 cm^{-1} at the same level of theory) of the ground state, which arises from the longer PP bond length after the $\pi \rightarrow \pi^*$ excitation in Eq. (2). The vibrational frequencies of the PP and PH stretching modes decrease with the inclusion of correlation effects, which is in agreement with the elongated bond lengths. Finally, the vibrational frequencies computed with aug-cc-pV(Q+d)Z basis sets are almost the same as those with aug-cc-pVQZ basis sets.

There is another triplet transition state $^3B_2$ *cis*-HPPH located on the same PES. The imaginary frequency of torsional mode (527i cm^{-1}) in Table 3.1 (and Table A4) indicates the triplet *cis*-structure is a transition state, although the corresponding *cis*-structure of the ground state is a minimum. The PP stretching mode (417 cm^{-1}) of $^3B_2$ *cis*-HPPH has a lower vibrational frequency than that (597 cm^{-1}) of the ground state due to the elongation of the PP bond. The vibrational frequencies of $^3B_2$ *cis*-HPPH computed using the aug-cc-pV(Q+d)Z and aug-cc-pVQZ basis sets are consistent within 5 cm^{-1}.

The skewed structure ^3B HPPH is a minimum structure on the triplet PES (in Table 3.1 and Table A5), and may be converted into another equivalent structure via either the ^3B_u *trans*-HPPH or $^3B_2$ *cis*-HPPH transition states through the torsional mode. The IR intensities of the six normal modes are explored using three different levels of theory combined with UHF as reference wavefunctions. Since this structure possesses C_2 symmetry, all of the modes are IR active and the two PH stretching modes [$\omega_1(a)$ and $\omega_5(b)$] present the strongest intensities as shown in Table A5.

The pyramidal $^3A''$ PPH_2 isomer is also a minimum on the triplet PES (in Table 3.1 and Table A6), as evidenced by its lack of imaginary frequencies. The PP stretching mode shows a lower frequency (444 cm^{-1}) compared to that (687 cm^{-1}) of the planar singlet state, which

is in agreement with the single bond character of the PP bond after the triplet excitation. In this C_s symmetry structure, all of the vibrational modes are IR active; the strongest intensities are generated by the PH stretching modes [$\omega_1(a')$ and $\omega_5(a'')$], while the weakest arises from the PP stretching mode [$\omega_4(a')$] (see Table A6).

The imaginary frequency [780i cm^{-1}, at the aug-cc-pVQZ RCCSD(T) level of theory] of the $^3A_2$ planar structure is assigned to the PH_2 wagging mode (in Table A7). Following this wagging mode yields two equivalent $^3A''$ pyramidal PPH_2 structures. Because of the $n \rightarrow \pi^*$ excitation in Eq. (6), the PP bond length of $^3A_2$ planar PPH_2 structure is substantially increased compared to the ground state planar PPH_2. This structural change correlates with the decrease of the PP stretch frequency (687 $\rightarrow$ 545 cm^{-1}). As shown in other structures above, the aug-cc-pV(Q+d)Z basis sets provide very close vibrational frequencies as the aug-cc-pVQZ basis sets at the RCCSD(T) level of theory.

As it is established that the employment of different reference and/or basis set with extra d function will not lead to significant differences, for the transition state connecting ^3B skewed HPPH and $^3A''$ pyramidal PPH_2 isomers, only the ROHF reference and standard basis sets are utilized to characterize the ^3A structure. The eigenvector (reaction coordinate) of the imaginary frequency in Table3.1 (and Table A8) is an admixture of P(1)-P(2)-H(4) bending and P(2)-H(4) stretching modes.

3.4.4 Energetics

The total energies and relative energies of the six structures at the nineteen levels of theory are presented in Tables A9 and A10. Focal point analyses of the energy difference and reaction barriers of isomerization reactions are provided in Tables A11-A15. The summary of the relative energies of the six structures with respect to the global minimum (closed-shell ^1A_g *trans*-HPPH) are shown in Table 3.2, Table 3.3, and Figure 3.2.

Non-planar Triplet Minima

In order to accurately predict the energy differences focal point analysis techniques are employed. At the HF-CBS limit the energy difference between the $^3A''$ pyramidal PPH_2 structure with respect to the global minimum is determined to be 5.74 kcal mol^{-1}(in Table 3.2 and Table A11). The energy difference is drastically increased with inclusion of correlation effects. At the UCCSDT(Q)-CBS limit the relative energy is extrapolated to be 27.68 kcal mol^{-1}. With consideration of FPA plus ZPVE, core-valence, and DBOC, the relative energy of the $^3A''$ pyramidal PPH_2 structure with respect to the global minimum ^1A_g *trans*-HPPH is determined to be 27.35±0.3 kcal mol^{-1} (in Table 3.2 and Table A11). In a similar manner, the energy separation between the two minima, $^3A''$ pyramidal PPH_2 and ^3B skewed HPPH on the triplet PES is extrapolated to be 5.99 kcal mol^{-1} at the UCCSD(T)-CBS limit. With the three corrections, the final energy difference is 5.09±0.3 kcal mol^{-1}(in Table 3.2 and Table A12), compared to 0.241 ev (5.6 kcal mol^{-1}) at the CCSD(T)/aug-cc-pVTZ//B3LYP/aug-cc-pVTZ level of theory by Ervin and Lineberger.[35] Therefore, the relative energy of the ^3B skewed HPPH with regard to the global minimum ^1A_g *trans*-HPPH is predicted to be 32.44±0.3 kcal mol^{-1} (in Table 3.3).

Planar Triplet Transition Sates

As mentioned above, *trans*-HPPH, *cis*-HPPH, and planar PPH_2, which are minima on the singlet ground state PES, become transition states on the triplet PES. With inclusion of FPA, ZPVE, core-valence, and DBOC the final energy separations become 41.53±0.3, 43.55±0.3, and 45.91±0.3 kcal mol^{-1}, respectively (as shown in Table 3.3). The ^3A transition state connecting the ^3B skewed HPPH and the $^3A''$ pyramidal PPH_2 is extrapolated to be 50.07 kcal mol^{-1} above the global minimum at the UCCSD(T)-CBS limit. The relative energy decreases to 48.85±0.3 kcal mol^{-1} with inclusion of the three corrections mentioned above (in Table 3.3).

Energy Barriers for Isomerization Reactions

At the HF-CBS limit the energy barrier for the isomerization reactions of two equivalent $^3A''$ pyramidal PPH_2 via $^3A_2$ planar PPH_2 transition state is extrapolated to be 25.35 kcal mol^{-1}(in Table A13). This energy barrier is sensitive to the basis sets at the MP2 level of theory. The energy difference between the cc-pV6Z and the CBS limit at the MP2 level of theory is computed to be 0.16 kcal mol^{-1}. The energy contribution from quadruple excitations is estimated by the difference between the UCCSDT(Q) and UCCSDT methods. As expected, the correction from quadruple excitations is very small, less than 0.05 kcal mol^{-1}. The UCCSD(T)-CBS limit value is estimated to be 19.25 kcal mol^{-1}. Additional corrections to the relative energies have been included to arrive at the final recommended values. One sees that the inclusion of the correction for core-valence effects is vital to predict relative energies to be accurate within 0.3 kcal mol^{-1}, while DBOC is negligible. The final energy barrier for the isomerization reactions of two equivalent $^3A''$ pyramidal PPH_2 via $^3A_2$ planar PPH_2 transition state is determined to be 18.56$\pm$0.3 kcal mol^{-1}(in Table 3.2 and Table A13).

Focal point analyses for the isomerization reactions of two equivalent ^3B skewed structures through ^3B_u *trans*-HPPH transition state and via $^3B_2$ *cis*-HPPH transition state are presented in Table A14. The extrapolated HF energies at the CBS limit are determined to be 6.54 and 8.51 kcal mol^{-1}. The energy barriers at the UCCSDT(Q)-CBS limit increase to 9.47 and 11.59 kcal mol^{-1}, respectively. The final reaction barriers are estimated to be 9.09$\pm$0.3 and 11.11$\pm$0.3 kcal mol^{-1} with consideration of the ZPVE, core-valence corrections, and DBOC. Ervin and Lineberger estimated the energy barrier via $^3B_2$ *cis*-HPPH transition state to be 0.448 ev (10.33 kcal mol^{-1}) at the CCSD(T)/aug-cc-pVTZ//B3LYP/aug-cc-pVTZ level of theory.[35] The HF-CBS limit overestimates the reaction barrier for the isomerization reaction (^3B skewed HPPH $\rightarrow$ $^3A''$ pyramidal PPH_2) (Table A15). Extrapolating to the UCCSDT(Q)-CBS limit lowers the reaction barrier to 17.40 kcal mol^{-1}. The additional three corrections decrease the barrier by 0.99 kcal mol^{-1} to 16.41$\pm$0.3 kcal mol^{-1}. In Figure 3.2 the

triplet potential energy surface has been schematically depicted using FPA with corrections for core-valence, ZPVE, and DBOC effects.

Singlet-Triplet Energy Crossing

Since the two singly occupied molecular orbital (SOMO) are perpendicular with each other in the ^3B skewed HPPH structure and the transition state ^1A HPPH (connecting ^1A_g *trans* and $^1A_1$ *cis*-HPPH), very weak spin coupling is anticipated. This may give rise to the energy crossing of the singlet and triplet potential energy hypersurfaces. In order to clarify this possibility, the Mk-MRCCSD method combined with cc-pVQZ basis sets is employed to optimize the geometries and compute the energies of the two structures. At the optimized geometry of the ^1A transition state, the energy of the singlet state is about 1.2 kcal mol^{-1} higher than the triplet state, while at the ^3B skewed HPPH optimized geometry, this triplet structure lies about 1.4 kcal mol^{-1} below the singlet state. Schoeller *et al*[88] also predicted that this triplet state shows lower energy, but the difference was estimated to be 0.5 kcal mol^{-1} using the MRCI method.

3.5 Conclusions

The low-lying triplet states of diphosphene (HPPH) and disphosphinylidene (PPH_2) have been systematically investigated in order to better understand about the relevant excitation processes. It is demonstrated that the theoretical computation of the six triplet state structurs is not very sensitive to reference wavefunctions (ROHF and UHF) and basis sets at higher levels of correlated methods, such as CCSD and CCSD(T). The *trans*- and *cis*-HPPH structures, which are minima on the ground singlet PES, become transition states on the triplet PES. These transition states connect two equivalent ^3B skewed structures; the lower barrier through ^3B_u *trans*-HPPH as transition state is estimated to be 9.1±0.3 kcal mol^{-1} using FPA plus three other corrections. The barrier between two equivalent $^3A''$ pyramidal PPH_2 via $^3A_2$ planar PPH_2 is determined to be 18.6±0.3 kcal mol^{-1}. The conversion

of the two minima on the triplet PES (^3B skewed HPPH $\rightarrow$ $^3A''$ pyamidal PPH_2) can be accomplished via hydrogen migration with a barrier of 16.4±0.3 kcal mol^{-1}. The crossover of the singlet and triplet adiabatic potential energy surfaces is studied using the Mk-MRCC method combined with the cc-pVQZ basis set. The ^3B skewed HPPH is estimated to be 1.4 kcal mol^{-1} lower than ^1A skewed HPPH transition state at the ^3B skewed HPPH optimized geometry.

3.6 Acknowledgments

T. Lu thanks Dr. Steven E. Wheeler, Dr. Yaoming Xie, and Jeremiah J. Wilke for their insightful discussions. This research was supported by the U.S. Department of Energy, Office of Basic Energy Sciences, Grant No. DE-FG02-00ER14748 and used resources of the National Energy Research Scientific Computing Center, which is supported by the Office of Science of the U.S. Department of Energy under Contract No. DE-AC02-05CH11231.

3.7 References

[1] Roncali, J. *Chem. Rev.* **1997**, *97*, 173–205

[2] Heeger, A. J. *Synth. Met.* **2001**, *125*, 23–42

[3] MacDiarmid, A. G. *Angew. Chem.-Int. Ed.* **2001**, *40*, 2581–2590

[4] Hissler, M.; Dyer, P. W.; Réau, R. *Coord. Chem. Rev.* **2003**, *244*, 1–44

[5] Babudri, F.; Farinola, G. M.; Naso, F. *J. Mater. Chem.* **2004**, *14*, 11–34

[6] Nielsen, M. B.; Diederich, F. *Chem. Rev.* **2005**, *105*, 1837–1867

[7] Kraft, A.; Grimsdale, A. C.; Holmes, A. B. *Angew. Chem.Int. Ed.* **1998**, *37*, 402–428

[8] Hay, C.; Fischmeister, C.; Hissler, M.; Toupet, L.; Réau, R. *Angew. Chem.-Int. Ed.* **2000**, *39*, 1812–1815

[9] Hay, C.; Hissler, M.; Fischmeister, C.; Rault-Berthelot, J.; Toupet, L.; Nyulászi, L.; Réau, R. *Chem.-Eur. J.* **2001**, *7*, 4222–4236

[10] Jin, Z.; Lucht, B. *J. Organomet. Chem.* **2002**, *653*, 167–176

[11] Fave, C.; Cho, T. Y.; Hissler, M.; Chen, C. W.; Luh, T. Y.; Wu, C. C.; Reau, R. *J. Am. Chem. Soc.* **2003**, *125*, 9254–9255

[12] Smith, R. C.; Protasiewicz, J. D. *Eur. J. Inorg. Chem.* **2004**, 998–1006

[13] Smith, R. C.; Protasiewicz, J. D. *J. Am. Chem. Soc.* **2004**, *126*, 2268–2269

[14] Shah, S.; Concolino, T.; Rheingold, A. L.; Protasiewicz, J. D. *Inorg. Chem.* **2000**, *39*, 3860–3867

[15] Sasamori, T.; Tokitoh, N. *Dalton Trans.* **2008**, 1395–1408

[16] Copeland, T.; Shea, M. P.; Milliken, M. C.; Smith, R. C.; Protasiewicz, J. D.; Simpson, M. C. *Anal. Chim. Acta* **2003**, *496*, 155–163

[17] Kawasaki, S.; Nakamura, A.; Toyota, K.; Yoshifuji, M. *Bull. Chem. Soc. Japan* **2005**, *78*, 1110–1120

[18] Pietschnig, R.; Niecke, E. *Organometallics* **1996**, *15*, 891–893

[19] Nagahora, N.; Sasamori, T.; Takeda, N.; Tokitoh, N. *Chem.-Eur. J.* **2004**, *10*, 6146–6151

[20] Moser, C.; Nieger, M.; Pietschnig, R. *Organometallics* **2006**, *25*, 2667–2672

[21] Nagahora, N.; Sasamori, T.; Tokitoh, N. *Chem. Lett.* **2006**, *35*, 220–221

[22] Allen, T. L.; Scheiner, A. C.; Yamaguchi, Y.; Schaefer, H. F. *Chem. Phys. Lett.* **1985**, *121*, 154–158

[23] Allen, T. L.; Scheiner, A. C.; Yamaguchi, Y.; Schaefer, H. F. *J. Am. Chem. Soc.* **1986**, *24*, 7579–7588

[24] Ito, K.; Nagase, S. *Chem. Phys. Lett.* **1986**, *126*, 531–536

[25] Nguyen, M. T. *Chem. Phys.* **1986**, *109*, 277–288

[26] Allen, T. L.; Scheiner, A. C.; Schaefer, H. F. *J. Phys. Chem.* **1990**, *94*, 7780–7784

[27] Esseffar, M.; Luna, A.; Mó, O.; Yáñez, M. *J. Phys. Chem.* **1993**, *97*, 6607–6615

[28] Sevin, A.; Gherbi, A.; Chaquin, P. *Chem. Phys. Lett.* **1994**, *223*, 227–232

[29] Mahé, L.; Barthelat, J. C. *J. Phys. Chem.* **1995**, *99*, 6819–6827

[30] Chaquin, P.; Gherbi, A.; Masure, D.; Sevin, A. *J. Mol. Struct.* **1996**, *369*, 85–92

[31] Schoeller, W.; Rozhenko, A. B. *Eur. J. Inorg. Chem.* **2001**, 845–850

[32] Amatatsu, Y. *J. Phys. Chem. A* **2008**, *112*, 8824–8828

[33] Lai, C.-H.; Su, M.-D. *J. Comp. Chem.* **2008**, *29*, 2487–2499

[34] Amatatsu, Y. *J. Phys. Chem. A* **2009**, *113*, 9667–9674

[35] Ervin, K. M.; Lineberger, W. C. *J. Chem. Phys.* **2005**, *122*, 194303

[36] Jin, S.; Colegrove, B. T.; Schaefer, H. F. *Inorg. Chem.* **1991**, *30*, 2969–2977

[37] Nguyen, M. T.; Keer, A. V.; Vanquickenborne, L. G. *J. Org. Chem.* **1996**, *61*, 7077–7084

[38] Wang, Y.; Ma, J.; Jiang, Y. *J. Phys. Chem. A* **2005**, *109*, 7197–7206

[39] Peng, H.-L.; Payton, J. L.; Protasiewicz, J. D.; Simpson, M. C. *J. Phys. Chem. A* **2009**, *113*, 7054–7063

[40] Lu, T.; Simmonett, A. C.; Evangelista, F. A.; Yamaguchi, Y.; Schaefer, H. F. *J. Phys. Chem. A* **2009**, *113*, 13227–13236

[41] Dunning, T. H. *J. Chem. Phys.* **1989**, *90*, 1007–1023

[42] Kendall, R. A.; Dunning, T. H.; Harrison, R. J. *J. Chem. Phys.* **1992**, *96*, 6796–6806

[43] Woon, D. E.; Dunning, T. H. *J. Chem. Phys.* **1993**, *98*, 1358–1371

[44] Dunning, T. H.; Peterson, K. A.; Wilson, A. K. *J. Chem. Phys.* **2001**, *114*, 9244–9253

[45] Purvis, G. D.; Bartlett, R. J. *J. Chem. Phys.* **1982**, *76*, 1910–1918

[46] Scuseria, G. E.; Scheiner, A. C.; Lee, T. J.; Rice, J. E.; Schaefer, H. F. *J. Chem. Phys.* **1987**, *86*, 2881–2890

[47] Scuseria, G. E.; Janssen, C. L.; Schaefer, H. F. *J. Chem. Phys.* **1988**, *89*, 7382–7387

[48] Rittby, M.; Bartlett, R. J. *J. Phys. Chem.* **1988**, *92*, 3033–3036

[49] Raghavachari, K.; Trucks, G. W.; Pople, J. A.; Head-Gordon, M. *Chem. Phys. Lett.* **1989**, *157*, 479–483

[50] Bartlett, R. J.; Watts, J. D.; Kucharski, S. A.; Noga, J. *Chem. Phys. Lett.* **1990**, *165*, 513–522

[51] Bartlett, R. J.; Watts, J. D.; Kucharski, S. A.; Noga, J. *Chem. Phys. Lett.* **1990**, *167*, 609

[52] Gauss, J.; Lauderdale, W. J.; Stanton, J. F.; Watts, J. D.; Bartlett, R. J. *Chem. Phys. Lett.* **1991**, *182*, 207–215

[53] Noga, J.; Bartlett, R. J. *J. Chem. Phys.* **1987**, *86*, 7041–7050

[54] Scuseria, G. E.; Schaefer, H. F. *Chem. Phys. Lett.* **1988**, *152*, 382–386

[55] Noga, J.; Bartlett, R. J. *J. Chem. Phys.* **1988**, *89*, 3401

[56] Watts, J. D.; Bartlett, R. J. *J. Chem. Phys.* **1990**, *93*, 6104–6105

[57] Bomble, Y. J.; Stanton, J. F.; Kallay, M.; Gauss, J. *J. Chem. Phys.* **2005**, *123*, 054101

[58] Kállay, M.; Gauss, J. *J. Chem. Phys.* **2005**, *123*, 214105

[59] Knowles, P. J.; Werner, H.-J. *Chem. Phys. Lett.* **1985**, *115*, 259

[60] Werner, H.-J.; Knowles, P. J. *J. Chem. Phys.* **1985**, *82*, 5053

[61] Mahapatra, U. S.; Datta, B.; Mukherjee, D. *Mol. Phys.* **1998**, *94*, 157–171

[62] Evangelista, F. A.; Allen, W. D.; Schaefer, H. F. *J. Chem. Phys.* **2006**, *125*, 154113

[63] Evangelista, F. A.; Allen, W. D.; Schaefer, H. F. *J. Chem. Phys.* **2007**, *127*, 024102

[64] Werner, H.-J. et al. *MOLPRO*, version 2006.1 (a package of ab initio programs); see http://www.molpro.net.

[65] Stanton, J. F.; Gauss, J.; Watts, J. D.; Szalay, P. G.; Bartlett, R. J.; with contributions from Auer, A. A.; Bernholdt, D. E.; Christiansen, O.; Harding, M. E.;

Heckert, M.; Heun, O.; Huber, C.; Jonsson, D.; Jusélius, J.; Lauderdale, W. J.; Metzroth, T.; Michauk, C.; O'Neill, D. P.; Price, D. R.; Ruud, K.; Schiffmann, F.; Tajti, A.; Varner, M. E.; Vázquez, J.; and the integral packages: MOLECULE (Almlöf, J.; Taylor, P. R.), PROPS (Taylor, P. R.), and ABACUS (Helgaker, T.; Jensen, H. J. Aa.; Jørgensen, P.; Olsen, J.). Current version see http://www.aces2.de.

[66] Crawford, T. D.; Sherrill, C. D.; Valeev, E. F.; Fermann, J. T.; King, R. A.; Leininger, M. L.; Brown, S. T.; Janssen, C. L.; Seidl, E. T.; Kenny, J. P.; Allen, W. D. *J. Comp. Chem.* **2007**, *28*, 1610–1616

[67] Evangelista, F. A. MCSCF is a program for multi-configuration self-consistent field calculations., 2008

[68] Evangelista, F. A.; Simmonett, A. C. PSIMRCC is a computer code written at the University of Georgia to perform multireference coupled cluster computations (2007). See http://www.ccc.uga.edu/psimrcc.

[69] East, A. L. L.; Allen, W. D. *J. Chem. Phys.* **1993**, *99*, 4638–4650

[70] Császár, A. G.; Allen, W. D.; Schaefer, H. F. *J. Chem. Phys.* **1998**, *108*, 9751–9764

[71] Gonzales, J. M.; Pak, C.; Cox, R. S.; Allen, W. D.; Schaefer, H. F.; Császár, A. G.; Tarczay, G. *Chem.-Eur. J.* **2003**, *9*, 2173–2192

[72] Schuurman, M. S.; Muir, S. R.; Allen, W. D.; Schaefer, H. F. *J. Chem. Phys.* **2004**, *120*, 11586–11599

[73] Allen, W. D.; East, A. L. L.; Császár, A. G. In *Structures and Conformations of Non-Rigid Molecules*; Laane, J., Dakkouri, M., van der Veken, B., Oberhammer, H., Eds.; Kluwer: Dordrecht, The Netherlands, 1993; pp 343–373

[74] Császár, A. G.; Tarczay, G.; Leininger, M. L.; Polyansky, O. L.; Tennyson, J.; Allen, W. D. In *Spectroscopy from Space*; Demaison, J., Sarka, K., Eds.; Kluwer: Dordrecht, The Netherlands, 2001; pp 317–339

[75] Wilke, J. J.; Allen, W. D.; Schaefer, H. F., III *J. Chem. Phys.* **2008**, *128*, 074308

[76] MRCC, a string-based quantum chemical program suite witten by M. Kállay.

[77] Kállay, M.; Surján, P. R. *J. Chem. Phys.* **2001**, *115*, 2945–2954

[78] Feller, D. *J. Chem. Phys.* **1993**, *98*, 7059–7071

[79] Helgaker, T.; Klopper, W.; Koch, H.; Noga, J. *J. Chem. Phys.* **1997**, *106*, 9639–9646

[80] Peterson, K. A.; Dunning, T. H. *J. Chem. Phys.* **2002**, *117*, 10548–10560

[81] Handy, N. C.; Yamaguchi, Y.; Schaefer, H. F. *J. Chem. Phys.* **1986**, *84*, 4481–4484

[82] Ioannou, A. G.; Amos, R. D.; Handy, N. C. *Chem. Phys. Lett.* **1996**, *251*, 52–58

[83] Handy, N. C.; Lee, A. M. *Chem. Phys. Lett.* **1996**, *252*, 425–430

[84] Kutzelnigg, W. *Mol. Phys.* **1997**, *90*, 909–916

[85] Valeev, E. F.; Sherrill, C. D. *J. Chem. Phys.* **2003**, *118*, 3921–3927

[86] Jayatilaka, D.; Lee, T. J. *J. Chem. Phys.* **1993**, *98*, 9734–9747

[87] Matus, M. H.; Nguyen, M. T.; Dixon, D. A. *J. Phys. Chem. A* **2007**, *111*, 1726–1736

[88] Schoeller, W. W.; Begemann, C.; Tubbesing, U.; Strutwolf, J. *J. Chem. Soc., Faraday Trans.* **1997**, *93*, 2957–2962

Table 3.1: Theoretical predictions of the total energy (in hartree), dipole moment (μ_e, in debye), harmonic vibrational frequencies (in cm^{-1}), and zero point vibrational energies (ZPVE, in kcal mol^{-1}) for the six triplet P_2H_2 structures at the cc-pVQZ RCCSD(T) level of theory.

Structures	Energy	μ_e	ω_1	ω_2	ω_3	ω_4	ω_5	ω_6	ZPVE
^3B_u *trans*-HPPH	-682.954596	0	2377(a_g)	905(a_g)	426(a_g)	486i(a_u)	2388(b_u)	645(b_u)	9.65
$^3B_2$ *cis*-HPPH	-682.951351	0.964	2397(a_1)	684(a_1)	417(a_1)	527i(a_2)	2381(b_2)	807(b_2)	9.56
^3B skewed HPPH	-682.969240	0.743	2354(a)	675(a)	471(a)	449(a)	2354(b)	655(b)	9.95
$^3A''$ pyramidal PPH_2	-682.979101	0.823	2384(a')	1079(a')	634(a')	444(a')	2395(a'')	670(a'')	10.88
$^3A_2$ planar PPH_2	-682.947804	1.299	2542(a_1)	1036(a_1)	545(a_1)	780i(b_1)	2583(b_2)	494(b_2)	10.30
^3A transition state	-682.942050	-	2360(a)	1680(a)	828(a)	624(a)	465(a)	1119i(a)	8.53

Table 3.2: Focal point analyses of the energy differences (in kcal mol^{-1}). All computations are performed at aug-cc-pVQZ RCCSD(T) optimized geometries.

Basis set	ΔE[HF]	$+\delta$[MP2]	$+\delta$[RCCSD]	$+\delta$[RCCSD(T)]	$+\delta$[RCCSDT]	$+\delta$[UCCSDT(Q)]	$= \Delta E$
^1A_g *trans*-HPPH $\rightarrow$ $^3A''$ pyramidal PPH_2							
CBS LIMIT	[+5.74]	[+23.10]	[-4.48]	[+3.42]	[-0.29]	[+0.20]	[+27.68]
$\Delta E^a_{final} = 27.68 - 0.22 - 0.10 - 0.01 = \mathbf{27.35}$ kcal mol^{-1}							
$^3A''$ pyramidal PPH_2 $\rightarrow$ ^3B skewed HPPH							
CBS LIMIT	[+8.95]	[-2.69]	[+0.05]	[-0.28]	[-0.05]	[+0.01]	[+5.99]
$\Delta E_{final} = 5.99 - 0.92 - 0.00 + 0.03 = \mathbf{5.09}$ kcal mol^{-1}							
$^3A''$ pyramidal PPH_2 $\rightarrow$ $^3A_2$ planar PPH_2 transition state							
CBS LIMIT	[+25.35]	[-6.80]	[+1.76]	[-1.05]	[+0.03]	[-0.03]	[+19.25]
$\Delta E_{final} = 19.25 - 0.58 - 0.09 - 0.01 = \mathbf{18.56}$ kcal mol^{-1}							
^3B skewed HPPH $\rightarrow$ ^3B_u *trans*-HPPH transition state							
CBS LIMIT	[+6.54]	[+3.04]	[-0.70]	[+0.61]	[-0.00]	[-0.02]	[+9.47]
$\Delta E_{final} = 9.47 - 0.31 - 0.09 + 0.02 = \mathbf{9.09}$ kcal mol^{-1}							
^3B skewed HPPH $\rightarrow$ $^3B_2$ *cis*-HPPH transition state							
CBS LIMIT	[+8.51]	[+3.37]	[-0.96]	[+0.70]	[-0.01]	[-0.02]	[+11.59]
$\Delta E_{final} = 11.59 - 0.39 - 0.10 + 0.01 = \mathbf{11.11}$ kcal mol^{-1}							
^3B skewed HPPH $\rightarrow$ ^3A transition state							
CBS LIMIT	[+30.39]	[-15.80]	[+5.13]	[-2.30]	[+0.01]	[-0.04]	[+17.40]
$\Delta E_{final} = 17.40 - 1.43 + 0.14 + 0.30 = \mathbf{16.41}$ kcal mol^{-1}							

a Δ_{ZPVE}=zero point vibrational energy correction from aug-cc-pVQZ RCCSD(T) harmonic frequencies; ΔE_{core}=core-valence correlation correction at the aug-cc-pCVQZ RCCSD(T) level of theory; Δ_{DBOC}=diagonal Born-Oppenheimer correction at the aug-cc-pVQZ ROHF level of theory; $\Delta E_{final} = \Delta E + \Delta_{ZPVE} + \Delta E_{core} + \Delta_{DBOC}$.

Table 3.3: Relative energies (in kcal mol^{-1}) of the six triplet structures with respect to the closed-shell ^1A_g *trans*-HPPH.

Energy[a]	^1A_g *trans*-HPPH	^3B_u *trans*-HPPH	$^3B_2$ *cis*-HPPH	^3B skewed HPPH	$^3A''$ pyramidal PPH_2	$^3A_2$ planar PPH_2	^3A transition state
ΔE	0.00	43.14	45.26	33.68	27.68	46.93	51.07
ΔE_{ZPVE}	0.00	41.69	43.72	32.53	27.46	46.13	48.50
$\Delta E_{ZPVE+core}$	0.00	41.49	43.51	32.42	27.36	45.93	48.53
$\Delta E_{ZPVE+core+DBOC}$	0.00	41.53	43.55	32.44	27.35	45.91	48.85

[a] ΔE=relative energies from focal point analyses; Δ_{ZPVE}=zero point vibrational energy correction from aug-cc-pVQZ RCCSD(T) harmonic frequencies; ΔE_{core}=core-valence correlation correction at the aug-cc-pCVQZ RCCSD(T) level of theory; Δ_{DBOC}=diagonal Born-Oppenheimer correction at the aug-cc-pVQZ ROHF level of theory.

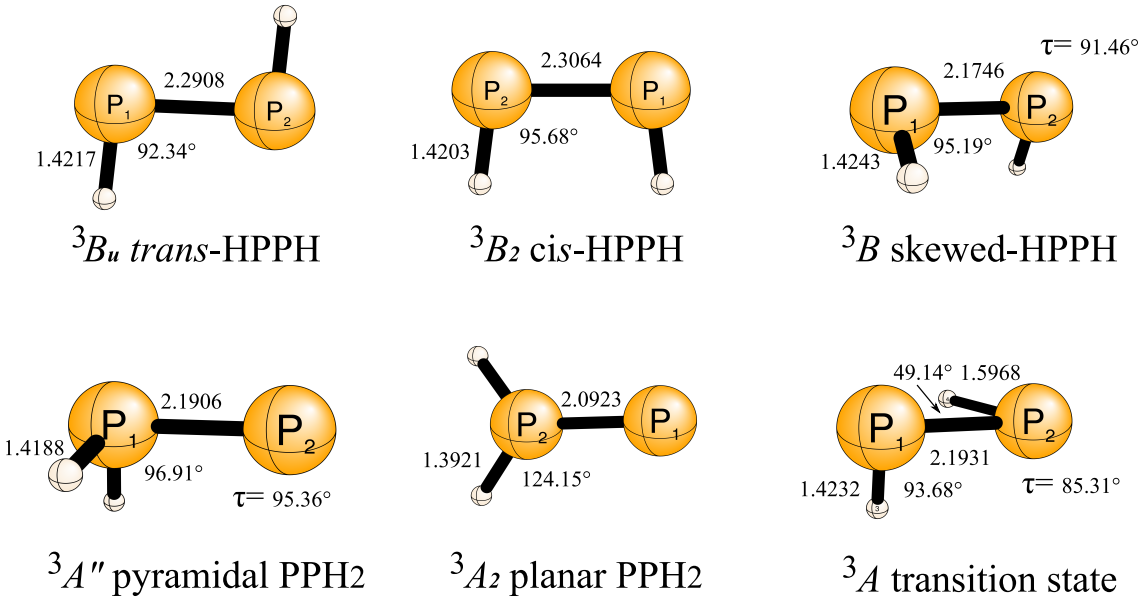

Figure 3.1: Predicted geometries for the six triplet P_2H_2 structures at the aug-cc-pVQZ RCCSD(T) level of theory, and bond lengths are in angstrom.

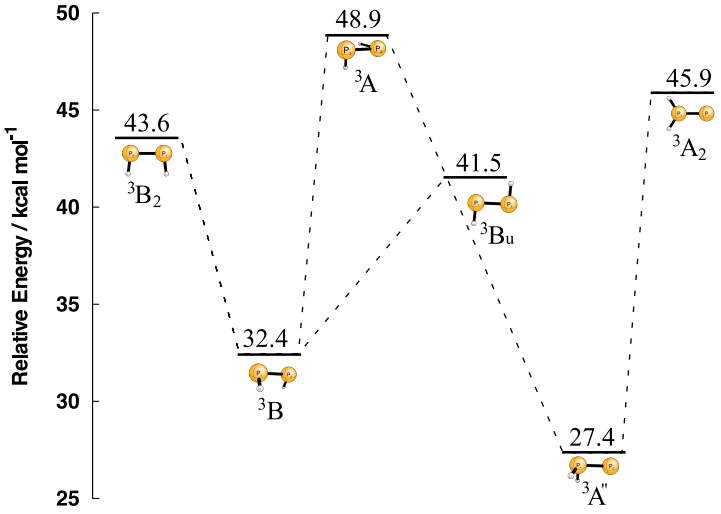

Figure 3.2: Schematic triplet potential energy surface using FPA with corrections for core-valence, ZPVE, and DBOC effects, and the relative energies are in kcal mol^{-1} with respect to the global minimum closed-shell ^1A_g *trans*-HPPH.

Chapter 4

Anharmonic vibrational analysis for disilacyclopropenylidene (Si_2CH_2)[1]

[1]T. Lu, J. J. Wilke, Y. Yamaguchi, and H. F. Schaefer, submitted to the Journal of Chemical Physics

4.1 Introduction and Literature Review

4.1.1 abstract

The global minimum on the Si_2CH_2 electronic singlet potential energy surface has been theoretically predicted to be a peculiar hydrogen bridged ($Si\cdots H\cdots Si$) disilacyclopropenylidene structure (Si_2CH_2-**1S**). An accurate quartic force field for Si_2CH_2-**1S** has been determined employing *ab initio* coupled-cluster (CC) theory with single and double excitations and a perturbative treatment for triple excitations [CCSD(T)], in combination with the correlation consistent core-valence quadruple zeta (cc-pCVQZ) basis set. The vibration-rotation coupling constants, equilibrium and zero-point vibration corrected rotational constants, centrifugal distortion constants, harmonic and fundamental vibrational frequencies for six isotopologues of Si_2CH_2-**1S** are predicted using vibrational second-order perturbation theory (VPT2). The anharmonic corrections for the vibrational motions involving the H bridged bonds are found to be more than 5% with respect to the corresponding harmonic vibrational frequencies. In this light an experimental detection and characterization of Si_2CH_2-**1S** is highly desired.

4.1.2 Introduction

Silicon is one of the most abundant elements in interstellar space and silicon harboring molecules are considered to be key molecules in astrochemistry.[1,2] It is already known that several silicon-containing molecules, such as SiC, *c*-SiC_2, and SiCN, are abundant in the circumstellar envelopes of the star IRC + 10 216.[3–10] In view of the similarity of hydrogenated silicon-carbon species ($Si_xC_yH_z$) to the important known hydrocarbon species (C_xH_y), $Si_xC_yH_z$ systems might be detectable in molecular clouds in interstellar space as well. The proposal concerning the parent cyclopropenylidene (C_3H_2) by J. P. Maier and coworkers[11] involving the diffuse interstellar bands (DIBs) is particularly fascinating. The Maier proposal (2011) has recently been carefully discussed by Oka and McCall.[12]

The dihydrogenated *c*-SiC_2, silacyclopropenylidene (SiC_2H_2), was first produced via the pulsed flash pyrolysis of 2-ethynyl-1,1,1-trimethyldisilane and was detected by matrix isolation spectroscopy,[13,14] in agreement with the early theoretical prediction that the silacyclopropenylidene is the global minimum on the electronic singlet SiC_2H_2 potential energy surface (PES).[15,16] Subsequently, a new experimental approach was employed to obtain silacyclopropenylidene from co-deposition of atomic silicon with acetylene in an argon matrix.[17] In addition, the measurement of rotational constants for silacyclopropenylidene using a source-modulated microwave spectrometer permitted the determination of the r_s structural parameters.[18]

More recently, theoretical investigations of silacyclopropenylidene as well as other SiC_2H_2 isomers have been performed employing highly correlated levels of *ab initio* theory.[19–31] The photochemical reaction pathway of silacyclopropenylidene was predicted to be drastically different from that of the parent cyclopropenylidene using an eight electrons/eight orbitals complete active space self-consistent field (CASSCF) method with the 6-311++G(3df,3pd) basis set.[32] In the most recent theoretical study, six minima and one transition state for SiC_2H_2 were located on the closed-shell singlet electronic state PES, in which the energy difference between silacyclopropenylidene and silacyclopropyne was predicted to be 46.1 kcal mol^{-1} with zero-point vibration energy corrections.[33]

In comparison with its isovalent structures, C_3H_2 and SiC_2H_2, relatively few studies of the Si_2CH_2 molecular system have been performed. In an early theoretical survey on the PES of Si_2CH_2,[34] the global minimum was reported to be disilacyclopropenylidene with both Si atoms possessing divalent character, at the MP2/6-31G*//HF/3-21G* level of theory. This was confirmed in a further investigation of geometrical structures and isomeric stabilities of various stationary points of Si_2CH_2 using coupled cluster theory in combination with correlation consistent basis sets.[35] Recently, nine structures of Si_2CH_2 were located by Wu and coworkers[33] on the electronic singlet PES, of which six structures are found to be minima, two structures to be transition states, and one structure to be a stationary point

of Hessian index two. The existence of the multi-centered hydrogen bridged structure, disilacyclopropenylidene (Si_2CH_2), as the global minimum was firmly established. The relative energies were reliably determined employing focal point analyses. The noticeable difference between Si_2CH_2 and its isovalent parent C_3H_2 was emphasized in that paper. In addition, the harmonic vibrational frequencies and associated infrared (IR) intensities were reported for all equilibirum structures.[33]

In the present investigation, the determination of molecular structural parameters was performed using the *ab initio* coupled cluster with single, double, and perturbative triple excitations [CCSD(T)] method,[36–38] with the correlation-consistent polarized core-valence quadruple zeta (cc-pCVQZ) basis set.[39–41] With the same level of theory, harmonic and anharmonic force fields are determined to provide vibration-rotation coupling constants, equilibrium and zero-point vibration corrected rotational constants, centrifugal distortion constants, harmonic and fundamental vibrational frequencies employing vibrational second-order perturbation (VPT2) theory.[42–48] The present study should provide a guide for the future spectroscopic identification of disilacyclopropenylidene.

4.2 Symmetry Internal Coordinates

The vibrational potential energy ($\overline{V}$) for disilacyclopropenylidene (Si_2CH_2) may be expanded in terms of displacement symmetry internal coordinates (Δ S_i) in the vicinity of the equilibrium point (E_e) as

$$\overline{V} = E_e + \frac{1}{2}\sum_{ij} F_{ij}\Delta S_i \Delta S_j + \frac{1}{6}\sum_{ijk} F_{ijk}\Delta S_i \Delta S_j \Delta S_k + \frac{1}{24}\sum_{ijkl} F_{ijkl}\Delta S_i \Delta S_j \Delta S_k \Delta S_l \quad (4.1)$$

In Eq. (2), F_{ij}, F_{ijk}, and F_{ijkl} denote quadratic, cubic, and quartic force constants. The nine symmetry internal coordinates for C_{2v} Si_2CH_2 structure are defined by

$S_1(a_1) = r_1$	CH stretch
$S_2(a_1) = \frac{1}{\sqrt{2}}(r_4 + r_5)$	SiH symmetric stretch
$S_3(a_1) = \frac{1}{\sqrt{2}}(r_2 + r_3)$	SiC symmetric stretch
$S_4(a_1) = \frac{1}{\sqrt{6}}(2\theta_6 - \theta_7 - \theta_8)$	SiCSi in-plane bend (SiSi stretch)
$S_5(b_1) = \pi_9$	CH out-of-plane bend
$S_6(b_1) = \tau_{10}$	SiH out-of-plane bend
$S_7(b_2) = \frac{1}{\sqrt{2}}(r_4 - r_5)$	SiH asymmetric stretch (SiH ip bend)
$S_8(b_2) = \frac{1}{\sqrt{2}}(r_2 - r_3)$	SiC asymmetric stretch
$S_9(b_2) = \frac{1}{\sqrt{2}}(\theta_7 - \theta_8)$	CH in-plane bend

where the internal coordinates are depicted in Figure 4.1.

4.3 Theoretical Procedures

In the present research, the correlation-consistent polarized core-valence quadruple zeta (cc-pCVQZ) basis set developed by Dunning and co-workers[39–41] was employed to correlate all electrons in the optimization of the structure and determination of the analytical potentials. The zeroth-order description of the ground state of Si_2CH_2 was obtained using single configuration self-consistent-field (SCF) [restricted Hartree-Fock (RHF)] wave functions. The coupled cluster with single, double, and perturbative triple excitations [CCSD(T)] approach[36–38] was used to construct the correlated wave functions.

The optimization of the structure of Si_2CH_2 was performed employing analytic derivative methods. In addition, the dipole moment, harmonic vibrational frequencies, and corresponding IR intensities were determined analytically. Electronic structure computations were carried out using the ACESII (Mainz-Austin-Budapest version)[49] and Molpro 2006.1 suites[50] quantum chemistry packages.

The C++ program GRENDEL[51] was used to generate the structural displacements and to compute force constants in the symmetry internal coordinates. The nonlinear transformation from the symmetry internal coordinates to the mass independent Cartesian coordinates for quadratic, cubic, and quartic force constants was performed using the INTDER 2005 code of Allen.[52–54] This approach allows the convenient evaluation of the force constants for each individual isotopic variant for Si_2CH_2.The vibration-rotation coupling constants, zero-point vibration corrected rotational constants, centrifugal distortion constants, and fundamental frequencies were obtained using the VPT2 method[42–48] based upon the Cartesian force constants through the ANHARM program.[55]

4.4 Results and Discussion

4.4.1 Electronic Structure Considerations

The $\widetilde{X}\ ^1A_1$ state of the disilacyclopropenylidene (Si_2CH_2) isomer arises from the following electron configuration

$$[\text{core}]6a_1^2 7a_1^2 5b_2^2 8a_1^2 2b_1^2 9a_1^2 6b_2^2 \quad \widetilde{X} \quad {}^1A_1 \tag{4.2}$$

where [core] (=$1a_1^2 1b_2^2 2a_1^2 3a_1^2 2b_2^2 4a_1^2 1b_1^2 1a_2^2 3b_2^2 5a_1^2 4b_2^2$) denotes the eleven lowest-lying core (Si: 1s,2s, 2p-like and C:1s-like) orbitals. The $2b_1$ MO describes an out-of-plane SiCSi π bonding, while the $9a_1$ and $6b_2$ MOs represent the SiHSi and SiC σ bonding orbitals, respectively.

4.4.2 Equilibrium Geometry and Dipole Moment

The geometrical parameters for the disilacyclopropenylidene molecule (Si_2CH_2) are shown in Figure 4.2 at the CCSD(T)/cc-pCVQZ level of theory. As expected, all of the bond lengths at this level of theory exhibit a slight shortening in comparison with those obtained at the cc-pVQZ CCSD(T) level,[33] this feature being due to the inclusion here of electron correlation involving the core orbitals.

The magnitude of the dipole moment using the CCSD(T) method with the cc-pCVQZ basis set is predicted to be 0.294 debye, which is comparable with that of 0.302 debye with

the cc-pV(Q+d) basis set.[33] The direction of the dipole moment is necessarily along the C_2(b) axis with sign $^{-}HSi_2CH^{+}$.

4.4.3 Vibration-Rotation Coupling Constants

The vibration-rotation interaction corrections to the equilibrium rotational constants, B_e, may be expressed by the following equation[44]

$$B_v = B_e - \sum_r \alpha_r^B (v + 1/2) + \text{higher terms} \tag{4.3}$$

where B_v (v being a vibrational quantum number) is the rotational constant and the sums run over all normal modes. Similar expressions hold for the vibrational dependence of the rotational constants A_v and C_v.

The vibration-rotation coupling constants α_r^B for an asymmetric top from perturbation theory are given by[44]

$$\begin{aligned} -\alpha_r^B &= \frac{2B_e^2}{\omega_r}\Bigg[\sum_\xi \frac{3\left(a_r^{(b\xi)}\right)^2}{4I_\xi} + \sum_s \left(\zeta_{r,s}^{(b)}\right)^2 \frac{(3\omega_r^2+\omega_s^2)}{\omega_r^2-\omega_s^2} \\ &+ \pi\left(\frac{c}{h}\right)^{\frac{1}{2}} \sum_s \phi_{rrs} a_s^{(bb)} \left(\frac{\omega_r}{\omega_s^{3/2}}\right)\Bigg] \end{aligned} \tag{4.4}$$

where ω_r is the rth harmonic vibrational frequency, I_ξ is the ξth principal moment of inertia, $\zeta_{r,s}^{(b)}$ is the Coriolis coupling constant about the b axis, and ϕ_{rrs} is the cubic force constants in terms of dimensionless normal coordinates. In this equation the $a_r^{\alpha\beta}$ constants are the derivatives of the matrix elements of the inertia tensor with respect to the rth normal coordinate Q_r

$$a_r^{(\alpha\beta)} = \left(\frac{\partial I_{\alpha\beta}}{\partial Q_r}\right)_e \tag{4.5}$$

The vibration-rotation coupling constants (α_r^A, α_r^B, and α_r^C) for the six isotopologues of disilacyclopropenylidene (Si_2CH_2) are presented in Table 4.1. The Coriolis resonances will be manifested in the second term in the square brackets of Eq. (4) when two vibrational frequencies are sufficiently close, *i.e.*, $\omega_r \approx \omega_s$. Since the vibrational frequencies for the

SiC s-stretching (ω_3, a_1) and CH out-of-plane bending (ω_5, b_1) modes for the undeuterated Si_2CH_2 molecule are reasonably close, the Coriolis resonances have been identified. In Table 4.1 the deperturbed α values with cutoff of the Coriolis resonances being 20 cm^{-1} are reported. In this light, it was pointed out by East, Johnson, and Allen that the B_0 constant (v=0) may be determined without terms involving the Coriolis resonances by taking the sums of the α_r^B constants over all normal modes in lieu of their individual values.[56] In Table 4.1, the magnitudes of the α^A constants involving the SiH vibrational motions (α_2^A, α_6^A, and α_7^A) are considerably larger than those of other α constants.

4.4.4 Rotational Constants and Centrifugal Distortion Constants

According to Ray's formula[57]

$$\kappa = \frac{2B - A - C}{A - C} \tag{4.6}$$

the disilacyclopropenylidene (Si_2CH_2) is classified as a near prolate top molecule (κ= -0.886). Consequently, both Watson's S-reducted and A-reduced rotational hamiltonians in the I^r representation are employed in the present rotational analysis.[43]

Table 4.2 presents the rotational constants and centrifugal distortion constants for the standard disilacyclopropenylidene (Si_2CH_2) and its five isotopologues evaluated at the CCSD(T)/cc-pCVQZ level of theory. In the following discussion, the vectors of the equilibrium (A_e, B_e, C_e) and zero-point vibration and centrifugal distortion corrected (A_0, B_0, C_0) rotational constants are abbreviated as $\mathbf{B_e}$ and $\mathbf{B_0}$, respectively. The equilibrium rotation constants $\mathbf{B_e}$ obtained in the present investigation are comparable to the corresponding values evaluated at the CCSD(T)/cc-pVTZ level of theory.[35] The prediction of the $\mathbf{B_0}$ values are obtained in terms of Watson's determinable rotational constants, which are independent of the type of reduction (A/S).[43] For all of the six species, the magnitudes of $\mathbf{B_0}$ are smaller than those of the corresponding $\mathbf{B_e}$, which reflects the lengthening of r_0 in comparison with the corresponding r_e. Moreover, in the case of the dideuterated isotopologues it is found that the magnitudes of A_e and A_0 show substantial decreases compared with those of their

parent structures, which can be rationalized by the increase of the corresponding principal moment of inertia, I_a. On the contrary, the other two rotational constants (B_0 and C_0) are less affected by the deuterium substitutions. This feature is due to the location of the two hydrogen atoms on the b principal axis. The substitutions of ^{29}Si and ^{13}C in the molecular structure show decreases in the rotational constants. It should be noted that the magnitudes of B_e and B_0 for ^{13}C substituted and its parent structures are practically the same, for the reasons outlined above for the two hydrogens.

The quartic centrifugal distortion constants of the six Si_2CH_2 species are also presented in Table 4.2. The magnitudes of D_K and D_{JK} in S-reduction and Δ_K and Δ_{JK} in A-reduction are decreased by a factor of 2 in Si_2CD_2 compared with Si_2CH_2. The prediction of these rotational constants and centrifugal distortion constants should assist in the future microwave spectroscopic identification of the disilacyclopropenylidene (Si_2CH_2) species.

4.4.5 Anharmonic Vibrational Constants

The rth anharmonic (fundamental) vibrational frequency (ν_r) is determined using the following equation:[42,44,58,59]

$$\nu_r = \omega_r + 2\chi_{rr} + \frac{1}{2}\sum_{s\neq r}\chi_{rs} \tag{4.7}$$

where ω_r is an rth harmonic vibrational frequency and χ_{rs} are anharmonic vibrational constants. The formulae obtained from perturbation theory for the χ_{rs} values are[42,44,59]

$$\chi_{rr} = \frac{1}{16}\phi_{rrrr} - \frac{1}{16}\sum_{s}\frac{\phi_{rrs}^2(8\omega_r^2 - 3\omega_s^2)}{\omega_s(4\omega_r^2 - \omega_s^2)} \tag{4.8}$$

for the diagonal elements and

$$\begin{aligned}\chi_{rs} &= \frac{1}{4}\phi_{rrss} - \frac{1}{4}\sum_{t}\frac{\phi_{rrt}\phi_{sst}}{\omega_t} - \frac{1}{2}\sum_{t}\frac{\phi_{rst}^2\omega_t(\omega_t^2 - \omega_r^2 - \omega_s^2)}{\Big[(\omega_r+\omega_s)^2 - \omega_t^2\Big]\Big[(\omega_r-\omega_s)^2 - \omega_t^2\Big]} \\ &+ \Big[A_e(\zeta_{r,s}^{(a)})^2 + B_e(\zeta_{r,s}^{(b)})^2 + C_e(\zeta_{r,s}^{(c)})^2\Big]\Big(\frac{\omega_r}{\omega_s} + \frac{\omega_s}{\omega_r}\Big)\end{aligned} \tag{4.9}$$

for the off-diagonal elements. Here, ϕ_{rrss} represents the quartic force constant in terms of dimensionless normal coordinates, and $\zeta_{(r,s)}^{(b)}$ denotes the Coriolis interaction constants. When

either of the following relationships is satisfied accidentally for an asymmetric top molecule, $2\omega_r \approx \omega_s$ and $\phi_{rrs} \neq 0$; $\omega_r + \omega_s \approx \omega_t$ and $\phi_{rst} \neq 0$, the quantities χ_{rr} [Eq. (8)] and χ_{rs} [Eq. (9)] may become indefinitely large and the perturbation theory may fail. Indeed, strong Fermi resonances have been identified as follows: Si_2CH_2: $2\omega_4 \approx \omega_3$, $2\omega_9 \approx \omega_2$, and $\omega_4 + \omega_8 \approx \omega_7$; $^{29}Si_2CH_2$: $2\omega_4 \approx \omega_3$ and $2\omega_9 \approx \omega_2$; $^{29}Si_2CD_2$: $2\omega_4 \approx \omega_3$; $Si_2{}^{13}CH_2$: $2\omega_4 \approx \omega_3$, $2\omega_9 \approx \omega_2$, $\omega_8 + \omega_9 \approx \omega_2$, and $\omega_4 + \omega_8 \approx \omega_7$. In such situations, the terms involving the resonances may be deleted following Nielsen's treatments.[42] The anharmonic vibrational constants (χ_{rs}) with cutoff of the Fermi resonances being 20 cm^{-1} for the six isotopologues are reported in Table 4.3, and the deperturbed vibrational frequencies are presented in Tables 4.4–4.9.

The anharmonic vibrational corrections for certain modes, specifically the SiH (SiD) s-stretching (ω_2, a_1) and SiH (SiD) bending (ω_7, b_2) modes, are more than 5% with respect to the corresponding harmonic vibrational frequencies, which are significantly larger than those for the tightly bound vibrations (see below). In order to partially compensate this inherent shortcoming of the VPT2 theory, the anharmonic frequencies with the assignment of χ_{72} (anharmonic vibrational coupling constants between the ω_2 and ω_7 modes) to zero are included in brackets as well.

4.4.6 Harmonic and Fundamental Vibrational Frequencies

In Tables 4.4–4.9 harmonic and fundamental vibrational frequencies and associated infrared (IR) intensities obtained at the CCSD(T)/cc-pCVQZ level of theory are given for the standard Si_2CH_2 and its five isotopologues species. These IR intensities are computed within the double harmonic approximation. The increase of all nine harmonic vibrational frequencies for the standard Si_2CH_2 with the cc-pCVQZ basis set in Table 4.4 are observed relative to those with the cc-pVQZ basis set[33,60] due to the shortening of bond lengths. The CH stretching and SiH symmetric stretching modes exhibit the highest frequencies among the nine modes. Moreover, the IR intensity of the ω_7 (b_2) mode is extraordinarily strong compared to the other eight modes, since it corresponds to a SiH bending (SiH a-stretch) motion with a large

change in dipole moment. The deviations of the fundamental frequencies with respect to the harmonic frequencies for the ω_2 (a_1, SiH s-str.) and ω_7 (b_2, SiH a-str. or SiH bend) modes of the standard Si_2CH_2 are 5.7 and 5.1%, respectively, which are likely to be a consequence of the H-bridged structure. The adjustment of χ_{72} to zero dramatically reduces the discrepancies between the harmonic and fundamental vibrational frequencies for the two modes to 3.6 and 2.5%, respectively (in brackets in Table 4.4). It is predicted that the anharmonic vibrational correction for the ω_9 (b_2, CH bend) mode is also substantial, 5.4%. For the other two undeuterated species, $^{29}Si_2CH_2$ (Table 4.6) and $Si_2{}^{13}CH_2$ (Table 4.8), the anharmonic vibrational features similar to the standard Si_2CH_2 have been predicted.

As shown in Table 4.5, the deviations of the fundamental frequencies relative to the harmonic frequencies for the ω_2 (a_1, SiD s-str.) and ω_7 (b_2, SiD a-str. or SiD bend) modes of the dideuterated isotopologue (Si_2CD_2-**1S**) are again relatively large, 5.2 and 5.3%, respectively, owing to the H(D)-bridged structure. By setting the χ_{72} constant to zero, the anharmonic vibrational corrections of the two modes are reduced to 4.5 and 4.6%, respectively (in brackets in Table 4.5). It is noted that the anharmonic vibrational correction for the ω_8 (b_2, SiC a-str.) mode is also quite large, 5.3%, probably due to its strong mixing with the ω_7 mode. For the other two deuterated species, $^{29}Si_2CD_2$ (in Table 4.7) and $Si_2{}^{13}CD_2$ (in Table 4.9), the anharmonic vibrational corrections are predicted in a manner similar to the Si_2CD_2-**1S** species.

In Table 4.10 theoretical isotopic shifts of harmonic and anharmonic vibrational frequencies for Si_2CD_2, $^{29}Si_2CH_2$, and $Si_2{}^{13}CH_2$ with respect to the standard Si_2CH_2 are summarized. Upon deuteration the six vibrational modes involving the H atoms, [ω_1 (a_1 CD str.), ω_2 (a_1, SiD s-str.), ω_5 (b_1, CD oop bend), ω_6 (b_1, SiD oop bend), ω_7 (b_2, SiD ip bend), and ω_9 (b_2, CD ip bend)] are dramatically red-shifted (in Tables 4.5, 4.7, and 4.9), as expected. Moreover, the corresponding IR intensities for most of the modes are reduced as well, especially for the SiH bending mode (318.7 $\rightarrow$ 210.0 km mol^{-1}) (in Table 4.5). In the case of ^{29}Si labelled isotopologue (in Table 4.6), all of the modes associated with the heavier isotopic substitution

are only slightly shifted. The largest red-shift of the SiSi stretching mode is estimated to be about 7.2 cm^{-1}. As for the ^{13}C labelled isotopologue (in Table 4.8), a considerable red-shift of the frequencies for the modes involving ^{13}C is observed. The SiC symmetric stretch mode (ω_8, b_2) yields the greatest red-shift, 15.5 cm^{-1}.

4.5 Conclusions

In the current research the equilibrium geometry and accurate quartic force field for the disilacyclopropenylidene (Si_2CH_2) molecule are obtained at the CCSD(T)/cc-pCVQZ level of theory. The analysis for the anharmonic force field has been carried out employing vibrational second-order perturbation theory (VPT2). The rotational constants for Si_2CH_2 and its D, ^{13}C, and ^{29}Si labelled isotopologues have been determined taking into account the vibration rotation interaction and centrifugal distortion contributions. The anharmonicity of the vibrational motions involving the H-bridged bonds is observed to be higher than for the more conventional vibrations. The present research should assist in the future detection of disilacyclopropenylidene with the high resolution spectroscopy.

4.6 Acknowledgments

We thank Dr. M. C. McCarthy at the Harvard-Smithsonian Center for Astrophysics and the School of Engineering and Applied Science, Harvard University and Dr. F. Tamassia in the Dipartimento di Chimica Fisica e Inorganica, Università di Bologna for their suggestion to initiate this research. We also acknowledge Dr. Q.-Y. Wu for many helpful discussions. This research was supported by the U.S. Department of Energy, Office of Basic Energy Sciences, Grant No. DE-FG02-97-ER14748 and used resources of the National Energy Research Scientific Computing Center (NERSC), which is supported by the Office of Science of the U.S. Department of Energy under Contract No. DE-AC02-05CH11231.

4.7 References

[1] Demyk, K.; Dartois, E.; Wiesemeyer, H.; Jones, A. P.; d'Hendecourt, L. *Astron. Astrophys.* **2000**, *364*, 170

[2] McCarthy, M. C.; Gottlieb, C. A.; Thaddeus, P. *Mol. Phys.* **2003**, *101*, 697

[3] Thaddeus, P.; Cummins, S. E.; Linke, R. A. *Astrophys. J.* **1984**, *283*, L45

[4] Cernicharo, J.; Gottlieb, C. A.; Guélin, M.; Thaddeus, P.; Vrtilek, J. M. *Astrophys. J.* **1989**, *341*, L25

[5] Ohishi, M.; Kaifu, N.; Kawaguchi, K.; Murakami, A.; Saito, S.; Yamamoto, S.; Ishikawa, S.; Fujita, Y.; Shiratori, Y.; Irvine, W. M. *Astrophys. J.* **1989**, *345*, L83

[6] Turner, B. E. *Astrophys. J.* **1992**, *388*, L35

[7] MacKay, D. D. S.; Charnley, S. B. *Mon. Not. Roy. Astron. Soc.* **1999**, *302*, 793

[8] Apponi, A. J.; McCarthy, M. C.; Gottlieb, C. A.; Thaddeus, P. *Astrophys. J.* **1999**, *516*, L103

[9] Guélin, M.; Muller, S.; Cernicharo, J.; Apponi, A. J.; McCarthy, M. C.; Gottlieb, C. A.; Thaddeus, P. *Astron. Astrophys.* **2000**, *363*, L9

[10] Guélin, M.; Muller, S.; Cernicharo, J.; McCarthy, M. C.; Thaddeus, P. *Astron. Astrophys.* **2004**, *426*, L49

[11] Maier, J. P.; Walker, G. A. H.; Bohlender, D. A.; Mazzotti, F. J.; Raghunandan, R.; Fulara, J.; Garkusha, I.; Nagy, A. *Astrophys. J.* **2011**, *726*, 41

[12] Oka, T.; McCall, B. J. *Science* **2011**, *331*, 293

[13] Maier, G.; Reisenauer, H. P.; Pacl, H. *Angew. Chem.Int. Edit.* **1994**, *33*, 1248

[14] Maier, G.; Pacl, H.; Reisenauer, H. P.; Meudt, A.; Janoschek, R. *J. Am. Chem. Soc.* **1995**, *117*, 12712

[15] Frenking, G.; Remington, R. B.; Schaefer, H. F. *J. Am. Chem. Soc.* **1986**, *108*, 2169

[16] Talbi, D. *Chem. Phys.* **2005**, *313*, 17

[17] Maier, G.; Reisenauer, H. P.; Egenolf, H. *Eur. J. Org. Chem.* **1998**, 1313

[18] Izuha, M.; Yamamoto, S.; Saito, S. *Can. J. Phys.* **1994**, *72*, 1206

[19] Francisco, J. S.; Kurz, C.; McDouall, J. J. W. *Chem. Phys. Lett.* **1989**, *162*, 79

[20] McDouall, J. J. W.; Schlegel, H. B.; Francisco, J. S. *J. Am. Chem. Soc.* **1989**, *111*, 4622

[21] Su, M. D.; Amos, R. D.; Handy, N. C. *J. Am. Chem. Soc.* **1990**, *112*, 1499

[22] Apeloig, Y.; Karni, M.; West, R.; Welsh, K. *J. Am. Chem. Soc.* **1994**, *116*, 9719

[23] Largo, A.; Barrientos, C. *J. Phys. Chem.* **1994**, *98*, 3978

[24] Ketvirtis, A. E.; Bohme, D. K.; Hopkinson, A. C. *J. Phys. Chem.* **1995**, *99*, 16121

[25] Vacek, G.; Colegrove, B. T.; Schaefer, H. F. *J. Am. Chem. Soc.* **1991**, *113*, 3192

[26] Sherrill, C. D.; Brandow, C. G.; Allen, W. D.; Schaefer, H. F. *J. Am. Chem. Soc.* **1996**, *118*, 7158

[27] Ikuta, S.; Saitoh, T.; Wakamatsu, S. *J. Chem. Phys.* **2004**, *121*, 3478

[28] Kassaee, M. Z.; Musavi, S. M.; Buazar, F.; Ghambarian, M. *J. Mol. Struct.* **2005**, *722*, 151

[29] Kassaee, M. Z.; Musavi, S. M.; Ghambarian, M. *Heteroatom Chem.* **2007**, *18*, 283

[30] Zdetsis, A. D. *J. Phys. Chem. A* **2008**, *112*, 5712

[31] Thorwirth, S.; Harding, M. E. *J. Chem. Phys.* **2009**, *130*, 214303

[32] Takahashi, M.; Sakamoto, K. *J. Phys. Chem. A* **2004**, *108*, 7301

[33] Wu, Q. Y.; Hao, Q.; Yamaguchi, Y.; Li, Q. S.; Fang, D.-C.; Schaefer, H. F. *J. Phys. Chem. A* **2010**, *114*, 7102

[34] Jemmis, E. D.; Prasad, B. V.; Tsuzuki, S.; Tanabe, K. *J. Phys. Chem.* **1990**, *94*, 5530

[35] Ikuta, S.; Wakamatsu, S. *J. Mol. Struct.* **2004**, *680*, 181

[36] Raghavachari, K.; Trucks, G. W.; Pople, J. A.; Head-Gordon, M. *Chem. Phys. Lett.* **1989**, *157*, 479

[37] Bartlett, R. J.; Watts, J. D.; Kucharski, S. A.; Noga, J. *Chem. Phys. Lett.* **1990**, *165*, 513

[38] Bartlett, R. J.; Watts, J. D.; Kucharski, S. A.; Noga, J. *Chem. Phys. Lett.* **1990**, *167*, 609

[39] Dunning, T. H. *J. Chem. Phys.* **1989**, *90*, 1007

[40] Woon, D. E.; Dunning, T. H. *J. Chem. Phys.* **1995**, *103*, 4572

[41] Peterson, K. A.; Dunning, T. H. *J. Chem. Phys.* **2002**, *117*, 10548

[42] Nielsen, H. H. *Rev. Mod. Phys.* **1951**, *23*, 90

[43] Watson, J. K. G. In *Vibrational Spectra and Structure*; Durig, J. R., Ed.; Elsevier, Amsterdam, 1997; Vol. 6; pp 1–89

[44] Mills, I. M. In *Molecular Spectroscopy: Modern Research*; Rao, K. N., Mathews, C. W., Eds.; Academic, New York, 1972; pp 115–140

[45] Papoušĕk, D.; Aliev, M. R. *Molecular Vibrational-Rotational Spectra*; Elsevier, Amsterdam, 1982

[46] Clabo, D. A.; Allen, W. D.; Remington, R. B.; Yamaguchi, Y.; Schaefer, H. F. *Chem. Phys.* **1988**, *123*, 187

[47] Allen, W. D.; Yamaguchi, Y.; Császár, A. G.; Clabo, D. A.; Remington, R. B.; Schaefer, H. F. *Chem. Phys.* **1990**, *145*, 427

[48] Aarset, K.; Császár, A. G.; Sibert, E. L.; Allen, W. D.; Schaefer, H. F.; Klopper, W.; Noga, J. *J. Chem. Phys.* **2000**, *112*, 4053

[49] J. F. Stanton, J. Gauss, J. D. Watts *et al.*, ACESII Mainz-Austin-Budapest version. For current version see http://www.aces2.de.

[50] H.-J. Werner, P. J. Knowles, R. Lindh, F. R. Manby, M. Schütz *et al.*, *MOLPRO*, version 2006.1 (a package of *ab initio* programs); see http://www.molpro.net.

[51] J. J. Wilke and H. F. Schaefer, GRENDEL++ (General energy derivatives for electron structure) is a C++ code for the computation of high-order energy derivatives from finite difference formulae for use in anharmonic vibrational analysis. http://www.ccc.uga.edu/ jjwilke/grendel.

[52] INTDER2005 is a general program developed by Wesley D. Allen which performs various vibrational analyses and higher-order nonlinear transformation among force field representations.

[53] Allen, W. D.; Császár, A. G. *J. Chem. Phys.* **1993**, *98*, 2983

[54] Allen, W. D.; Császár, A. G.; Szalay, V.; Mills, I. M. *Mol. Phys.* **1996**, *89*, 1213

[55] ANHARM is a FORTRAN vibrational anharmonicity program for VPT2 analysis written by Y. Yamaguchi and H. F. Schaefer. Center for Computational Quantum Chemistry, University of Georgia, Athens, GA.

[56] East, A. L. L.; Johnson, C. S.; Allen, W. D. *J. Chem. Phys.* **1993**, *98*, 1299

[57] See discussion in G. W. King, R. M. Hainer, and P. C. Cross, J. Chem. Phys. **11**, 27 (1943).

[58] Nielsen, H. H. *Phys. Rev.* **1941**, *60*, 794

[59] Nielsen, H. H. *Phys. Rev.* **1945**, *68*, 181

[60] In Table 1 of reference 33, the assignment of the SiC a-stretch and CH bend for Si_2CH_2-1**S** should be reversed.

Table 4.1: Theoretical Prediction of Vibration-Rotation Coupling Constants (in MHz) for Disilacyclopropenylidene (Si_2CH_2-**1S**) and its Five Isotopologues at the cc-pCVQZ CCSD(T) Level of Theory.

	Si_2CH_2	Si_2CD_2	$^{29}Si_2CH_2$	$^{29}Si_2CD_2$	$Si_2{}^{13}CH_2$	$Si_2{}^{13}CD_2$
Rotational Constants						
A_e	23659.8	18360.2	23546.5	18285.5	22594.4	17724.8
B_e	5650.6	5650.6	5455.7	5455.7	5650.6	5650.6
C_e	4561.3	4320.8	4429.4	4202.0	4520.2	4284.7
A_0	23619.0	18296.8	23506.5	18222.9	22561.3	17667.4
B_0	5593.5	5606.5	5400.7	5413.3	5593.8	5606.7
C_0	4517.3	4286.5	4386.8	4168.7	4477.2	4251.1
Quartic Centrifugal Distortion Constants						
$S(I^r)$ reduction						
10^3D_J	2.407	2.228	2.264	2.097	2.374	2.203
10^3D_{JK}	-5.380	-2.118	-5.339	-2.167	-4.933	-2.071
10^3D_K	86.158	40.407	85.625	40.348	79.784	38.373
10^3d_1	-0.592	-0.659	-0.544	-0.606	-0.606	-0.669
10^3d_2	-0.053	-0.076	-0.047	-0.068	-0.056	-0.079
$A(I^r)$ reduction						
$10^3\Delta_J$	2.513	2.380	2.359	2.234	2.486	2.360
$10^3\Delta_K$	86.688	41.170	86.099	41.032	80.347	39.162
$10^3\Delta_{JK}$	-6.016	-3.034	-5.908	-2.989	-5.609	-3.018
$10^3\delta_K$	7.227	6.177	6.963	5.913	7.065	5.931
$10^3\delta_J$	0.592	0.659	0.544	0.606	0.606	0.669

Table 4.2: Theoretical Prediciton of Rotational Constants (in MHz) and Quartic Centrifugal Distortion Constants (in MHz) for Disilacyclopropenylidene (Si_2CH_2-**1S**) and its Five Isotopologues at the cc-pCVQZ CCSD(T) Level of Theory.

	Si_2CH_2	Si_2CD_2	$^{29}Si_2CH_2$	$^{29}Si_2CD_2$	$Si_2{}^{13}CH_2$	$Si_2{}^{13}CD_2$
Rotational Constants						
A_e	23659.8	18360.2	23546.5	18285.5	22594.4	17724.8
B_e	5650.6	5650.6	5455.7	5455.7	5650.6	5650.6
C_e	4561.3	4320.8	4429.4	4202.0	4520.2	4284.7
A_0	23619.0	18296.8	23506.5	18222.9	22561.3	17667.4
B_0	5593.5	5606.5	5400.7	5413.3	5593.8	5606.7
C_0	4517.3	4286.5	4386.8	4168.7	4477.2	4251.1
Quartic Centrifugal Distortion Constants						
$S(I^r)$ reduction						
10^3D_J	2.407	2.228	2.264	2.097	2.374	2.203
10^3D_{JK}	-5.380	-2.118	-5.339	-2.167	-4.933	-2.071
10^3D_K	86.158	40.407	85.625	40.348	79.784	38.373
10^3d_1	-0.592	-0.659	-0.544	-0.606	-0.606	-0.669
10^3d_2	-0.053	-0.076	-0.047	-0.068	-0.056	-0.079
$A(I^r)$ reduction						
$10^3\Delta_J$	2.513	2.380	2.359	2.234	2.486	2.360
$10^3\Delta_K$	86.688	41.170	86.099	41.032	80.347	39.162
$10^3\Delta_{JK}$	-6.016	-3.034	-5.908	-2.989	-5.609	-3.018
$10^3\delta_K$	7.227	6.177	6.963	5.913	7.065	5.931
$10^3\delta_J$	0.592	0.659	0.544	0.606	0.606	0.669

Table 4.3: Theoretical Prediction of Anharmonic Vibrational Constants (in cm^{-1}) for Disilacyclopropenylidene (Si_2CH_2-**1S**) and its Five Isotopologues at the cc-pCVQZ CCSD(T) Level of Theory.

	Si_2CH_2	Si_2CD_2	$^{29}Si_2CH_2$	$^{29}Si_2CD_2$	$Si_2{}^{13}CH_2$	$Si_2{}^{13}CD_2$
χ_{11}	-58.661	-31.468	-58.662	-31.470	-58.314	-31.152
χ_{21}	-3.82	-2.217	-3.820	-2.219	-3.779	-2.155
χ_{22}	-16.112	-7.608	-16.102	-7.602	-16.167	-7.741
χ_{31}	-1.855	-1.798	-1.861	-1.800	-1.734	-1.632
χ_{32}	-4.842	-4.584	-4.868	-4.587	-4.676	-4.261
χ_{33}	-2.267	-2.104	-2.252	-2.091	-2.126	-1.999
χ_{41}	-1.828	-1.435	-1.791	-1.405	-1.829	-1.421
χ_{42}	-2.662	-2.172	-2.629	-2.164	-2.714	-2.197
χ_{43}	-2.622	-2.269	-2.560	-1.969	-2.499	-2.059
χ_{44}	-0.332	-0.295	-0.318	-0.339	-0.339	-0.333
χ_{51}	-11.691	-7.229	-11.696	-7.234	-11.502	-6.977
χ_{52}	2.974	3.583	2.953	3.526	2.674	3.429
χ_{53}	-3.333	-4.117	-3.326	-4.069	-3.152	-3.578
χ_{54}	-0.218	-0.05	-0.216	-0.048	-0.244	-0.065
χ_{55}	-1.529	-1.132	-1.533	-1.135	-1.453	-1.078
χ_{61}	-6.862	-3.504	-6.853	-3.495	-6.882	-3.508
χ_{62}	6.655	4.884	6.620	4.818	6.505	4.808
χ_{63}	-2.661	-2.815	-2.665	-2.751	-2.424	-2.381
χ_{64}	-2.312	-1.738	-2.262	-1.705	-2.304	-1.733
χ_{65}	-13.874	-6.215	-13.831	-6.178	-13.876	-6.719
χ_{66}	2.606	1.155	2.601	1.145	2.587	1.184
χ_{71}	-2.854	2.104	-2.876	2.028	-2.991	1.355
χ_{72}	-65.046	-15.067	-65.146	-15.262	-66.968	-17.282
χ_{73}	-7.112	-7.016	-7.211	-7.005	-6.586	-6.372
χ_{74}	34.089	-15.797	31.958	-16.636	21.789	-15.202
χ_{75}	-11.685	-4.076	-11.696	-4.093	-11.896	-4.266
χ_{76}	-16.426	-5.997	-16.439	-6.033	-16.543	-6.354
χ_{77}	-24.097	-6.339	-24.127	-6.379	-24.705	-6.891
χ_{81}	-7.03	0.158	-9.447	0.261	-14.447	0.172
χ_{82}	-18.266	-37.94	-5.557	-37.926	-8.253	-35.751
χ_{83}	-5.043	-3.144	-4.479	-3.071	-2.771	-3.350
χ_{84}	-1.689	-3.447	-5.303	-3.151	-0.075	-2.820
χ_{85}	-2.035	-6.255	-0.967	-6.242	0.682	-5.915
χ_{86}	-2.902	-4.613	-2.532	-4.559	-1.029	-4.128
χ_{87}	1.708	-20.053	5.347	-20.179	-2.863	-18.405
χ_{88}	-1.449	-0.453	-1.689	-0.418	-0.392	-0.163
χ_{91}	-6.164	-7.671	-3.725	-7.724	1.185	-7.519
χ_{92}	-29.648	-31.924	-21.451	-31.806	-21.155	-35.709
χ_{93}	-0.684	-1.141	-1.073	-1.120	-2.927	-0.937
χ_{94}	-50.471	5.861	-44.386	6.659	-39.762	4.670
χ_{95}	-5.526	-0.232	-6.562	-0.213	-7.902	-0.289
χ_{96}	1.114	0.062	0.764	0.056	-0.433	0.128
χ_{97}	34.513	-13.472	28.608	-14.136	29.082	-12.252
χ_{98}	8.446	-0.547	-0.907	-0.518	-6.096	-0.041
χ_{99}	-9.355	3.695	-9.620	3.718	-7.267	4.352

Table 4.4: Theoretical Prediction of the Harmonic and Anharmonic (Fundamental) Vibrational Frequencies (in cm^{-1}), and IR Intensities (in km mol^{-1}, in parentheses) for the Standard Disilacyclopropenylidene (Si_2CH_2-**1S**) Molecule at the cc-pCVQZ CCSD(T) Level of Theory.

Normal modes (assignment)	harmonic	Δ(anh.-harm.)[a]	anharmonic[a]
1 (a_1) CH str	3259.6(1.8)	-138.4	3121.3
2 (a_1) SiH s-str	1566.4(9.2)	-89.6[-57.0]	1476.9[1509.4]
3 (a_1) SiC s-str	897.9(15.6)	-18.6	879.3
4 (a_1) SiSi str	448.0(0.9)	-14.5	433.5
5 (b_1) CH oop bend	894.8(10.9)	-25.8	869.1
6 (b_1) SiH oop bend	497.1(18.8)	-13.4	483.6
7 (b_2) SiH a-str	1263.8(318.7)	-64.6[-32.1]	1199.2[1231.8]
8 (b_2) SiC a-str	802.1(6.2)	-16.3	785.8
9 (b_2) CH ip bend	789.6(6.2)	-42.9	746.7

[a] The Δ(anh.-harm.) and anharmonic frequencies with the adjustment of χ_{72} to zero are given in brackets. See text for discussion.

Table 4.5: Theoretical Prediction of the Harmonic and Anharmonic (Fundamental) Vibrational Frequencies (in cm^{-1}), and IR Intensities (in km mol^{-1}, in parentheses) for the Dideuterodisilacyclopropenylidene (Si_2CD_2-**1S**) Molecule at the cc-pCVQZ CCSD(T) Level of Theory.

Normal modes (assignment)	harmonic	Δ(anh.-harm.)[a]	anharmonic[a]
1 (a_1) CD str	2408.4(2.8)	-73.7	2334.7
2 (a_1) SiD s-str	1121.0(3.0)	-57.9[-50.4]	1063.1[1070.6]
3 (a_1) SiC s-str	864.6(15.1)	-17.7	846.9
4 (a_1) SiSi str	446.6(0.9)	-11.1	435.5
5 (b_1) CD oop bend	654.7(7.8)	-14.6	640.1
6 (b_1) SiD oop bend	391.4(10.2)	-7.7	383.8
7 (b_2) SiD a-str	984.5(210.0)	-52.4[-44.8]	932.1[939.7]
8 (b_2) SiC a-str	737.6(0.9)	-38.8	698.8
9 (b_2) CD ip bend	574.8(0.1)	-17.1	557.7

[a] The Δ(anh.-harm.) and anharmonic frequencies with the adjustment of χ_{72} to zero are given in brackets. See text for discussion.

Table 4.6: Theoretical Prediction of the Harmonic and Anharmonic (Fundamental) Vibrational Frequencies (in cm^{-1}), and IR Intensities (in km mol^{-1}, in parentheses) for the ^{29}Si Labelled Disilacyclopropenylidene ($^{29}Si_2CH_2$-**1S**) Molecule at the cc-pCVQZ CCSD(T) Level of Theory.

Normal modes (assignment)	harmonic	Δ(anh.-harm.)[a]	anharmonic[a]
1 (a_1) CH str	3259.7(1.7)	-138.4	3121.3
2 (a_1) SiH s-str	1566.2(9.1)	-79.2[-46.6]	1487.1[1519.6]
3 (a_1) SiC s-str	893.7(15.5)	-18.5	875.1
4 (a_1) SiSi str	440.8(0.9)	-14.2	426.6
5 (b_1) CH oop bend	894.7(11.0)	-25.7	869.0
6 (b_1) SiH oop bend	496.6(18.8)	-13.4	483.2
7 (b_2) SiH a-str	1262.7(317.6)	-67.0[-34.4]	1195.7[1228.3]
8 (b_2) SiC a-str	798.3(4.6)	-15.3	783.0
9 (b_2) CH ip bend	789.1(7.9)	-43.6	745.4

[a] The Δ(anh.-harm.) and anharmonic frequencies with the adjustment of χ_{72} to zero are given in brackets. See text for discussion.

Table 4.7: Theoretical Prediction of the Harmonic and Anharmonic (Fundamental) Vibrational Frequencies (in cm^{-1}), and IR Intensities (in km mol^{-1}, in parentheses) for the ^{29}Si Labelled Dideuterodisilacyclopropenylidene ($^{29}Si_2CD_2$-**1S**) Molecule at the cc-pCVQZ CCSD(T) Level of Theory.

Normal modes (assignment)	harmonic	Δ(anh.-harm.)[a]	anharmonic[a]
1 (a_1) CD str	2408.4(2.8)	-73.7	2334.6
2 (a_1) SiD s-str	1120.8(2.9)	-58.0[-50.4]	1062.8[1070.4]
3 (a_1) SiC s-str	860.1(15.0)	-17.4	842.7
4 (a_1) SiSi str	439.5(0.9)	-10.9	428.6
5 (b_1) CD oop bend	654.6(7.8)	-14.5	640.1
6 (b_1) SiD oop bend	390.7(10.1)	-7.6	383.1
7 (b_2) SiD a-str	982.0(209.2)	-53.4[-45.8]	928.5[936.2]
8 (b_2) SiC a-str	734.7(0.7)	-38.5	696.2
9 (b_2) CD ip bend	574.2(0.1)	-17.0	557.3

[a] The Δ(anh.-harm.) and anharmonic frequencies with the adjustment of χ_{72} to zero are given in brackets. See text for discussion.

Table 4.8: Theoretical Prediction of the Harmonic and Anharmonic (Fundamental) Vibrational Frequencies (in cm^{-1}), and IR Intensities (in km mol^{-1}, in parentheses) for the ^{13}C Labelled Disilacyclopropenylidene ($Si_2{}^{13}CH_2$-**1S**) Molecule at the cc-pCVQZ CCSD(T) Level of Theory.

Normal modes (assignment)	harmonic	Δ(anh.-harm.)[a]	anharmonic[a]
1 (a_1) CH str	3248.9(1.6)	-137.6	3111.3
2 (a_1) SiH s-str	1565.6(9.4)	-81.5[-48.0]	1484.1[1517.6]
3 (a_1) SiC s-str	874.9(14.5)	-17.6	857.2
4 (a_1) SiSi str	446.6(1.0)	-14.5	432.1
5 (b_1) CH oop bend	892.7(10.6)	-25.5	867.2
6 (b_1) SiH oop bend	493.3(18.7)	-13.3	480.0
7 (b_2) SiH a-str	1259.9(313.1)	-77.9[-44.4]	1182.0[1215.5]
8 (b_2) SiC a-str	797.7(1.1)	-18.2	779.5
9 (b_2) CH ip bend	774.1(12.2)	-38.5	735.5

[a] The Δ(anh.-harm.) and anharmonic frequencies with the adjustment of χ_{72} to zero are given in brackets. See text for discussion.

Table 4.9: Theoretical Prediction of the Harmonic and Anharmonic (Fundamental) Vibrational Frequencies (in cm^{-1}), and IR Intensities (in km mol^{-1}, in parentheses) for the ^{13}C Labelled Dideuterodisilacyclopropenylidene ($Si_2{}^{13}CD_2$-**1S**) Molecule at the cc-pCVQZ CCSD(T) Level of Theory.

Normal modes (assignment)	harmonic	Δ(anh.-harm.)[a]	anharmonic[a]
1 (a_1) CD str	2392.2(2.4)	-73.1	2319.0
2 (a_1) SiD s-str	1119.3(3.3)	-60.0[-51.4]	1059.3[1067.9]
3 (a_1) SiC s-str	845.9(14.1)	-16.3	829.7
4 (a_1) SiSi str	445.2(1.0)	-11.1	434.1
5 (b_1) CD oop bend	651.4(7.4)	-14.3	637.1
6 (b_1) SiD oop bend	387.3(10.2)	-7.6	379.7
7 (b_2) SiD a-str	971.9(205.9)	-53.2[-44.5]	918.8[927.4]
8 (b_2) SiC a-str	726.9(0.2)	-35.4	691.4
9 (b_2) CD ip bend	573.9(0.1)	-17.3	556.6

[a] The Δ(anh.-harm.) and anharmonic frequencies with the adjustment of χ_{72} to zero are given in brackets. See text for discussion.

Table 4.10: Theoretical Isotopic Shifts of Harmonic and Anharmonic Vibrational Frequencies (in cm^{-1}) for Si_2CD_2, $^{29}Si_2CH_2$, and $Si_2{}^{13}CH_2$ with Respect to Si_2CH_2 at the cc-pCVQZ CCSD(T) Level of Theory.

Modes (symmetry)	Si_2CD_2	$^{29}Si_2CH_2$	$Si_2{}^{13}CH_2$
$\Delta\omega_1(a_1)$ CH str	-851.2	0.0	-10.7
$\Delta\omega_2(a_1)$ SiH s-str	-445.4	-0.2	-0.8
$\Delta\omega_3(a_1)$ SiC s-str	-33.4	-4.2	-23.1
$\Delta\omega_4(a_1)$ SiSi str	-1.4	-7.2	-1.4
$\Delta\omega_5(b_1)$ CH oop bend	-240.1	-0.1	-2.1
$\Delta\omega_6(b_1)$ SiH oop bend	-105.7	-0.5	-3.8
$\Delta\omega_7(b_2)$ SiH a-str	-279.3	-1.2	-3.9
$\Delta\omega_8(b_2)$ SiC a-str	-64.5	-3.8	-4.4
$\Delta\omega_9(b_2)$ CH ip bend	-214.8	-0.6	-15.5
$\Delta\nu_1(a_1)$ CH str	-786.6	-0.0	-10.0
$\Delta\nu_2(a_1)$ SiH s-str	-413.8	+10.2	+7.2
$\Delta\nu_3(a_1)$ SiC s-str	-32.4	-4.2	-22.1
$\Delta\nu_4(a_1)$ SiSi str	+2.0	-6.9	-1.4
$\Delta\nu_5(b_1)$ CH oop bend	-228.9	-0.1	-1.9
$\Delta\nu_6(b_1)$ SiH oop bend	-99.9	-0.5	-3.7
$\Delta\nu_7(b_2)$ SiH a-str	-267.1	-3.6	-17.2
$\Delta\nu_8(b_2)$ SiC a-str	-87.0	-2.8	-6.3
$\Delta\nu_9(b_2)$ CH ip bend	-189.0	-1.2	-11.1

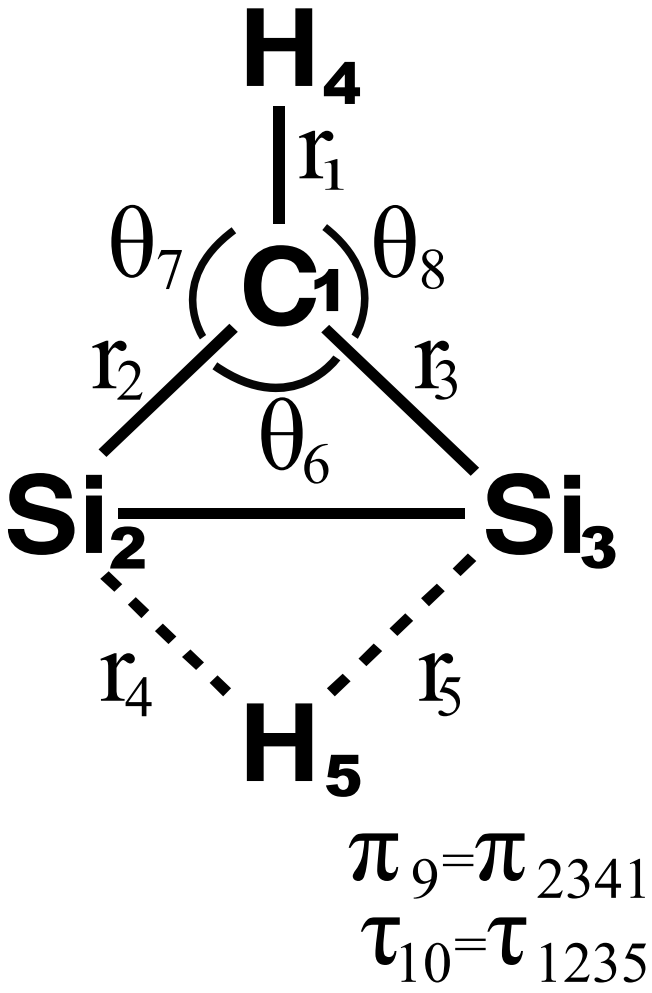

Figure 4.1: Simple internal coordinates for the disilacyclopropenylidene (Si_2CH_2-**1S**) structure.

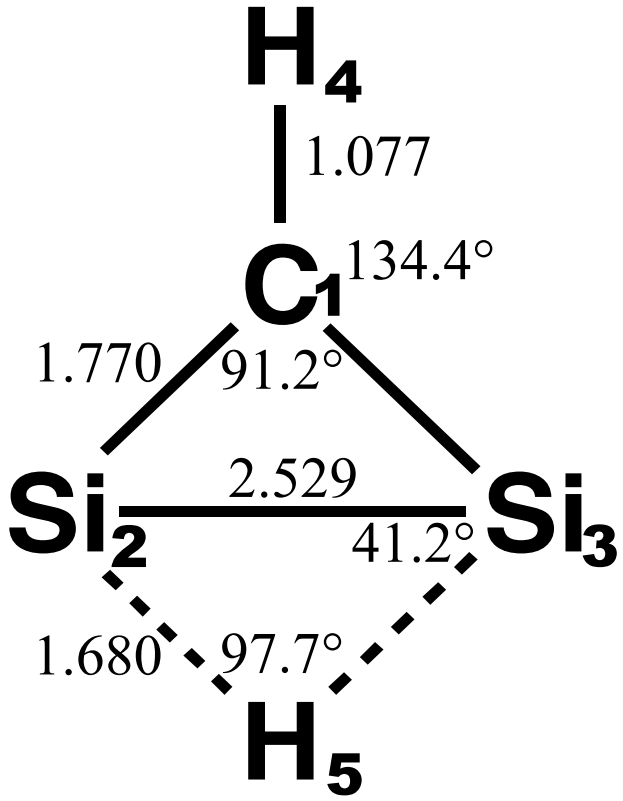

Figure 4.2: Predicted equilibrium geometry for the disilacyclopropenylidene (Si_2CH_2-**1S**) structure at the cc-pCVQZ CCSD(T) level of theory. Bond lengths are in Å.

Chapter 5

Summary and Conclusions

5.1 Conclusions

The first principles method, *ab initio* electronic structure theory, in computational quantum chemistry has been employed to carry out the present research. A variety of properties for targeted molecules have been predicted in the dissertation. The understanding of small molecules serves as a guide to future investigate large systems.

In the initial stage of our research, *trans*- and *cis*-HPPH diphosphene as well as planar PPH_2 diphosphinylidene have been studied using highly correlated *ab initio* electronic structure theory. Multireference wavefunctions were required to investigate the isomerization transition state between the *trans* and *cis* structures. The *trans-cis* isomerization transition state barrier is predicted to be 35.2 kcal mol^{-1} using the Mk-MRCCSD method. At the highest level of theory, aug-cc-pVTZ CCSD(T), the barrier for the isomerization transition state between *trans*-HPPH and planar PPH_2 is predicted to be 48.2 kcal mol^{-1}. The results for this unusual non-planar transition state should be of aid in understanding the nature of 1,2 hydrogen shifts for phosphorus compounds involving the PP double bond.

We proceeded to study the low-lying triplet states of diphosphene (HPPH) and disphosphinylidene (PPH_2) in order to better understand about the relevant excitation processes. It has been demonstrated that the theoretical computation of the six triplet state structurs is not very sensitive to reference wavefunctions (ROHF and UHF) and basis sets at higher levels of correlated methods, such as CCSD and CCSD(T). The *trans*- and *cis*-HPPH structures, which are minima on the ground singlet PES, become transition states on the triplet PES. These transition states connect two equivalent ^3B skewed structures; the lower barrier through ^3B_u *trans*-HPPH as transition state is estimated to be 9.1±0.3 kcal mol^{-1} using FPA plus three other corrections. The barrier between two equivalent $^3A''$ pyramidal PPH_2 via $^3A_2$ planar PPH_2 is determined to be 18.6±0.3 kcal mol^{-1}. The conversion of the two minima on the triplet PES (^3B skewed HPPH $\rightarrow$ $^3A''$ pyamidal PPH_2) can be accomplished via hydrogen migration with a barrier of 16.4±0.3 kcal mol^{-1}. The crossover of the singlet and triplet adiabatic potential energy surfaces is studied using the Mk-MRCC method combined

with the cc-pVQZ basis set. The ^3B skewed HPPH is estimated to be 1.4 kcal mol^{-1} lower than ^1A skewed HPPH transition state at the ^3B skewed HPPH optimized geometry.

In the chapter 4, the equilibrium geometry and accurate quartic force field for the disilacyclopropenylidene (Si_2CH_2-**1S**) molecule are obtained at the cc-pCVQZ CCSD(T) level of theory. The analysis for the anharmonic force field has been carried out employing vibrational second-order perturbation theory (VPT2). The rotational constants for Si_2CH_2 and its D, ^{13}C, and ^{29}Si labelled isotopologues have been determined taking into account the vibration rotation interaction and centrifugal distortion contributions. The anharmonicity of the vibrational motions involving the H-bridged bonds is observed to be higher than for the more conventional vibrations. The present research should assist in the future detection of disilacyclopropenylidene with the high resolution spectroscopy.

The present research has demonstrated that computational chemistry provides an effective means to make predictions of structures, energetics, vibrational frequencies, and other physical properties. Currently, the high accurate computations are limited within small molecules. In view of the development of the computing power and new methodologies, the application of *ab initio* approach may be extended to more practical systems.

Appendix A

Supplementary Material for Chapter 2

Table A.1: CI expansion coefficients ($|C_I| \geq 0.060$) of the aug-cc-pVQZ CASSCF wavefunctions for the six triplet structures at the aug-cc-pVQZ RCCSD(T) optimized geometries.

Structures	Configuration	CI coefficients
^3B_u *trans*-HPPH	$\Phi_1 : (core)(5a_g)^2(5b_u)^2(6b_u)^2(6a_g)^2(7a_g)^2(2a_u\alpha)(2b_g\alpha)$	0.970
	$\Phi_2 : (core)(5a_g)^2(5b_u)^2(6b_u)^2(6a_g)^2(2a_u\alpha)(2b_g\alpha)(7b_u)^2$	-0.116
	$\Phi_3 : (core)(5a_g)^2(5b_u)^2(6b_u)^2(6a_g)^2(7a_g\alpha)(2a_u)^2(7b_u\alpha)$	0.068
$^3B_2$ *cis*-HPPH	$\Phi_1 : (core)(5a_1)^2(5b_2)^2(6a_1)^2(6b_2)^2(7a_1)^2(2b_1\alpha)(2a_2\alpha)$	0.969
	$\Phi_2 : (core)(5a_1)^2(5b_2)^2(6a_1)^2(6b_2)^2(2b_1\alpha)(2a_2\alpha)(7b_2)^2$	-0.120
	$\Phi_3 : (core)(5a_1)^2(5b_2)^2(6a_1)^2(6b_2)^2(7a_1\alpha)(2b_1)^2(7b_2\alpha)$	0.070
	$\Phi_4 : (core)(5a_1)^2(5b_2)^2(6a_1)^2(7a_1)^2(2b_1\alpha)(2a_2\alpha)(8a_1)^2$	0.061
^3B skewed HPPH	$\Phi_1 : (core)(6a)^2(6b)^2(7b)^2(7a)^2(8a)^2(9a\alpha)(8b\alpha)$	0.971
	$\Phi_2 : (core)(6a)^2(6b)^2(7b)^2(7a)^2(9a\alpha)(8b\alpha)(9b)^2$	-0.078
$^3A''$ pyramidal PPH_2	$\Phi_1 : (core)(9a')^2(10a')^2(3a'')^2(11a')^2(12a')^2(4a''\alpha)(13a'\alpha)$	0.974
	$\Phi_2 : (core)(9a')^2(10a')^2(3a'')^2(11a')^2(4a''\alpha)(13a'\alpha)(14a')^2$	-0.083
	$\Phi_3 : (core)(9a')^2(10a')^2(11a')^2(12a')^2(4a''\alpha)(13a'\alpha)(5a'')^2$	-0.067
$^3A_2$ planar PPH_2	$\Phi_1 : (7a_1)^2(8a_1)^2(3b_2)^2(9a_1)^2(3b_1)^2(4b_2\alpha)(4b_1\alpha)$	0.973
	$\Phi_2 : (7a_1)^2(8a_1)^2(3b_2)^2(3b_1)^2(4b_2\alpha)(4b_1\alpha)(10a_1)^2$	-0.067
	$\Phi_3 : (7a_1)^2(8a_1)^2(3b_2)^2(9a_1\beta)(3b_1\alpha)(4b_2\alpha)(4b_1)^2(10a_1\alpha)$	-0.065
^3A transition state connecting	$\Phi_1 : (11a)^2(12a)^2(13a)^2(14a)^2(15a)^2(16a\alpha)(17a\alpha)$	0.961
pyramidal PPH_2 and skewed HPPH	$\Phi_2 : (11a)^2(12a)^2(13a)^2(14a\alpha)(15a)^2(16a\alpha)(17a\beta)(18a\alpha)$	0.085
	$\Phi_3 : (11a)^2(12a)^2(13a)^2(14a)^2(16a\alpha)(17a\alpha)(19a)^2$	-0.080
	$\Phi_4 : (11a)^2(12a)^2(13a)^2(15a)^2(16a\alpha)(17a\alpha)(18a)^2$	-0.070

Table A.2: Electron occupation numbers of the valence MOs of the aug-cc-pVQZ CASSCF wavefunctions at the aug-cc-pVQZ RCCSD(T) optimized geometries.

MO\ Structures	^3B_u *trans*-HPPH	$^3B_2$ *cis*-HPPH	^3B skewed HPPH	$^3A''$ pyramidal PPH_2	$^3A_2$ planar PPH_2	^3A transition state connecting pyramidal PPH_2 and skewed HPPH
11	$1.994(5a_g)$	$1.994(5a_1)$	$1.994(6a)$	$1.994(9a')$	$1.992(7a_1)$	1.998(11a)
12	$1.990(5b_u)$	$1.990(5b_2)$	$1.988(6b)$	$1.988(10a')$	$1.983(8a_1)$	1.991(12a)
13	$1.976(6b_u)$	$1.977(6a_1)$	$1.973(7b)$	$1.973(3a'')$	$1.975(3b_2)$	1.978(13a)
14	$1.973(6a_g)$	$1.973(6b_2)$	$1.974(7a)$	$1.979(11a')$	$1.967(9a_1)$	1.956(14a)
15	$1.958(7a_g)$	$1.958(7a_1)$	$1.967(8a)$	$1.972(12a')$	$1.984(3b_1)$	1.951(15a)
16	$1.005(2a_u)$	$1.005(2b_1)$	$1.004(9a)$	$1.001(4a'')$	$1.000(4b_2)$	1.005(16a)
17	$0.996(2b_g)$	$0.996(2a_2)$	$1.004(8b)$	$1.002(13a')$	$1.011(4b_1)$	1.001(17a)
18	$0.049(7b_u)$	$0.048(7b_2)$	$0.038(9b)$	$0.038(14a')$	$0.045(10a_1)$	0.052(18a)
19	$0.031(8b_u)$	$0.033(8a_1)$	$0.030(10a)$	$0.029(5a'')$	$0.022(5b_2)$	0.049(19a)
20	$0.028(8a_g)$	$0.027(8b_2)$	$0.029(10b)$	$0.024(15a')$	$0.021(11a_1)$	0.018(20a)
VMOs[a]	0.108	0.108	0.097	0.091	0.088	0.119

[a] A total electron occupation number in the virtual MOs.

Table A.3: Theoretical harmonic vibrational frequencies (in cm^{-1}) and zero point vibrational energies (ZPVE, in kcal mol^{-1}) for the ^3B_u *trans*-HPPH structure.

Theory	$\omega_1(a_g)$ sym PH stretch	$\omega_2(a_g)$ sym bend	$\omega_3(a_g)$ PP stretch	$\omega_4(a_u)$ torsion	$\omega_5(b_u)$ asym PH stretch	$\omega_6(b_u)$ asym bend	ZPVE
cc-pVDZ ROHF	2502	982	452	382i	2514	694	10.22
cc-pVTZ ROHF	2499	985	458	398i	2511	696	10.23
cc-pVQZ ROHF	2503	988	459	401i	2516	698	10.25
aug-cc-pVDZ ROHF	2499	978	454	386i	2511	694	10.21
aug-cc-pVTZ ROHF	2501	984	459	397i	2514	696	10.24
aug-cc-pVQZ ROHF	2504	988	460	400i	2517	698	10.25
cc-pVDZ RCCSD	2385	907	416	410i	2395	646	9.66
cc-pVTZ RCCSD	2391	915	432	446i	2402	650	9.72
cc-pVQZ RCCSD	2401	921	438	465i	2413	655	9.77
aug-cc-pVDZ RCCSD	2368	897	411	433i	2378	641	9.58
aug-cc-pVTZ RCCSD	2388	913	430	454i	2400	651	9.71
aug-cc-pVQZ RCCSD	2400	921	437	466i	2411	656	9.77
cc-pVDZ RCCSD(T)	2365	894	403	415i	2376	635	9.55
cc-pVTZ RCCSD(T)	2369	900	421	460i	2381	639	9.60
cc-pVQZ RCCSD(T)	2379	906	427	483i	2391	644	9.66
aug-cc-pVDZ RCCSD(T)	2347	882	397	441i	2357	630	9.46
aug-cc-pVTZ RCCSD(T)	2366	898	419	469i	2377	640	9.59
aug-cc-pVQZ RCCSD(T)	2377	905	426	486i	2388	645	9.65
aug-cc-pV(Q+d)Z RCCSD(T)	2381	908	427	489i	2393	646	9.67
aug-cc-pVQZ UHF	2500	986	461	355i	2512	696	10.23
aug-cc-pVTZ UCCSD	2389	914	431	453i	2400	651	9.70
aug-cc-pVTZ UCCSD(T)	2366	898	419	467i	2378	640	9.58

Table A.4: Theoretical dipole moments (μ_e, in debye), harmonic vibrational frequencies (in cm^{-1}), and zero point vibrational energies (ZPVE, in kcal mol^{-1}) for the $^3B_2$ *cis*-HPPH structure.

Theory		$\omega(a_1)$	$\omega_2(a_1)$	$\omega_3(a_1)$	$\omega_4(a_2)$	$\omega_5(b_2)$	$\omega_6(b_2)$	
	μ_e	sym PH stretch	sym bend	PP stretch	torsion	asym PH stretch	asym bend	ZPVE
cc-pVDZ ROHF	1.281	2524	744	446	458i	2505	904	10.19
cc-pVTZ ROHF	1.187	2524	739	453	469i	2505	903	10.19
cc-pVQZ ROHF	1.176	2528	741	453	473i	2509	904	10.21
aug-cc-pVDZ ROHF	1.198	2524	741	448	456i	2504	897	10.17
aug-cc-pVTZ ROHF	1.179	2526	739	453	470i	2506	900	10.19
aug-cc-pVQZ ROHF	1.172	2529	741	454	473i	2509	904	10.21
cc-pVDZ RCCSD	1.053	2402	691	407	473i	2385	818	9.59
cc-pVTZ RCCSD	1.014	2412	688	424	500i	2395	822	9.64
cc-pVQZ RCCSD	1.015	2423	696	430	516i	2406	827	9.70
aug-cc-pVDZ RCCSD	0.913	2389	683	402	489i	2371	799	9.50
aug-cc-pVTZ RCCSD	0.968	2409	690	422	506i	2392	819	9.63
aug-cc-pVQZ RCCSD	0.992	2421	697	429	516i	2404	827	9.69
cc-pVDZ RCCSD(T)	1.030	2382	679	394	476i	2365	801	9.47
cc-pVTZ RCCSD(T)	0.994	2390	675	412	508i	2374	803	9.52
cc-pVQZ RCCSD(T)	0.992	2400	683	418	527i	2384	808	9.57
aug-cc-pVDZ RCCSD(T)	0.883	2367	671	388	495i	2349	779	9.37
aug-cc-pVTZ RCCSD(T)	0.937	2386	677	410	515i	2369	800	9.50
aug-cc-pVQZ RCCSD(T)	0.964	2397	684	417	527i	2381	807	9.56
aug-cc-pV(Q+d)Z RCCSD(T)	0.958	2402	686	418	530i	2386	809	9.58
aug-cc-pVQZ UHF	1.169	2525	740	455	451i	2506	902	10.19
aug-cc-pVTZ UCCSD	0.968	2409	690	423	505i	2392	820	9.63
aug-cc-pVTZ UCCSD(T)	0.938	2386	677	410	515i	2370	800	9.50

Table A.5: Theoretical dipole moments (μ_e, in debye), harmonic vibrational frequencies (in cm^{-1}), infrared intensities (in parentheses, in km mol^{-1}), and zero point vibrational energies (ZPVE, in kcal mol^{-1}) for the ^3B skewed HPPH structure.

Theory		$\omega_1(a)$	$\omega_2(a)$	$\omega_3(a)$	$\omega_4(a)$	$\omega_5(b)$	$\omega_6(b)$	
	μ_e	sym PH stretch	sym bend	PP stretch	torsion	asym PH stretch	asym bend	ZPVE
cc-pVDZ ROHF	0.910	2492	761	462	411	2490	765	10.56
cc-pVTZ ROHF	0.856	2489	763	470	419	2488	764	10.58
cc-pVQZ ROHF	0.858	2493	765	471	421	2492	765	10.60
aug-cc-pVDZ ROHF	0.871	2489	761	464	409	2489	762	10.56
aug-cc-pVTZ ROHF	0.862	2491	763	470	417	2490	763	10.58
aug-cc-pVQZ ROHF	0.859	2493	765	471	420	2493	765	10.60
cc-pVDZ RCCSD	0.781	2372	687	436	431	2372	682	9.99
cc-pVTZ RCCSD	0.764	2375	688	454	447	2375	676	10.04
cc-pVQZ RCCSD	0.775	2383	693	464	455	2384	678	10.10
aug-cc-pVDZ RCCSD	0.701	2356	683	433	425	2355	673	9.91
aug-cc-pVTZ RCCSD	0.741	2372	689	453	445	2372	676	10.03
aug-cc-pVQZ RCCSD	0.762	2381	693	464	454	2381	678	10.09
cc-pVDZ RCCSD(T)	0.773	2350	673	439	425	2350	666	9.88
cc-pVTZ RCCSD(T)	0.759	2350	670	460	442	2350	655	9.91
cc-pVQZ RCCSD(T)	0.769	2357	674	472	450	2357	655	9.97
aug-cc-pVDZ RCCSD(T)	0.689	2331	667	434	421	2331	656	9.79
aug-cc-pVTZ RCCSD(T)	0.731	2345	671	459	441	2346	654	9.90
aug-cc-pVQZ RCCSD(T)	0.743	2354	675	471	449	2354	655	9.95
aug-cc-pV(Q+d)Z RCCSD(T)	0.759	2358	675	474	450	2359	655	9.98
aug-cc-pVQZ UHF	0.851	2491(51.2)	760(16.1)	468(0.4)	409(1.8)	2490(64.9)	760(25.4)	10.56
aug-cc-pVTZ UCCSD	0.741	2372(33.4)	689(9.9)	453(1.1)	445(0.0)	2372(43.4)	676(14.0)	10.02
aug-cc-pVTZ UCCSD(T)	0.731	2346(31.0)	672(8.8)	459(0.6)	441(0.6)	2346(40.6)	655(12.0)	9.89

Table A.6: Theoretical dipole moments (μ_e, in debye), harmonic vibrational frequencies (in cm^{-1}), infrared intensities (in parentheses, in km mol^{-1}), and zero point vibrational energies (ZPVE, in kcal mol^{-1}) for the $^3A''$ pyramidal PPH_2 structure.

Theory		$\omega_1(a')$	$\omega_2(a')$	$\omega_3(a')$	$\omega_4(a')$	$\omega_5(a'')$	$\omega_6(a'')$	
	μ_e	sym PH stretch	sym bend	wagging	PP stretch	asym PH stretch	asym bend	ZPVE
cc-pVDZ ROHF	0.847	2519	1188	738	460	2523	750	11.70
cc-pVTZ ROHF	0.827	2517	1191	735	468	2520	749	11.71
cc-pVQZ ROHF	0.838	2520	1193	736	469	2522	751	11.72
aug-cc-pVDZ ROHF	0.850	2513	1185	739	463	2518	748	11.68
aug-cc-pVTZ ROHF	0.845	2517	1190	734	468	2521	749	11.70
aug-cc-pVQZ ROHF	0.842	2520	1192	736	469	2522	751	11.72
cc-pVDZ RCCSD	0.760	2403	1105	667	427	2415	684	11.02
cc-pVTZ RCCSD	0.793	2405	1100	657	445	2415	684	11.03
cc-pVQZ RCCSD	0.825	2412	1097	654	453	2421	686	11.05
aug-cc-pVDZ RCCSD	0.721	2382	1096	655	424	2394	680	10.92
aug-cc-pVTZ RCCSD	0.787	2400	1096	654	444	2410	685	11.00
aug-cc-pVQZ RCCSD	0.816	2409	1097	653	452	2419	686	11.04
cc-pVDZ RCCSD(T)	0.758	2383	1093	654	418	2396	671	10.89
cc-pVTZ RCCSD(T)	0.799	2382	1084	639	437	2393	668	10.87
cc-pVQZ RCCSD(T)	0.834	2387	1079	635	445	2398	670	10.89
aug-cc-pVDZ RCCSD(T)	0.716	2360	1083	640	415	2373	666	10.78
aug-cc-pVTZ RCCSD(T)	0.789	2375	1079	636	436	2387	669	10.84
aug-cc-pVQZ RCCSD(T)	0.823	2384	1079	634	444	2395	670	10.88
aug-cc-pV(Q+d)Z RCCSD(T)	0.820	2388	1080	634	445	2399	670	10.89
aug-cc-pVQZ UHF	0.853	2515(42.4)	1189(24.9)	729(13.7)	467(1.8)	2518(53.7)	748(17.6)	11.67
aug-cc-pVTZ UCCSD	0.787	2400(27.5)	1097(18.7)	654(7.8)	444(3.1)	2410(35.2)	685(11.5)	10.99
aug-cc-pVTZ UCCSD(T)	0.788	2375(25.3)	1079(18.2)	636(6.6)	436(3.5)	2387(32.5)	669(10.6)	10.84

Table A.7: Theoretical dipole moments (μ_e, in debye), harmonic vibrational frequencies (in cm^{-1}), and zero point vibrational energies (in kcal mol^{-1}) for the $^3A_2$ planar PPH_2 structure.

Theory		$\omega_1(a_1)$	$\omega_2(a_1)$	$\omega_3(a_1)$	$\omega_4(b_1)$	$\omega_5(b_2)$	$\omega_6(b_2)$	
	μ_e	sym PH stretch	sym bend	PP stretch	wagging	asym PH stretch	asym bend	ZPVE
cc-pVDZ ROHF	0.966	2676	1109	537	889i	2718	550	10.86
cc-pVTZ ROHF	0.978	2672	1120	539	879i	2712	559	10.87
cc-pVQZ ROHF	0.978	2677	1125	539	879i	2716	563	10.90
aug-cc-pVDZ ROHF	0.889	2671	1103	531	885i	2714	549	10.82
aug-cc-pVTZ ROHF	0.931	2671	1118	537	876i	2712	559	10.87
aug-cc-pVQZ ROHF	0.949	2676	1125	538	878i	2716	563	10.90
cc-pVDZ RCCSD	1.140	2573	1037	532	838i	2615	492	10.37
cc-pVTZ RCCSD	1.256	2568	1050	545	808i	2608	502	10.40
cc-pVQZ RCCSD	1.292	2572	1053	552	801i	2612	509	10.44
aug-cc-pVDZ RCCSD	1.053	2553	1023	525	817i	2598	497	10.29
aug-cc-pVTZ RCCSD	1.200	2561	1040	543	799i	2603	499	10.36
aug-cc-pVQZ RCCSD	1.258	2569	1050	551	799i	2609	509	10.42
cc-pVDZ RCCSD(T)	1.186	2552	1030	527	830i	2595	481	10.27
cc-pVTZ RCCSD(T)	1.302	2543	1038	539	793i	2585	486	10.29
cc-pVQZ RCCSD(T)	1.335	2546	1040	547	783i	2587	495	10.32
aug-cc-pVDZ RCCSD(T)	1.094	2529	1013	518	805i	2575	485	10.19
aug-cc-pVTZ RCCSD(T)	1.243	2535	1027	537	781i	2578	484	10.24
aug-cc-pVQZ RCCSD(T)	1.299	2542	1036	545	780i	2583	494	10.30
aug-cc-pV(Q+d)Z RCCSD(T)	1.300	2545	1039	547	782i	2586	496	10.32
aug-cc-pVQZ UHF	1.113	2676	1126	548	932i	2715	563	10.90
aug-cc-pVTZ UCCSD	1.214	2561	1040	543	802i	2603	499	10.36
aug-cc-pVTZ UCCSD(T)	1.241	2535	1027	537	782i	2579	485	10.29

Table A.8: Theoretical harmonic vibrational frequencies (in cm^{-1}) and zero point vibrational energies (in kcal mol^{-1}) for the ^3A transition state connecting ^3B skewed HPPH and $^3A''$ pyramidal PPH_2 structure.

Theory	$\omega_1(a)$	$\omega_2(a)$	$\omega_3(a)$	$\omega_4(a)$	$\omega_5(a)$	$\omega_6(a)$	ZPVE
cc-pVDZ ROHF	2503	1757	917	724	493	2320i	9.15
cc-pVTZ ROHF	2501	1757	911	721	499	2273i	9.14
cc-pVQZ ROHF	2504	1757	910	721	500	2268i	9.15
aug-cc-pVDZ ROHF	2499	1746	908	719	492	2275i	9.11
aug-cc-pVTZ ROHF	2502	1754	908	719	499	2262i	9.13
aug-cc-pVQZ ROHF	2504	1757	909	721	500	2265i	9.15
cc-pVDZ RCCSD	2383	1671	846	650	456	1414i	8.60
cc-pVTZ RCCSD	2385	1687	843	644	472	1353i	8.63
cc-pVQZ RCCSD	2392	1698	844	646	479	1342i	8.67
aug-cc-pVDZ RCCSD	2364	1647	845	640	447	1382i	8.50
aug-cc-pVTZ RCCSD	2381	1679	847	643	469	1340i	8.61
aug-cc-pVQZ RCCSD	2389	1695	847	646	477	1338i	8.67
cc-pVDZ RCCSD(T)	2360	1658	830	634	444	1242i	8.48
cc-pVTZ RCCSD(T)	2358	1674	823	624	460	1146i	8.50
cc-pVQZ RCCSD(T)	2363	1684	824	625	467	1125i	8.53
aug-cc-pVDZ RCCSD(T)	2338	1632	828	622	434	1192i	8.38
aug-cc-pVTZ RCCSD(T)	2352	1665	828	622	457	1126i	8.48
aug-cc-pVQZ RCCSD(T)	2360	1680	828	624	465	1119i	8.53

Table A.9: The total energies (in hartree) for the ^3B_u *trans*-HPPH, $^3B_2$ *cis*-HPPH, and ^3B skewed HPPH structures.

Theory	^1A_g *trans*-HPPH	^3B_u *trans*-HPPH[a]			$^3B_2$ *cis*-HPPH			^3B skewed HPPH		
	energy	energy	ΔE_e	ΔE_0	energy	ΔE_e	ΔE_0	energy	ΔE_e	ΔE_0
cc-pVDZ HF	-682.612667	-682.583432	18.35	16.64	-682.580270	20.33	18.59	-682.593316	12.14	10.78
cc-pVTZ HF	-682.641862	-682.609025	20.61	18.93	-682.605936	22.54	20.82	-682.619322	14.14	12.81
cc-pVQZ HF	-682.650518	-682.616519	21.33	19.66	-682.613393	23.30	21.57	-682.626894	14.82	13.49
aug-cc-pVDZ HF	-682.617668	-682.587311	19.05	17.38	-682.584268	20.96	19.26	-682.597301	12.78	11.46
aug-cc-pVTZ HF	-682.643184	-682.610082	20.77	19.10	-682.606937	22.75	21.03	-682.620293	14.36	13.04
aug-cc-pVQZ HF	-682.650899	-682.616855	21.36	19.69	-682.613690	23.35	21.63	-682.627176	14.89	13.56
cc-pVDZ RCCSD	-682.884746	-682.828507	35.29	33.76	-682.825279	37.32	35.72	-682.840170	27.97	26.78
cc-pVTZ RCCSD	-682.972302	-682.913154	37.12	35.61	-682.909991	39.10	37.52	-682.926036	29.03	27.85
cc-pVQZ RCCSD	-682.998244	-682.936708	38.61	37.10	-682.933499	40.63	39.04	-682.950352	30.05	28.87
aug-cc-pVDZ RCCSD	-682.901011	-682.844524	35.45	33.94	-682.841504	37.34	35.76	-682.856803	27.74	26.57
aug-cc-pVTZ RCCSD	-682.978383	-682.918866	37.35	35.84	-682.915717	39.32	37.74	-682.931950	29.14	27.95
aug-cc-pVQZ RCCSD	-683.000584	-682.938925	38.69	37.18	-682.935719	40.70	39.12	-682.952627	30.09	28.91
cc-pVDZ RCCSD(T)	-682.896990	-682.835825	38.38	36.91	-682.832554	40.43	38.88	-682.847852	30.83	29.69
cc-pVTZ RCCSD(T)	-682.991391	-682.926585	40.67	39.22	-682.923375	42.68	41.15	-682.940211	32.12	30.98
cc-pVQZ RCCSD(T)	-683.019299	-682.952037	42.21	40.76	-682.948781	44.25	42.72	-682.966597	33.07	31.93
aug-cc-pVDZ RCCSD(T)	-682.915231	-682.853750	38.58	37.14	-682.850710	40.49	38.95	-682.866536	30.56	29.44
aug-cc-pVTZ RCCSD(T)	-682.998344	-682.933161	40.90	39.46	-682.929982	42.90	41.37	-682.947057	32.18	31.05
aug-cc-pVQZ RCCSD(T)	-683.021992	-682.954596	42.29	40.84	-682.951351	44.33	42.79	-682.969240	33.10	31.96
aug-cc-pV(Q+d)Z RCCSD(T)	-683.024595	-682.956722	42.59	41.13	-682.953436	44.65	43.11	-682.971504	33.31	32.17

[a] Relative energies (ΔE_e) and ZPVE-corrected relative energies (ΔE_0) are in kcal mol^{-1} with respect to the global minimum structure closed-shell ^1A_g *trans*-HPPH obtained by the same method and basis set.

Table A.10: The total energies (in hartree) for the $^3A''$ pyramidal PPH_2, $^3A_2$ planar PPH_2, and ^3A transition state connecting skewed HPPH and pyramidal PPH_2.

Theory	^1A_g *trans*-HPPH	$^3A''$ pyramidal PPH_2[a]			$^3A_2$ planar PPH_2			^3A transition state connecting pyramidal PPH_2 and skewed HPPH		
	energy	energy	ΔE_e	ΔE_0	energy	ΔE_e	ΔE_0	energy	ΔE_e	ΔE_0
cc-pVDZ HF	-682.612667	-682.607987	2.94	2.72	-682.564548	30.19	29.13	-682.544091	43.03	40.26
cc-pVTZ HF	-682.641862	-682.633642	5.16	4.95	-682.592562	30.94	29.90	-682.570686	44.66	41.89
cc-pVQZ HF	-682.650518	-682.641123	5.90	5.69	-682.600571	31.34	30.31	-682.578233	45.36	42.58
aug-cc-pVDZ HF	-682.617668	-682.611588	3.82	3.62	-682.568729	30.71	29.65	-682.548272	43.55	40.78
aug-cc-pVTZ HF	-682.643184	-682.634483	5.46	5.26	-682.593818	30.98	29.94	-682.571661	44.88	42.11
aug-cc-pVQZ HF	-682.650899	-682.641374	5.98	5.77	-682.600900	31.38	30.35	-682.578537	45.41	42.63
cc-pVDZ RCCSD	-682.884746	-682.853018	19.91	19.74	-682.814235	44.25	43.43	-682.808744	47.69	45.10
cc-pVTZ RCCSD	-682.972302	-682.937053	22.12	21.92	-682.902466	43.82	43.00	-682.895321	48.31	45.71
cc-pVQZ RCCSD	-682.998244	-682.960738	23.53	23.30	-682.927699	44.27	43.42	-682.919488	49.42	46.80
aug-cc-pVDZ RCCSD	-682.901011	-682.869133	20.00	19.84	-682.832429	43.04	42.25	-682.825913	47.12	44.55
aug-cc-pVTZ RCCSD	-682.978383	-682.942657	22.42	22.21	-682.908818	43.65	42.81	-682.901465	48.27	45.67
aug-cc-pVQZ RCCSD	-683.000584	-682.962914	23.64	23.41	-682.930047	44.26	43.41	-682.921846	49.41	40.86
cc-pVDZ RCCSD(T)	-682.896990	-682.860324	23.01	22.88	-682.822347	46.84	46.09	-682.819184	48.82	46.28
cc-pVTZ RCCSD(T)	-682.991391	-682.950861	25.43	25.26	-682.917622	46.29	45.53	-682.912929	49.24	46.68
cc-pVQZ RCCSD(T)	-683.019299	-682.976571	26.81	26.59	-682.945068	46.58	45.79	-682.939305	50.20	47.62
aug-cc-pVDZ RCCSD(T)	-682.915231	-682.878420	23.10	22.97	-682.842822	45.44	44.72	-682.838637	48.06	45.53
aug-cc-pVTZ RCCSD(T)	-682.998344	-682.957362	25.72	25.53	-682.924996	46.03	45.24	-682.920072	49.12	46.57
aug-cc-pVQZ RCCSD(T)	-683.021992	-682.979101	26.91	26.70	-682.947804	46.55	45.75	-682.942050	50.16	47.59
aug-cc-pV(Q+d)Z RCCSD(T)	-683.024595	-682.981330	27.15	26.92	-682.950226	46.67	45.86	-682.944342	50.36	

[a] Relative energies (ΔE_e) and ZPVE-corrected energies (ΔE_0) are in kcal mol^{-1} with respect to the global minimum structure closed-shell ^1A_g *trans*-HPPH obtained by the same method and basis set.

Table A.11: Focal point analysis of the energy difference (in kcal mol^{-1}) between ^1A_g *cis*-HPPH and $^3A''$ pyramidal PPH_2.

Basis set	ΔE[HF]	$+\delta$[MP2]	$+\delta$[RCCSD]	$+\delta$[RCCSD(T)]	$+\delta$[RCCSDT]	$+\delta$[UCCSDT(Q)]	$=\Delta E$
^1A_g *trans*-HPPH $\rightarrow$ $^3A''$ pyramidal PPH_2							
cc-pVDZ	+2.92	+20.05	-2.82	+2.94	-0.09	+0.20	[+23.20]
cc-pVTZ	+4.74	+21.03	-3.62	+3.29	-0.29	[+0.20]	[+25.35]
cc-pVQZ	+5.33	+22.06	-3.92	+3.33	[-0.29]	[+0.20]	[+26.71]
cc-pV5Z	+5.59	+22.51	-4.13	+3.37	[-0.29]	[+0.20]	[+27.25]
cc-pV6Z	+5.69	+22.76	[-4.28]	[+3.39]	[-0.29]	[+0.20]	[+27.47]
CBS LIMIT	[+5.74]	[+23.10]	[-4.48]	[+3.42]	[-0.29]	[+0.20]	[+27.68]
Function	$a+be^{-cX}$	$d+eX^{-3}$	$d+eX^{-3}$	$d+eX^{-3}$	Additive	Additive	
Fit Points ($X=$)	4,5,6	5,6	4,5	4,5			
$^a\Delta E_0 = \Delta E_{\rm fp} + \Delta_{ZPVE} + \Delta E_{core} + \Delta_{DBOC}$							
$= 27.68 - 0.22 - 0.10 - 0.01 =$ **27.35** kcal mol^{-1}							

[a] The symbol δ denotes the increment in the energy difference (ΔE) with respect to the previous level of theory. Bracketed numbers are the results of basis set extrapolation, while unbracketed numbers were explicitly computed. Δ_{ZPVE}=zero point vibrational energy correction from aug-cc-pVQZ RCCSD(T) harmonic frequencies; ΔE_{core}=core-valence correlation correction at the aug-cc-pCVQZ RCCSD(T) level of theory; Δ_{DBOC}=diagonal Born-Oppenheimer correction at the aug-cc-pVQZ ROHF level of theory. All computations are performed at aug-cc-pVQZ RCCSD(T) optimized geometries.

Table A.12: Focal point analysis of the energy difference (in kcal mol^{-1}) between $^3A''$ pyramidal PPH_2 and ^3B skewed HPPH.

Basis set	ΔE[HF]	$+\delta$[MP2]	$+\delta$[RCCSD]	$+\delta$[RCCSD(T)]	$+\delta$[RCCSDT]	$+\delta$[UCCSDT(Q)]	$=\Delta E$
			$^3A''$ pyramidal $PPH_2 \rightarrow {}^3B$ skewed HPPH				
cc-pVDZ	+9.31	-1.30	+0.05	-0.27	-0.08	+0.01	[+7.73]
cc-pVTZ	+9.06	-2.05	-0.09	-0.25	-0.05	[+0.01]	[+6.64]
cc-pVQZ	+8.99	-2.39	-0.08	-0.26	[-0.05]	[+0.01]	[+6.22]
cc-pV5Z	+8.97	-2.51	-0.05	-0.27	[-0.05]	[+0.01]	[+6.11]
cc-pV6Z	+8.96	-2.59	[-0.01]	[-0.27]	[-0.05]	[+0.01]	[+6.05]
CBS LIMIT	[+8.95]	[-2.69]	[+0.05]	[-0.28]	[-0.05]	[+0.01]	[+5.99]
Function	$a+be^{-cX}$	$d+eX^{-3}$	$d+eX^{-3}$	$d+eX^{-3}$	Additive	Additive	
Fit Points ($X=$)	4,5,6	5,6	4,5	4,5			
			$^a\Delta E_0 = \Delta E_{\rm fp} + \Delta_{ZPVE} + \Delta E_{core} + \Delta_{DBOC}$				
			$= 5.99 - 0.92 - 0.00 + 0.03 = \mathbf{5.09}$ kcal mol^{-1}				

[a] The symbol δ denotes the increment in the energy difference (ΔE) with respect to the previous level of theory. Bracketed numbers are the results of basis set extrapolation, while unbracketed numbers were explicitly computed. Δ_{ZPVE}=zero point vibrational energy correction from aug-cc-pVQZ RCCSD(T) harmonic frequencies; ΔE_{core}=core-valence correlation correction at the aug-cc-pCVQZ RCCSD(T) level of theory; Δ_{DBOC}=diagonal Born-Oppenheimer correction at the aug-cc-pVQZ ROHF level of theory. All computations are performed at aug-cc-pVQZ RCCSD(T) optimized geometries.

Table A.13: Focal point analysis of the energy barriers (in kcal mol^{-1}) for the isomerization reactions of two equivalent $^3A''$ pyramidal PPH_2 via the $^3A_2$ planar PPH_2 transition state.

Basis set	ΔE[HF]	$+\delta$[MP2]	$+\delta$[RCCSD]	$+\delta$[RCCSD(T)]	$+\delta$[RCCSDT]	$+\delta$[UCCSDT(Q)]	$=\Delta E$
$^3A''$ pyramidal $PPH_2 \rightarrow {}^3A_2$ planar PPH_2							
cc-pVDZ	+27.24	-4.69	+1.67	-0.51	-0.03	-0.03	[+23.65]
cc-pVTZ	+25.77	-5.72	+1.63	-0.84	+0.03	[-0.03]	[+20.84]
cc-pVQZ	+25.44	-6.30	+1.61	-0.97	[+0.03]	[-0.03]	[+19.76]
cc-pV5Z	+25.39	-6.52	+1.66	-1.01	[+0.03]	[-0.03]	[+19.51]
cc-pV6Z	+25.36	-6.64	[+1.70]	[-1.02]	[+0.03]	[-0.03]	[+19.42]
CBS LIMIT	[+25.35]	[-6.80]	[+1.76]	[-1.05]	[+0.03]	[-0.03]	[+19.25]
Function	$a+be^{-cX}$	$d+eX^{-3}$	$d+eX^{-3}$	$d+eX^{-3}$	Additive	Additive	
Fit Points ($X=$)	4,5,6	5,6	4,5	4,5			
$^a\Delta E_0 = \Delta E_{\rm fp} + \Delta_{ZPVE} + \Delta E_{core} + \Delta_{DBOC}$							
$= 19.25 - 0.58 - 0.09 - 0.01 =$ **18.56** kcal mol^{-1}							

[a] The symbol δ denotes the increment in the energy difference (ΔE) with respect to the previous level of theory. Bracketed numbers are the results of basis set extrapolation, while unbracketed numbers were explicitly computed. Δ_{ZPVE}=zero point vibrational energy correction from aug-cc-pVQZ RCCSD(T) harmonic frequencies; ΔE_{core}=core-valence correlation correction at the aug-cc-pCVQZ RCCSD(T) level of theory; Δ_{DBOC}=diagonal Born-Oppenheimer correction at the aug-cc-pVQZ ROHF level of theory. All computations are performed at aug-cc-pVQZ RCCSD(T) optimized geometries.

Table A.14: Focal point analysis of the energy barrier (in kcal mol^{-1}) for the isomerization reaction of two equivalent ^3B skewed HPPH via ^3B_u *trans*-HPPH or via $^3B_2$ *cis*-HPPH transition states.

Basis set	ΔE[HF]	$+\delta$[MP2]	$+\delta$[RCCSD]	$+\delta$[RCCSD(T)]	$+\delta$[RCCSDT]	$+\delta$[UCCSDT(Q)]	$=\Delta E$
^3B skewed HPPH $\rightarrow$ ^3B_u *trans*-HPPH							
cc-pVDZ	+5.87	+2.19	-0.91	+0.31	-0.02	-0.02	[+7.42]
cc-pVTZ	+6.36	+2.53	-0.85	+0.49	-0.00	[-0.02]	[+8.51]
cc-pVQZ	+6.47	+2.83	-0.73	+0.57	[-0.00]	[-0.02]	[+9.11]
cc-pV5Z	+6.53	+2.92	-0.71	+0.59	[-0.00]	[-0.02]	[+9.31]
cc-pV6Z	+6.54	+2.97	[-0.70]	[+0.60]	[-0.00]	[-0.02]	[+9.38]
CBS LIMIT	[+6.54]	[+3.04]	[-0.70]	[+0.61]	[-0.00]	[-0.02]	[+9.47]
$\Delta E_0 = \Delta E_{\rm fp} + \Delta_{ZPVE} + \Delta E_{core} + \Delta_{DBOC}$							
$= 9.47 - 0.31 - 0.09 + 0.02 =$ **9.09** kcal mol^{-1}							
^3B skewed HPPH $\rightarrow$ $^3B_2$ *cis*-HPPH							
cc-pVDZ	+7.81	+2.48	-1.14	+0.34	-0.02	-0.02	[+9.45]
cc-pVTZ	+8.26	+2.86	-1.10	+0.52	-0.01	[-0.02]	[+10.51]
cc-pVQZ	+8.40	+3.17	-0.98	+0.59	[-0.01]	[-0.02]	[+11.15]
cc-pV5Z	+8.49	+3.26	-0.97	+0.65	[-0.01]	[-0.02]	[+11.40]
cc-pV6Z	+8.51	+3.31	[-0.97]	[+0.67]	[-0.01]	[-0.02]	[+11.49]
CBS LIMIT	[+8.51]	[+3.37]	[-0.96]	[+0.70]	[-0.01]	[-0.02]	[+11.59]
Function	$a + be^{-cX}$	$d + eX^{-3}$	$d + eX^{-3}$	$d + eX^{-3}$	Additive	Additive	
Fit Points (X =)	4,5,6	5,6	4,5	4,5			
$^a\Delta E_0 = \Delta E_{\rm fp} + \Delta_{ZPVE} + \Delta E_{core} + \Delta_{DBOC}$							
$= 11.59 - 0.39 - 0.10 + 0.01 =$ **11.11** kcal mol^{-1}							

[a]The symbol δ denotes the increment in the energy difference (ΔE) with respect to the previous level of theory. Bracketed numbers are the results of basis set extrapolation, while unbracketed numbers were explicitly computed. Δ_{ZPVE}=zero point vibrational energy correction from aug-cc-pVQZ RCCSD(T) harmonic frequencies; ΔE_{core}=core-valence correlation correction at the aug-cc-pCVQZ RCCSD(T) level of theory; Δ_{DBOC}=diagonal Born-Oppenheimer correction at the aug-cc-pVQZ ROHF level of theory. All computations are performed at aug-cc-pVQZ RCCSD(T) optimized geometries.

Table A.15: Focal point analysis of the energy barrier (in kcal mol^{-1}) for the isomerization reaction between ^3B skewed HPPH and $^3A''$ pyramidal PPH_2 via ^3A transition state.

Basis set	ΔE[HF]	$+\delta$[MP2]	$+\delta$[RCCSD]	$+\delta$[RCCSD(T)]	$+\delta$[RCCSDT]	$+\delta$[UCCSDT(Q)]	$=\Delta E$
^3B skewed HPPH $\rightarrow$ ^3A transition state							
cc-pVDZ	+30.53	-14.19	+3.29	-1.61	+0.02	-0.04	[+17.99]
cc-pVTZ	+30.30	-15.41	+4.46	-2.08	+0.01	[-0.04]	[+17.24]
cc-pVQZ	+30.37	-15.66	+4.92	-2.21	[+0.01]	[-0.04]	[+17.39]
cc-pV5Z	+30.38	-15.73	+5.03	-2.25	[+0.01]	[-0.04]	[+17.40]
cc-pV6Z	+30.39	-15.76	[+5.07]	[-2.27]	[+0.01]	[-0.04]	[+17.41]
CBS LIMIT	[+30.39]	[-15.80]	[+5.13]	[-2.30]	[+0.01]	[-0.04]	[+17.40]
$^a\Delta E_0 = \Delta E_{\rm fp} + \Delta_{ZPVE} + \Delta E_{core} + \Delta_{DBOC}$							
$= 17.40 - 1.43 + 0.14 + 0.30 =$ **16.41** kcal mol^{-1}							

[a] The symbol δ denotes the increment in the energy difference (ΔE) with respect to the previous level of theory. Bracketed numbers are the results of basis set extrapolation, while unbracketed numbers were explicitly computed. Δ_{ZPVE}=zero point vibrational energy correction from aug-cc-pVQZ RCCSD(T) harmonic frequencies; ΔE_{core}=core-valence correlation correction at the aug-cc-pCVQZ RCCSD(T) level of theory; Δ_{DBOC}=diagonal Born-Oppenheimer correction at the aug-cc-pVQZ ROHF level of theory. All computations are performed at aug-cc-pVQZ RCCSD(T) optimized geometries.

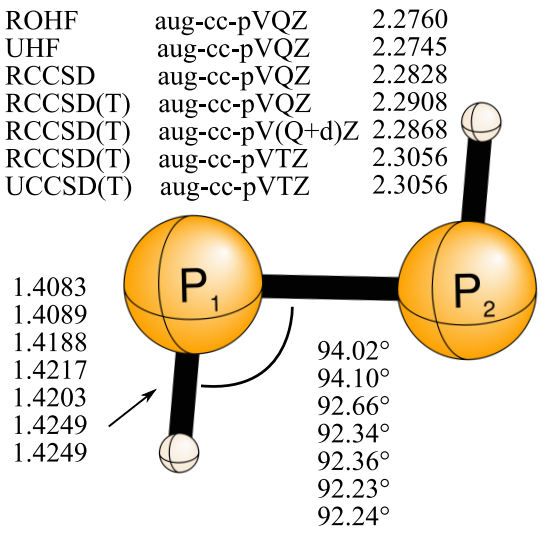

Figure A.1: Theoretical geometries for ^3B_u *trans*-HPPH. Bond lengths are in angstrom.

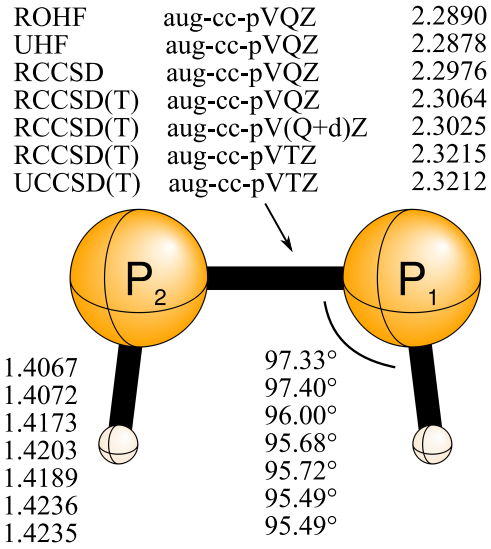

Figure A.2: Theoretical geometries for $^3B_2$ *cis*-HPPH. Bond lengths are in angstrom.

			dihedral angle
ROHF	aug-cc-pVQZ	2.2015	89.93°
UHF	aug-cc-pVQZ	2.2050	89.63°
RCCSD	aug-cc-pVQZ	2.1771	91.19°
RCCSD(T)	aug-cc-pVQZ	2.1746	91.46°
RCCSD(T)	aug-cc-pV(Q+d)Z	2.1700	91.49°
RCCSD(T)	aug-cc-pVTZ	2.1919	91.32°
UCCSD(T)	aug-cc-pVTZ	2.1921	91.31°

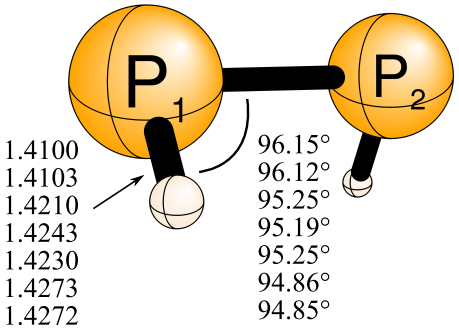

Figure A.3: Theoretical geometries for ^3B skewed HPPH. Bond lengths are in angstrom.

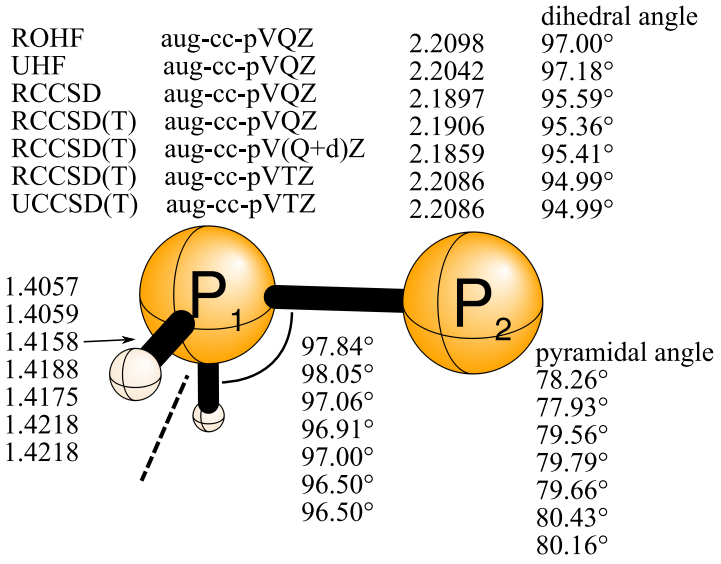

Figure A.4: Theoretical geometries for $^3A''$ pyramidal PPH_2. Bond lengths are in angstrom.

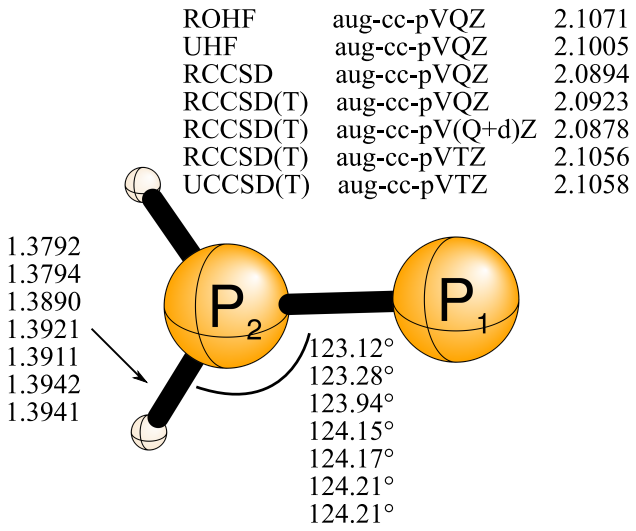

Figure A.5: Theoretical geometries for $^3A_2$ planar PPH_2. Bond lengths are in angstrom.

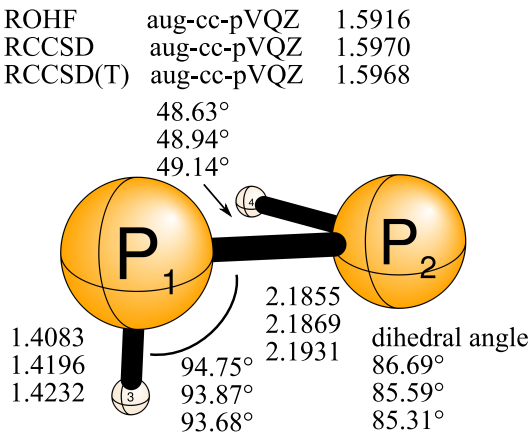

Figure A.6: Theoretical geometries for the transition state connecting ${}^3B$ skewed HPPH and ${}^3A''$ pyramidal PPH_2. Bond lengths are in angstrom.